UNIVERSITY OF TECHNOLOGY, SYDNEY

Design of a Biologically Inspired Climbing Robot and an Adhesion Mechanism for Reliable and Versatile Climbing in Complex Steel Structures

by

Peter Kenneth Ward

A thesis submitted in partial fulfillment for the
Degree of Masters of Engineering by Research

in the
Faculty of Engineering and IT
Intelligent Mechatronic Systems Group

July 2016

Declaration of Authorship

I, Peter Kenneth Ward , declare that this thesis titled, 'Design of a Biologically Inspired Climbing Robot and an Adhesion Mechanism for Reliable and Versatile Climbing in Complex Steel Structures' and the work presented in it is my own. I confirm that:

- This work was done wholly or mainly while in candidature for a research degree at this University.
- Where any part of this thesis has previously been submitted for a degree or any other qualification at this University or any other institution, this has been clearly stated.
- Where I have consulted the published work of others, this is always clearly attributed.
- Where I have quoted from the work of others, the source is always given. With the exception of such quotations, this thesis is entirely my own work.
- I have acknowledged all main sources of help.
- Where the thesis is based on work done by myself jointly with others, I have made clear exactly what was done by others and what I have contributed myself.

Signed: _____

Date: 22/07/2016

UNIVERSITY OF TECHNOLOGY, SYDNEY

Abstract

Faculty of Engineering and IT
Intelligent Mechatronic Systems Group

Masters of Engineering by Research

by Peter Kenneth Ward

Steel infrastructure is the backbone of modern day society, however it requires regular inspection and maintenance to ensure integrity and prolong the life of services. The inspection of steel infrastructure such as steel bridges, often requires inspection at heights, in confined spaces, in hazardous environments or in areas which simply cannot be accessed by humans. With more stringent Work Health and Safety requirements, the ability to carry out comprehensive inspection becomes more challenging, to the extent that particular locations can no longer be inspected. There is significant motivation for climbing robots to carry out the inspection of such locations; however very few solutions have been successfully deployed.

The difficulty in deploying a climbing robot is largely attributed to robot configurations which lack versatility and adhesion systems which lack reliability. Inspired biologically from the inchworm caterpillar, a climbing robot is developed to addresses these two issues. This research presents the kinematic design of a climbing robot and the design of a novel magnetic adhesion mechanism which overcomes the challenges faced by the current state-of-the-art climbing robots.

The inchworm inspired climbing robot has a unique kinematic design consisting of 7 Degrees of Freedom to achieve its versatile climbing ability. This unique configuration allows the robot to navigate complex structures and pass through narrow obstacles, such as manholes.

This research presents an optimisation model for developing robust and reliable adhesion systems which consist of multiple adhesion modules. The optimisation model maximises particular adhesion performance criteria, whilst minimising weight. The model allows for tailored designs depending on the means of adhesion being used.

In verifying the optimisation model, a novel adhesion mechanism is developed with the means of attaching and detaching a permanent magnet to a steel surface. The adhesion module consists of a quarter gear segment to rotate the magnet between attached and detached states. Using the novel adhesion mechanism, an adhesion system is developed based on the optimisation model and verified through testing.

The inchworm inspired robot configuration and the novel magnetic adhesion system enable the practical deployment of the robot. The Climbing RObot Caterpillar (CROC) has undergone extensive testing in simulated environments, mock-up environments and has been deployed for the real world inspection of complex steel structures. Over 50 site trials have been conducted over a three year period inside the hollow archways of the Sydney Harbour Bridge. CROC extends the state of the art, being the first of its kind deployed with the capability of autonomous inspection in complex steel structures.

Acknowledgements

Firstly, I would like to express my sincere gratitude to my supervisor Prof. Dikai Liu who introduced me to this field of research and allowed me to join the Climbing Robot team. Since taking me on as an intern, he has provided continuous guidance and motivation for my personal development through my studies and work related experience.

Besides my supervisor, I would like to thank the rest of the Climbing Robot project team, Prof. Kenneth Waldron, Prof. Gamini 'Dissa' Dissanayake, Dr. Gavin Paul, Chia-Han 'John' Yang, Phillip Quin, David Pagano and Liyang Liu. Also to Jack Liang and the many interns and capstone students who have assisted me during the project. Thank you for your insightful comments, encouragement, patience and support in broadening my research knowledge from various perspectives. Also, for the trials and tribulations, with many sleepless nights, even weeks, leading to the eventual success of the project. My sincere thanks also goes to the rest of the research staff and students at the Centre for Autonomous Systems. There has always been someone to lend a hand.

I would like to thank Laurent Matkovic, Peter Mann, Waruna Kaluarachchi, Philip Brooks and Palitha Manamperi from the NSW Roads and Maritime Services, who have supported us and beleived in us throughout the project. It has been fantastic to work in collaboration with them.

A very special thank you to the FEIT Workshop, Laurence Stonard, John Funnel, Scott Graham, Peter Bracken, Siegfried Holler, Ron Smith and Bill Firth (RIP), for supporting me throughout my research. With each iteration of the robot, they have taught me many valuable technical skills. Also to Peter Waterson for his valuable knowledge on magnets and John Hazelton for his time in proof reading my thesis.

I am thankful to all my friends who have made my time in Sydney enjoyable, particularly my past colleagues Greg Peters and Freek De Bruijn who also shared many insightful discussions during our coffee breaks.

Last but not the least, I would like to thank my family and friends. My parents Anthea and Trevor Ward have driven my curiosity and passion for learning, inventing and never giving up. Without their encouragement, I may not have undertaken this research and without their proof reading, my thesis would not read as well. Also to my brother Martin Ward, my grandparents and relatives who have supported me throughout the undertaking of this thesis and my life in general. Finally to Sandra Palm for your patience over the past four years, I promise I will start cooking and cleaning again.

Contents

List of Figures

List of Tables

Abbreviations

CAD	Computer Aided Design
CAS	Centre for Autonomous Systems
CROC	Climbing Robot Caterpillar
DOF	Degrees Of Freedom
EPM	Electro Permanent Magnet
FEA	Finite Element Analysis
HD	High Definition
MAV	Micro Aerial Vehicle
MFEA	Magnetic Static Finite Element Analysis
NDT	Non-Destructive Testing
NSW	New South Wales (Australia)
PEM	Permanent Electro Magnet
RGB	Red Green Blue
RMS	Roads and Maritime Service New South Wales
UTS	University of Technology, Sydney
UAV	Unmanned Aerial Vehicle
WHS	Work Health and Safety

Glossary of Terms

Actuator	On a robot, the actuators are devices responsible for controlled motion of the system. They may be powered by electrical energy, hydraulic fluids, or pneumatic pressure.
Degrees of Freedom	The Degrees of Freedom (DOF) in a robotic system, is the number of unique ways in which the system can move, whether the movements are translations or angular motions.
Environment	Includes all characteristic of the 3D surroundings in which the robot is operates.
Electro-mechanical servo	A type of actuator consisting of an electric motor, typically a gear train and control board. Normally can be controlled given a specific position, velocity, acceleration or torque.
Joints	In robotics, joints are objects which have at least one degree of freedom and represent the relationship between different reference frames. Joints by be of revolute, prismatic, translation or spherical type. They may also be passive or actively controlled. Actuators typically referred to as joints.

Manipulator	An articulated robotic arm consisting of several actuators. The manipulators end-effector allows it to manipulate objects in 3D space.
Map	Model of the geometry and material-type of surfaces in the surrounding environment.
Obstacle	An object within the robot's environment which it must overcome by climbing around, over or through.
Planning	The act of generating a path (and motion) course which the robot can then follow to get between two poses.
Pose	The position the robot or manipulator takes given a set of joint angles.
Unstructured	A real-world environment that has not been set up to facilitate ease of robot movements. These environments contain many uncertainties.
Workspace	The set of points which can be reached by the end-effector of a robot manipulator.

Chapter 1

Introduction

A robot can be defined as,

> "any automatically operated machine that replaces human effort, though it may not resemble human beings in appearance or perform functions in a humanlike manner."[1]

Modern day industrial robots were first created for industrial lines in the 1950s [2]. Since then, they have disrupted traditional industries. They have thrived in carrying out repetitive tasks on well organised assembly lines, day in, day out. Today's researchers face much greater challenges in pushing the forefront of robotics outside of the boxes, in which these assembly line robots operate from.

This new breed of robots will be more disruptive than industrial robots, being able to operate in environments which are unstructured. These environments will not be accurately known and may be subject to many uncertainties. This is the case for many industries including the agricultural, construction, healthcare, maritime, military and transportation to name a few.

These robots are referred to as service robotics. Service robotics incorporate greater mobility and autonomy than industrial robotics as they require environmental and situational

awareness. One of the more specialised branches of service robots, are those which are capable of climbing 3D structures; these are referred to as climbing robots. Climbing robots are expected to traverse 3D environments through means of adhesion principles.

There is significant research concentrating on developing climbing robots with the means and intelligence to move freely outside of well defined environments. These types of robots are expected to climb large structures, explore complex and unknown environments, build detailed three dimensional maps, localise themselves within their environment, carry out advanced tasks, avoid obstacles and adapt to uncertainties in their environments. Robots capable of performing these tasks will benefit many industries and advance the robot revolution.

1.1 Background

1.1.1 Inspection of Steel Infrastructure

The inspection of steel infrastructure is one of many tasks which will benefit greatly from these advancements in robotics.

Steel is one of the most important and widely used construction materials in the world. Steel is the backbone of many structures across most industries, including bridges in the transport industry; oil and gas platforms, power plants, wind turbines, silos and transfer chutes in the energy industry; and ship hulls and shipping ports in the maritime industry.

While steel is clearly versatile, it suffers an inherent problem of oxidation, leading to rust degradation over time. The primary failure in steel bridges is corrosion [3]. Hence, regular and ongoing inspection, condition assessment and maintenance are essential tasks to achieve the designed service life and to prolong aesthetics.

For comprehensive inspection and condition assessment, it is essential that the entire structure is analysed. Inspectors are often faced with inadequate access to locations on the structure, preventing comprehensive condition assessment. The integrity of the structure may be compromised through undetected aging, corrosion or mechanical stress leading

to severe risks including loss of life, economic costs, lack of dependable transport and environmental damage.

> "The collapse of the Silver Bridge in 1967 resulted in loss of 47 lives. ... The cost of this disaster was [USD]175 million dollars but some experts estimate the same occurrence today would cost between 2.1 and 5.6 billion [USD]dollars. Furthermore, these cost figures do not take into account factors such as loss of business resulting from loss of access or detours, the cost resulting from blockage of a major river shipping channel and potential environmental damage due to hazardous materials being transported over the bridge at the time of collapse." [4]

Following the collapse of the Silver Bridge, The National Bridge Inspection Program was initiated in the USA, stipulating that bridge inspections must be performed every 24 months.

In 2007 an unexpected collapse of an Interstate arch truss bridge in the USA killed 13 people, placing further scrutiny on inspection and maintenance programs and allocated spending. The following tactics were identified as crucial steps to ensure bridge structures are maintained in acceptable condition [5]:

- Advanced inspection technologies that can detect damage early
- Quality control measures to ensure the accuracy of inspections and serve as additional training for inspectors
- Advanced systems for managing and organising inspection data
- Innovative approaches to prioritising repairs
- Preventive maintenance measures to extend bridge life span.

It is evident that the ancillary cost of infrastructure failure is vast and that the monetary value for the inspection and preventative maintenance of structures will be more than compensated for. However, despite the growing effort, tactics and increased expenditure for inspection and maintenance, the ability to comprehensively assess the health of structures

is often limited by the ability to access particular locations in hazardous environments, at heights or in confined spaces. These matters are complicated further by ever increasing stringency imposed by Work Health and Safety (WHS) regulations.

1.1.2 Current Inspection Methods and Their Hazards

This section presents the current methods for inspection and maintenance, then discusses the severity of risks faced by human inspectors.

There are many inspection methods available, however visual assessment is the first and primary means used. This is in part due to the difficulty in access to sites, as a consequence particular locations are never thoroughly examined and degraded areas may be left unnoticed until failure.

Where there is cause for action, inspectors will need to access the site to perform a more thorough condition assessment. In performing thorough inspections, workers may be placed at greater risk in order to access the inspection sites. Access to such locations may require permits for working at heights, in confined spaces and in hazardous environments. Some of the common access methods and associated risks are as follows: [6]

- **Ladders**: are commonly used to access areas of the bridge where risk is low, however, they are the largest cause for falls from height in the workplace.
- **Inspection Vehicles**: such as 'boom buckets' or 'cherry pickers' are used to elevate workers to high regions or lower workers for sub-structure inspection (Fig 1.1a). Unexpected loads and disturbances have caused tipping resulting in injuries and fatalities. Furthermore, they delay or prevent traffic from passing due to road closures.
- **Boats, barges**: may be used for bridges over water where access to traffic can not be interrupted. Inspections may be performed using binoculars or booms depending on complexity of structure, barge traffic and required inspection methods.
- **Rigging/floats**: typically uses cables and platforms supported at heights (Fig 1.1b). This method can only be used when there is sufficient clearance and when access by other means is not feasible.

- **Scaffolds**: are typically used for lower heights providing greater mobility and support than rigging; however they are subject to strict compliance. Some scaffolds known as 'spiders' may be used to support climbers for inspecting high structures.
- **Climbers**: are generally used if other access methods are not feasible. In most cases free climbing is prohibited and climbers must be always be secured to the structure and a safety line (Fig 1.1c & 1.1d).

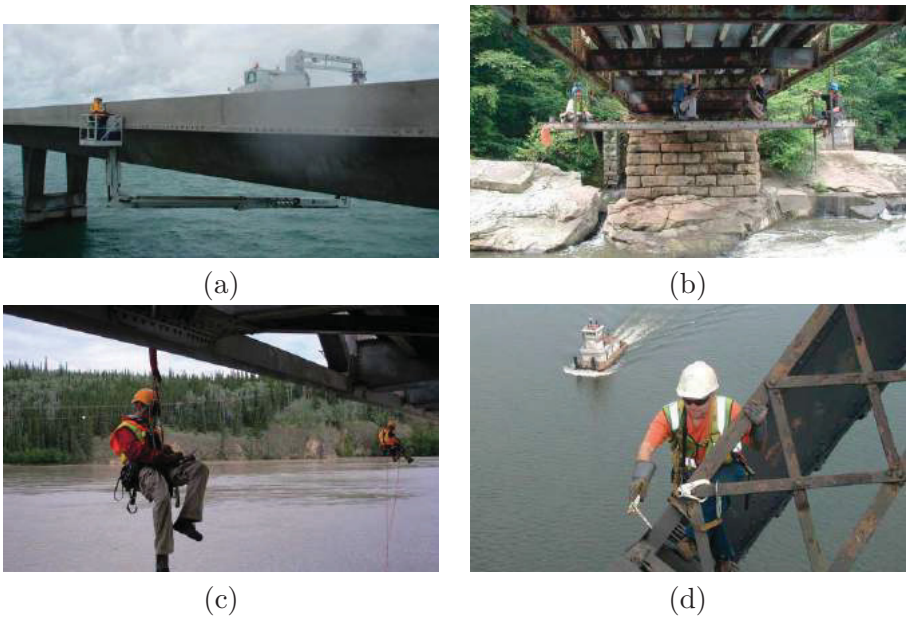

(a) (b) (c) (d)

FIGURE 1.1: Traditional methods of inspection place workers at risk. (a) Boom suspends worker for understructure inspection (b) Floats suspended below bridge deck as platform for workers (c) Multiple climbers suspended along bridge length to inspect beneath bridge decking (d) Climber operating tool with one hand and holding on to structure with other.

The ability to inspect exterior surfaces of the structure is possible, albeit difficult at times. The inspection of internal areas, such as box girders, is very limited. In the past inspectors have been able to inspect confined spaces with specialised training; however with increased WHS requirements trained inspectors are no longer permitted to work in these confined locations. Statistics from around the world highlight these necessary precautions for working in confined spaces.

In Australia,

> "OSHA estimates that there are 5,000 serious injuries and 63 fatalities annually associated with confined spaces." [7]

In the United States,

> "a five year study into the statistics of confined space fatalities was performed. During this five year period between 2005 to 2009, 481 fatalities were recorded in 28 states. This equates to one fatality every four days with over 61% of these fatalities occurring in the construction and maintenance sectors." [8]

Due to the severity of the risks and consequences posed to workers in confined spaces and at heights, there is strong emphasis on risk mitigation.

1.1.3 Potential and Motivation for Climbing Robots

A 2011 bridge inspection project [9] covered the challenges in performing inspection work on a complex bridge structure. Numerous hazards were present, including overhead and adjacent power lines, heavy train traffic, barge traffic, working in confined spaces, working from heights and limited working hours. All low risk inspection methods were ruled out due to the imposed restrictions and complexity of the structure. As a result, climbers were required to work at heights and in confined spaces as seen in Fig 1.2 (a) and (b) to carry out inspection.

If a robotic solution was realised, the elevated risks, extra costs and extended time may have been alleviated from an early stage. A climbing robot could have inspected the internal and external structure without interfering with the train or barge traffic. Risk of interfering with power lines would be mitigated without the use of booms, climbers or rigging. The entire structure could have been inspected efficiently with a coordinated team of climbing robots. The collected inspection data could be stored in a database for comparison with future inspections.

Industries are becoming more aware of the limitations in current inspection and maintenance methods, and the potential for deploying robots. With the ability to overcome

(a)

(b)

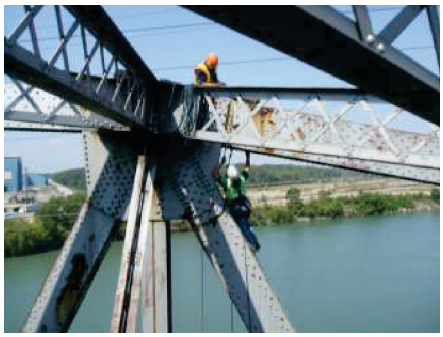

(c)

FIGURE 1.2: (a) Bridge No. 16.9 over Little Calumet River in Riverdale, Illinois. (b) Confined spaces requiring climbers (c) Main trusses near power lines requiring access with climbers [9]

obstacles and climb surfaces irrespective of orientation, many benefits can be realised with a climbing robot:

- Access to inspection sites previously inaccessible to humans
- Access to high risk locations at heights and in confined spaces, mitigating and eliminating the risk for human workers
- Utilising multiple Non-Destructive Testing techniques (such as visual, hyper-spectral, electromagnetic, ultrasonic, and laser) to provide detailed condition assessment of the structure
- Storing detailed records with organised inspection data detailing location and condition
- Repairs can be performed at the time of inspection

- Regular, efficient and ongoing inspection and maintenance can be performed with minimal effort using coordinated teams of climbing robots
- Reduced time and cost in set up of work platforms, equipment and plant.

With so much potential and motivation, one may wonder why this technological gap in the inspection of infrastructure worldwide has not been addressed with climbing robots. To understand this, the challenges faced by climbing robots in real world scenarios must first be considered.

1.1.4 Challenges Faced in Developing Climbing Robots

While the benefits of introducing robots into the inspection industry are widely recognised, the practical deployment of robots has been largely limited to industrial manipulators with very structured environments. In these structured environments, robots have little to no requirement of mobility as work is brought to the robots. Industrial robots with mobility are limited to operate within structured and sanctioned work zones with very few uncertainties. These environments are carefully designed to ensure reliable, robust and safe operation.

The greatest challenge faced by robots and their deployment in real world scenarios pertains to their operating environment. The environment effects all aspects of the robot including design, required intelligence and operation. The successful deployment of state-of-the-art climbing robots today, is largely constrained for operation in simple and semi-structured environments.

These environments contain large flat planar surfaces, ideal surface conditions, with simple and known obstacles. These environments require simple mobility and little to no autonomy. Robots in these scenarios can be controlled by human operators with simple controllers.

Real world infrastructure, on the other hand, contains complex geometry and intersecting planes, surface irregularities, and unforeseen obstacles. This poses two challenges for the designers of such climbing robots; these being the requirement for advanced robot

intelligence and the requirement for advanced robot designs which are capable of dealing with the environment and operational goals.

1.1.4.1 Robot Intelligence

Climbing robots need a sense of environmental and situational awareness in order to overcome obstacles and to cater for uncertainties. This requires sensory information which must be interpreted and acted upon in an accurate and timely manner. Therefore these robots are expected to have advanced intelligence through sophisticated algorithms to address the challenges of autonomy. The fundamental principles for autonomous operation include exploration, mapping, localisation, planning, motion control and task execution.

This thesis does not focus on the fundamental research for these aspects of intelligence. Instead, this thesis focuses on the design of the robot, to provide a body which enables the robot to its full potential and permits operation in real world scenarios.

1.1.4.2 Robot Design

Assuming high level autonomy is achieved, robots are also limited by constraints of their design. There are several aspects to the design which require careful consideration; these are the task definition, locomotion and adhesion. These aspects are fundamental in the design of climbing robots, requiring carefully consideration and selection to enable practical deployment.

The task definition: The first step in the design process is identifying the task definition. This defines the scope and mission of the climbing robot, including the procedures which must be carried out, the required application scenarios and environmental influences. This determines the required payload capacity and equipment which must be incorporated into the design. The task definition largely influences the design of the locomotion and adhesion principles.

Locomotion: Climbing robots need a means of moving from one location to another, the form that this takes is referred to as locomotion. Locomotion plays an important role in

the mobility, dexterity and manoeuvrability of a climbing robot in order to carry out its task definition. Climbing robots may adopt locomotion such as wheeled, tanked, legged, limbless or rolling. Each type of locomotion has numerous forms of implementations with advantages and disadvantages defined by the task definition.

Mobility: The mobility of a robot is a performance criteria which defines the effectiveness of the climbing robot in moving from one location to another. The implementation of a particular locomotion can provide greater mobility for a specific task, application scenario or environmental conditions. Therefore, as the complexity of the task definition increases, the design of a climbing robot becomes increasingly more challenging.

Adhesion: Another challenging aspect in the design of a climbing robot is the adhesion method. There are many principles of adhesion, each largely dependant on the task definition, in particular the intended operating environment and surface conditions. Adhesion mechanisms may adopt principles such as chemical, electrostatic, Van Der Waals, pneumatic, grasping, electromagnets or permanent magnets. Each method comes with advantages and disadvantages that differ for specific environmental conditions and operational goals.

1.2 Aims for This Research

This research was funded in part, by the New South Wales Roads and Maritime Services (NSW RMS), the Australian Research Council and The University of Technology Sydney, to investigate a robotic solution for the inspection of steel structures where it is not feasible or poses too great a risk to send human inspection workers.

This thesis considers the challenges for a climbing robot to be deployed in the inspection industry. In doing so, it addresses these challenges and presents a climbing robot for the inspection of complex steel structures. Whilst human made machines deal well with structured environment, they can not compare to the versatility of biological systems when placed into unstructured environments. Biologically systems have spent millions of years adapting to their environment, thereby providing a wealth of knowledge which can be utilised when considered the design and operation of robots.

This research draws upon the inchworm caterpillar for inspiration in the design of a climbing robot. The inchworm is highly versatile in its ability to overcome complex unstructured environments. Biological systems such as the inchworm caterpillar are very complex, however inspiration can be drawn from different levels. This research primarily uses abstract inspiration in the design, for example the method of locomotion, being an inchworm step, the concept of using feet on either end of a slender body with many degrees of freedom, and the arrangement of adhesion modules at the extremities of its feet.

By drawing upon the inspiration from the inchworm caterpillar, this research aimed to demonstrate how biologically inspiration can be used to improve the reliability and versatility of climbing robots in complex and unstructured environments such as steel bridges.

1.2.1 Scope

The Sydney Harbour Bridge has been used as the primary application scenario for the climbing robot. The primary goal of the climbing robot is to carry out inspection of the internal steel box girder sections of the Sydney Harbour Bridge. The robot must self-contained with the necessary inspection equipment including high definition colour images and video. Furthermore, as the robot can not be seen remotely, and complex obstacles are expected, the robot must carry the necessary computing hardware and sensors to enable autonomous operation and inspection.

The Sydney Harbour Bridge pictured in Fig 1.3 a, is a prime example of a complex steel structure which requires ongoing inspection and maintenance.

The containment and access level for inspection and maintenance of this bridge has been identified as Level 6, being the highest on a scale of one to six.

> "Level 6 Complex structure over $30m$. Staged internal and specialised external access required. Operating requirements of other plant and equipment must be considered." [10]

The Sydney Harbour Bridge presents many challenging real world inspection sites which are either high risk or not feasible for human inspections due to risks working at heights,

in confined spaces, or ergonomics. Several challenging obstacles and application scenarios that the climbing robot must overcome have been identified.

- **Complex Intersecting Planes**

  The Sydney Harbour Bridge consists of many web-like trusses and box girders as pictured in Fig 1.3 b. The surface planes intersect at varying angles both concave and convex. The robot must be able to transfer between planes at any angle and orientation with respect to gravity as shown in Figures 1.5a to 1.5d.

(a) (b)

FIGURE 1.3: The Sydney Harbour Bridge. a) The bridge has a Level 6 rating for containment and access in performing inspection and maintenance (b) Complex web like structures of the Sydney Harbour Bridge[11].

- **Confined Spaces**

  The bridge has four primary arches which span the width of the harbour. Each arch contains three chords with internal chambers. The chambers are confined and are divided by manhole plates (Fig 1.4a) or partition plates (Fig 1.4b). Some manhole scenarios have a clearance of no more than $300mm$ by $380mm$. Partition plates have a clearance of no more than $300mm$ by $760mm$ between the ground and partition plate. Fig 1.4c highlights the challenge of inspecting the chambers, particularly whilst carrying the required tools and inspection equipment. With more stringent WHS regulations, the risks for human inspectors to inspect these chambers has been deemed too significant. Therefore the robot must be able to navigate the confined sections and pass through manhole and partition plate scenarios. To climb through

the manhole the climbing robot must be able to perform a 180° plane transition on plates between 10 to 70mm in thickness as shown in Fig 1.5e.

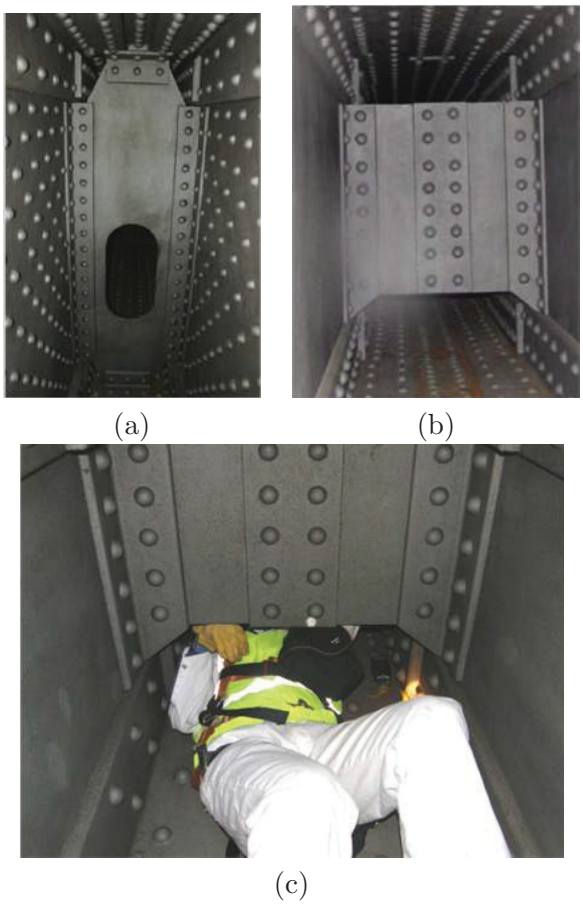

FIGURE 1.4: Obstructions faced by inspectors in the archways of the Sydney Harbour Bridge. a) Manhole scenario b) Partition plate scenario c) Inspection worker investigating beyond partition plate

- **Rivets**

  The Sydney Harbour Bridge is densely riveted with over 6 million rivets. The size and patterns of the rivets vary across locations. The most common occurring rivets are 50mm diameter and 25mm in height.

- **Surface Conditions**

  The opening of the Sydney Harbour Bridge in 1932 required 272,000 litres of lead based paint to provide a three coat foundation; since then it has been continuously repainted as part of ongoing maintenance and preservation of aesthetics.

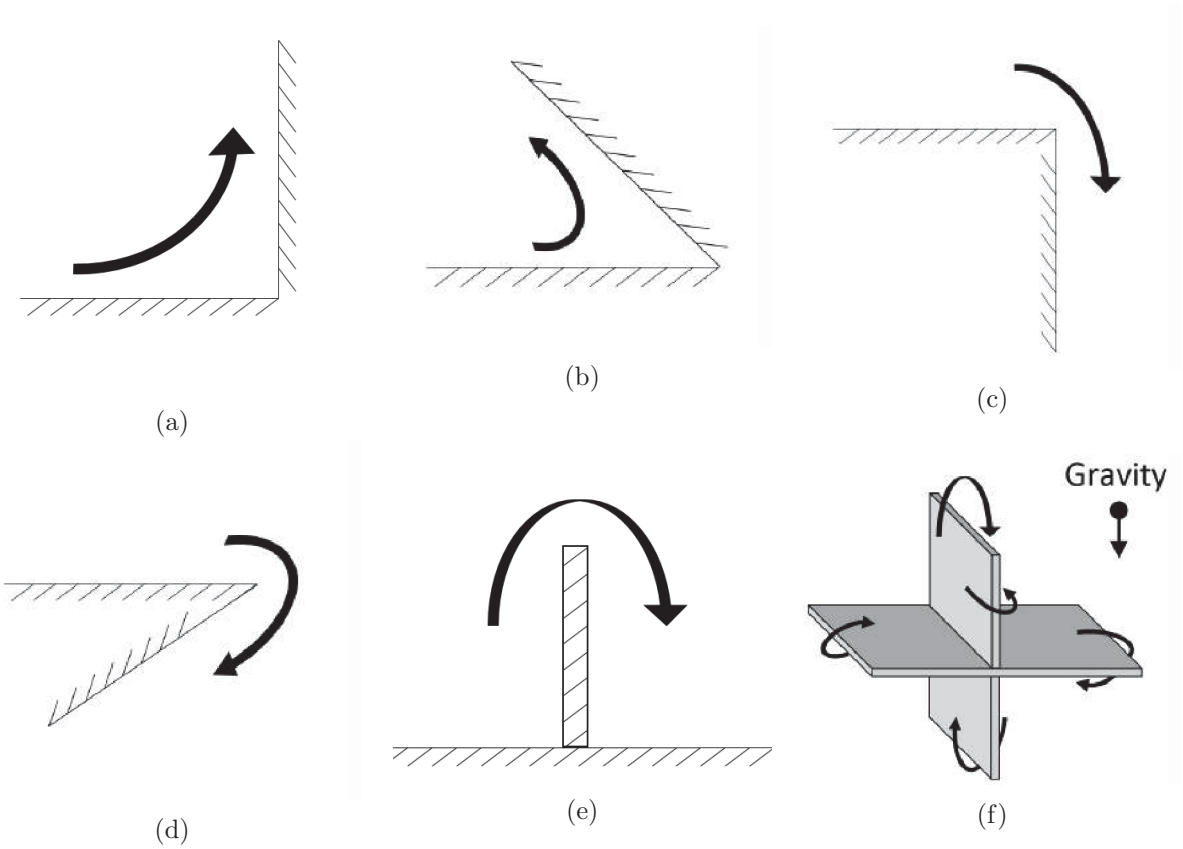

FIGURE 1.5: Plane transitions required for climbing robot. (a) 90° concave transition (b) Acute concave transition (c) 90° convex transition (d) 90° Obtuse convex transition (e) 180° thin plane transition. (f) Required 180° plane transitions with respect to gravity.

The typical paint thickness on the structural steel ranges from $300\mu m$ to $750\mu m$. However, some areas of the bridge have been identified with a paint thickness greater than $1.6mm$ and is susceptible to peeling.

> "This is a significant issue as there is a limit to the thickness of paint that can be applied to a surface before it starts to fall off under its own weight and due to degradation over time."[12]

Hence, it is often difficult to determine the surface condition beneath the paint through visual inspection, as seen in Fig 1.6a. The adhesion system for the climbing robot must be robust and reliable, catering for varying surface conditions, including variation in surface profile and integrity of the surface, including extreme cases as seen in Fig 1.6b.

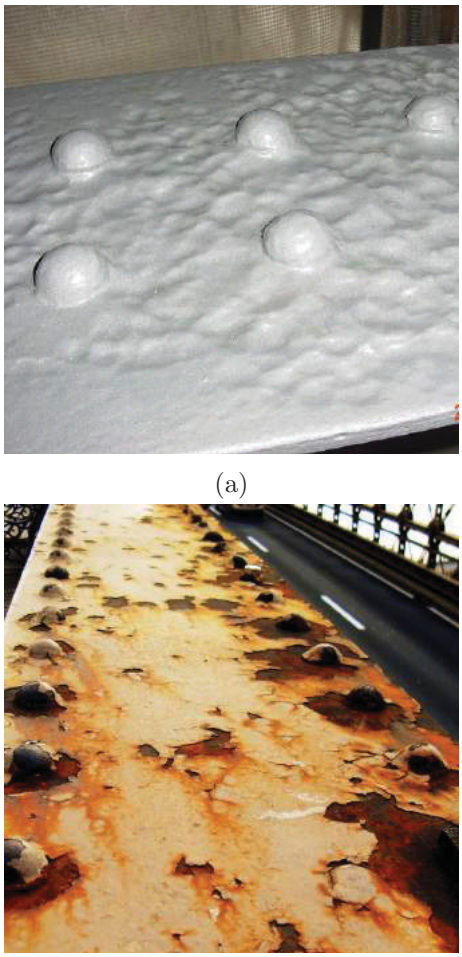

(a)

(b)

FIGURE 1.6: Surface conditions expected in real world inspection sites. (a) New paint coating covering pitted surface of steel member[13]. (b) Significant build up of paint dirt and rust[11].

A robot capable of traversing these scenarios would provide inspectors with a valuable tool for comprehensive assessment of the structure. To this cause, this research has investigated the design of a climbing robot capable of traversing these scenarios in order to carry out inspection.

1.3 Contributions

The outcomes of this thesis are developed through an extensive literature review, theoretical modelling, design optimisations, experimental results, real world testing and a reflection of research conducted.

The main contributions of this thesis are:

- A novel, biologically inspired 7 DOF robot configuration with high mobility. The climbing robot can climb on planar surfaces and perform complex plane transitions, including the ability to climb through narrow manholes, at any orientation with respect to gravity. The superior mobility allows the climbing robot to access previously inaccessible inspection locations and carry out a broad range of tasks.
- A novel, permanent magnetic adhesion module. The magnetic adhesion module yields high capacity with a light weight, high robustness to surfaces conditions, and is power-fail safe ensuring safe operation. The system uses a gear train to provide attached and detached states on ferromagnetic structures.
- An optimisation model to design an adhesion system consisting of multiple adhesion modules, maximising performance characteristics, and minimising the system weight and size.
- The integration of the biologically inspired robot configuration and the novel adhesion system to form a climbing robot for inspection of complex environments. The robot extends the state of the art in climbing ability for complex steel structures, being able to perform 180° plane transitions between 0 to 100mm in thickness, in any orientation with respect to gravity.

1.3.1 Publications and Presentations

- Peter Ward, Dikai Liu, "Design of a High Capacity Electro Permanent Magnetic Adhesion for Climbing Robots", Robotics and Biomimetics (ROBIO), 2012 IEEE International Conference on , pp.217,222, 11-14 Dec. 2012

- Peter Ward, Dikai Liu, Ken Waldron, Mahdi Hassan, "Optimal Design of a Magnetic Adhesion for Climbing Robots", Climbing And Walking Robots (CLAWAR), 16th International Conference on , July 2013.

- Peter Ward, Phillip Quin, David Pagano, Chia-Han Yang, Dikai Liu, Ken Waldron, Gamini Dissanayake, Gavin Paul, Philip Brooks, Peter Mann, Waruna Kaluarachchi, Palitha Manamperi, Laurent Matkovic, "Climbing Robot for Steel Bridge Inspection: Design Challenges", 9th Austroads Bridge Conference, ARRB Group Ltd and Authors, Sydney, NSW 2014

1.3.2 Abstracts and Presentations

- Peter Ward, Dikai Liu, Gavin Paul, John Yang, Liyang Liu, Phillip Quin, David Pagano, Ken Waldron, Gamini Dissanayake, Philip Brooks, Peter Mann, Waruna Kaluarachchi, Palitha Manamperi, Laurent Matkovic, "Lessons Learnt From Field Trials of a Biologically Inspired Inspection Robot on the Sydney Harbour Bridge", 10th RMS Annual Bridge Conference, Bridge Engineering Bridges, Safe and Effective Road Network, 2 - 3 December 2015, Sydney

1.3.3 Patents

- Peter Ward, Dikai Liu (2015). Adhesion system for a climbing vehicle. University of Technology Sydney, New South Wales, Australia. Publication No.: WO/2015/003221. International Application nuermber: PCT/AU2014/000719. Priority number: AU20130902595 20130712. International Classifications: B62D55/265; B62D57/024. Published 15th January 2015.

1.3.4 Awards

The outcomes of this research are part of the key innovations of a biologically inspired autonomous climbing robot that has won the following awards:

- July 2015 NSW iAwards - Merit Award for New Product Category, 'A Bio-Inpired Climbing Robot for the Inspection of Steel Infrastructure'. University of Technology Sydney / NSW Roads and Maritime Services.
- July 2015 National iAwards, Australia - Merit Award for New Product Category. 'A Bio-Inspired Climbing Robot for the Inspection of Steel Infrastructure'. University of Technology Sydney / NSW Roads and Maritime Services.
- October 2015 SafeWork NSW Awards - Best solution to an identified workplace health and safety issue, Robotic Bridge Inspector. NSW Roads and Maritime Services / University of Technology Sydney.
- November 2015 Asia Pacific ICT Alliance (APICTA) Awards, Sri Lanka - Winner of Industry Application Category, 'Biologically Inspired Climbing Robot'. University of Technology Sydney / NSW Roads and Maritime Services.

1.4 Thesis Outline

This thesis is structured as follows:

Chapter 1 outlines the thesis, provides background, motivation, and the scope, contributions and outcomes that result from this research.

Chapter 2 presents a comprehensive literature review on climbing robots. Two challenging research aspects emerging from the literature are reviewed: robot locomotion; and adhesion systems. The review and analysis of the state-of-the-art climbing robots provides a valuable resource to robot designers highlighting the necessary considerations in designing a climbing robot, with attention to the required mobility and adhesion to perform the required tasks and tackle the application scenarios.

Chapter 3 considers how biological inspiration can be used to conceive a robot configuration capable of exploring complex environments. The inchworm caterpillar is studied and found capable of performing the required complex plane transitions. The inspiration is used to achieve high mobility in real-world inspection scenarios. The robot configuration is presented and is validated in simulation and from thorough testing of a prototype in a mock structure.

Chapter 4 presents the design of a novel permanent magnetic adhesion module and an optimisation model to design an adhesion system consisting of multiple adhesion modules. The adhesion system is evaluated through testing in laboratory conditions and in real world site conditions.

Chapter 5 provides an overview of the system integration of the climbing robot and adhesion system. The system is tested and evaluated in laboratory conditions and in real world conditions. Upon evaluation the system is improved to meet the challenges for deployment with real world operating conditions carrying out the required task definition.

Chapter 6 concludes the thesis with a discussion on current limitations and avenues for future research work are proposed.

The conclusions are followed by **Appendices** and the **Bibliography**.

Chapter 2

Literature Review

This chapter provides a comprehensive literature review on climbing robots by presenting and analysing different methods of locomotion and adhesion. This literature review considers feasibility in respect to the intended operating environment and inspection tasks.

2.1 Locomotion

There are many types of locomotion which have been explored for climbing robots, some of the more common types include wheeled, tracked, limbless and legged. These solutions are analysed in terms of their ability to overcome the intended scenarios, focusing on achieving high mobility, in particular the ability to perform complex plane transitions.

Whilst not a climbing robot, flying robots are briefly discussed in order to highlight their lack of feasibility in the application scenarios, and in carrying out the task definition.

2.1.1 Flying Robots

In recent years flying robots, otherwise referred to as unmanned aerial vehicles (UAVs), drones, quad-copters, multi-copters, or micro aerial vehicles (MAVs) have shown great potential in inspection applications with extended flight times, great stability and higher

payloads. Their ability to span uneven terrain is unmatched; however, the miniaturisation of UAVs for confined and complex environments, greatly effects these performance characteristics.

There are several reasons that flying robots are not considered feasible for the inspection of the archways in the Sydney Harbour Bridge. These include control complexity in confined and complex environments, size limitations in the environment, payload capacity, flight time, and maintenance capabilities.

Size limitation: An industry leading quad rotor UAV with ideal performance is the AscTec Pelican by Ascending Technologies. The UAV is capable of up to 15mins of autonomous navigation using an on-board lidar for 3D mapping. However with blade tip to tip dimensions of 700mm, the UAV cannot pass through the 300mm manholes in the archways. For inspections in the archways of the Sydney Harbour Bridge, a drone would be limited in size by the 300mm width of the manholes. Based on this wingspan, an expected flight time of up to 8 minutes is achievable [14].

Payload Capability: The payload capability of drones is largely proportional to their size. Due to the complexity and confinement in the archways, the drone would require numerous cameras and sensory equipment at several positions and orientations. Due to the constraint in size and flight time a drone would not be able to handle the required payload capacity. Finally, drones have very limited ability to perform maintenance tasks due to the lack of payload capacity.

For these reasons flying robots have not been considered as a possible form of locomotion for the inspection robot.

2.1.2 Wheeled and Tracked Robots

Wheeled and tracked type robots are dominant in the field of climbing robots. Wheel and tracked type robots offer many advantages including high mobility, high payload capacity and simple control methods.

Mobility: There are several advantages and disadvantages regarding the mobility of wheeled and tracked robots. They tend to have much greater speed and simpler control

requirements. However as the environment becomes more complex with obstacles, surface irregularities, discontinuities and plane transitions, their ability is greatly compromised.

There are numerous examples of climbing robots which are highly mobile on smooth and planer surfaces, scaling windows [15–19], concrete buildings [18–22] and steel structures [15, 18, 23–33]. However, plane transitions is one of the greatest challenges for these robots.

> "The difficulty of plane transition is to secure weight by adhesion on the new surface while releasing it on the previous surface. The robot has to be safe and stable at any time of the transition." [20]

Despite the challenge, several techniques have been developed to tackle surface transitions. Tripillar [20], Fig 2.1 a, is capable of performing concave wall transitions such as from the floor to ceiling. However, Tripillar can not perform convex plane transitions. Combot [34], Fig 2.1 b, is another tracked robot with magnetic adhesion, capable of overcoming obstacles up 30mm and capable of performing 90 degree concave and convex transfers, assisted by the added degrees of freedom along its body.

MagneBike, Fig 2.1 c, may be considered one of the most successful with commercial potential being demonstrated. Its success can be attributed to its high mobility in comparison to other wheeled and tracked forms. Its ability to transfer from one plane to another is achieved by integrating lateral lever arms to lift the magnetic assembly off the surface. The decrease in magnetic attraction force from one plane allows the wheel to continue on the other plane. Although this robot provides high mobility with the ability to perform 90° convex and concave transition angles, it is not capable of performing 180° plane transitions on thin sections as required in the intended application scenario.

There are two robots that have been identified with the ability to perform 180° thin plane transitions. Cymag [31] is a wheeled robot that can perform most plane transitions regardless of the orientation of gravity, including a 180° plane transition in select orientations with respect to gravity. However due to its simple rolling structure it would face similar challenges to other wheel robots including build up of ferromagnetic particles, difficulty in overcoming surface irregularities, discontinuities and obstacles such as

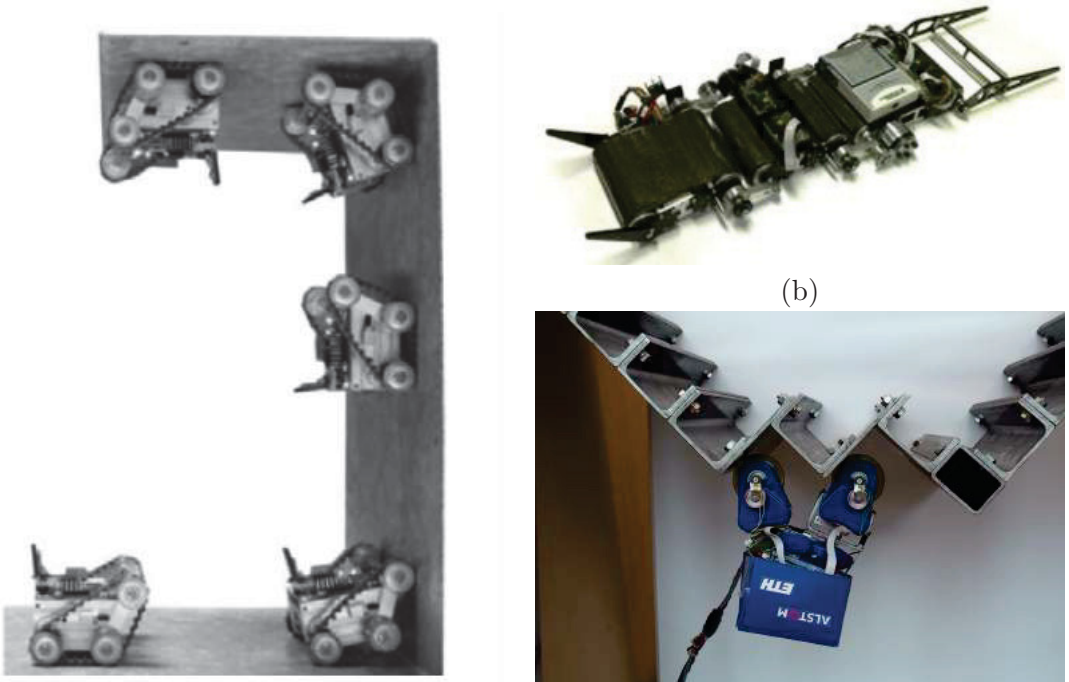

(a) (b) (c)

FIGURE 2.1: Wheeled and tracked robots capable of plane transitions. (a) Tripillar: Moving from floor to ceiling [20]. (b) Combot, capable of 90° concave and complex plane transitions. [35] (c) MagneBike performing 90° concave and complex plane transitions [36].

rivets. Furthermore, the design principle limits capability of performing inspection and maintenance tasks. Another tracked climbing robot [37] with the capability to perform the required 180° thin plane transition has been identified. However, this robot can only perform thin plane transition in one orientation with respect to gravity, as gravity assists the transition. This robot, along with other tracked style robots are susceptible to peeling from the surface with changes in load distribution and gravity.

Many robots have been demonstrated in laboratory or ideal site environments. When environmental conditions deteriorate the performance of the robots also suffers. Experiments have shown that collecting ferromagnetic dust on wheels and tracks rapidly reduces the effective adhesion strength, which may lead to failure of the adhesion.

"First tests have been done with a simplified version of the MagneBike,

> which rolls on rubber-covered magnetic wheels and implements several innovative mechanisms for dealing with difficult combinations of obstacles. After a few cm, this robot already failed, as the ferromagnetic rust was sticking to all parts of the magnetic wheel not only destroying the rubber but also penetrating into the gears. For this reason, the idea to use magnetic wheeled robots with additional mechanisms for passing specific obstacles had to be rejected very soon." [38]

Paylaod: Another challenge for wheeled and tracked robots is managing the careful balance between total system weight and adhesion strength. With insufficient adhesion the climbing robot may fall off, with too strong adhesion the robot might not move due to the required torque to turn the wheels. This also means that changes in the load, due to added equipment, manipulation tasks or changes in orientation with respect to gravity, could alter the performance of the robot and reduce reliability, as noted with Tripillar.

> "The major disadvantage of our caterpillar is the low force needed to detach it when peeling it off. ... In the case of the caterpillar, the force needed to lift one magnet is sufficient to detach the whole caterpillar." [20]

For the inspection of clean, flat and smooth surfaces, wheeled and tracked robots are ideal methods of locomotion. They offer simple control and high speeds. However, they are not ideal in environments which contain complex obstacles, complex intersection of planes, surface irregularities and discontinuities. For these environments researchers have looked toward biologically inspired systems, particularly those with legs.

2.1.3 Biologically Inspired Robots

Biological systems have been an important source of inspiration to researchers, in unlocking the mechanism in which they are able to navigate through complex environments and over complex 3D structures. Biological inspiration is drawn from many animals such as snakes, geckos, ants, spiders, monkeys and caterpillars to name a few. There are

many classifications for biological inspiration for climbing robots, however the primary distinction that can be made, is between limbless and legged climbing robots.

2.1.3.1 Limbless Robots

Limbless robots are typically inspired by caterpillars, worms, snakes or slug-like animals. The gaits for these robots may adopt principles of propagation [39–41], rolling [39, 42, 44], side-winding [43] or bracing [45, 46]. Without the use of limbs, wheels or tank treads, they have the advantage of not posing the risk in getting limbs caught on obstacles in complex environments. Limbless robots have been researched by . Example propagation gaits for a caterpillar type and earthworm type robot can be seen in Figs. 2.2a and 2.2b.

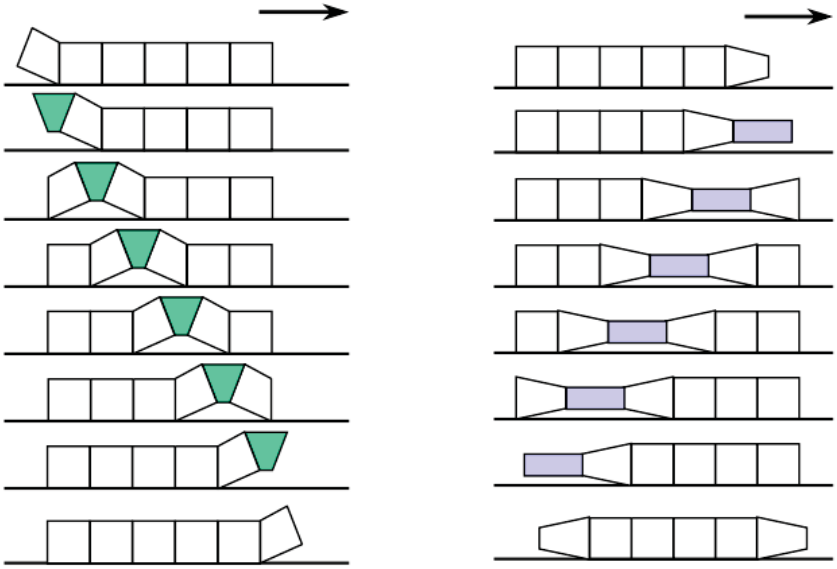

(a) (b)

FIGURE 2.2: Example movement gaits for limbless type robots (a) Caterpillar propagation gait. (b) Earth worm propagation gait.

Several limbless climbing robots have been noted to climb pole like structures such as trees with the ability to grip around their trunks as seen in Fig 2.3. These robots are often hyper redundant and offer a high degree of mobility; however thus far they have lacked the capability for good exploration and manipulation tasks, and most importantly, the ability to scale vertical planar surfaces. The incorporation of adhesion along the body is

considered feasible; however this is expected to pose similar challenges to the wheeled and tracked type robots, such as overcoming friction in order to enable the sliding motion.

FIGURE 2.3: Snake type robot climbing a tree branch through means of grasping and bracing. [46]

2.1.3.2 Legged Robots

When the ability to overcome obstacles is critical, researchers most often look toward legged animals for inspiration. The inspiration of these robots are often derived from animals such as geckos, ants, spiders, caterpillars, and monkeys to name a few. There are several characteristics which are important to considered for legged climbing robots:

Mobility and Climbing Gaits: The advantage in legged robots lies in their ability to overcome many of the problems faced by wheeled, tanked and limbless locomotion. In particular, legged robots are often implemented to overcome obstacles and discontinuities in the environment, and to perform plane transitions. Legged robots carry their body weight above the surface allowing them to step over obstacles in the way.

Stability and Payload: As the centre of mass for the climbing robot moves further away from a vertical plane, the robot requires greater adhesion and stronger actuators to maintain a grip and support its body.

One approach to supporting the body is incorporating more legs. Adding more legs to the robot often provides greater stability and redundancy in adhesion. It is also thought to

add extra degrees of freedom in the system which allows for greater mobility in overcoming obstacles. However in practice, using more legs has tended to reduce the practical mobility due to an increase in control complexity and overall weight of the system.

Control Complexity and Speed: Additional degrees of freedom through extra legs or body segments increases the control complexity in coordinating the legs and body. Therefore in comparison to other forms of locomotion, legged robots tend to be much slower. With increased control complexity, the success for legged robots to overcome obstacles in real testing has been limited. This is particularly true for operating in performing plane transitions and operating in confined spaces.

In comparison to wheeled or tracked robots which normally utilise two degrees of freedom, legged robots may contain many degrees of freedom. It is an extremely difficult process for a human operator to simultaneously control multiple joints of the robot, as required to perform climbing trajectories successfully.

Therefore legged robots require a largely autonomous approach with complex motion planning algorithms. This has been one of the greatest challenges for practical use of legged robots.

2.1.3.3 Comparison of Legged Robots

There are many legged robots designed with the intention to carry out inspection and maintenance tasks. These robots differ largely in size, weight and mobility often due to the application scenario, environment, and operational tasks. In identifying characteristics suitable for this research Table 2.1 has been created to highlight the practical ability between robot configuration and plane transition capabilities. The plane transition capabilities are defined in Fig 1.5 . For each of the climbing and transition abilities listed, a tick signifies that it has been demonstrated. This comparison then seeks to learn what attributes in legged robot design is best suited to performing 180° thin plane transitions.

TABLE 2.1: Comparison of legged climbing robots. Degree of Freedom (DOF) are active joints, unless otherwise specified as passive. For bipedal robots, joint axis have been standardised using Rx - Rotation in x direction, Ry - Rotation in y direction, Rz - Rotation in z direction

Robot	**Type of Locomotion**	**Details**	**Climbing & Transition Ability**		**Adhesion Method**
GeckoBot [47] 	Quadruped 12DOF 3DOF per leg	$100g$ 210mm length $5cm/s$ Floor $1cm/s$ Incline	Floor Incline Vertical Horizontal Inverted Concave Convex	✓ ✓	Synthetic fibrillar dry adhesive
Biped Robot [48] 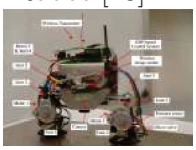	Bipedal 5DOF Under-actuated: 3 active DOF RxRzTzRzRx		Floor Incline Vertical Horizontal Inverted Concave Convex	✓ ✓	Vacuum pumped suction cups
Stickybot [49, 50] 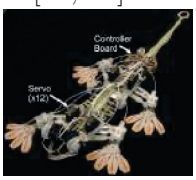	Quadruped $38DOF$ $12ActiveDOF$	$370g$ 600mm length $4cm/sec$ vertical $24cm/sec$ horizontal	Floor Incline Vertical Horizontal Inverted Concave Convex	✓ ✓ ✓ ✓	Synthetic fibrillar dry adhesive, directional

Continued on next page

Table 2.1 – continued from previous page

Robot	Type of Locomotion	Details	Climbing & Transition Ability		Adhesion Method
REST1 [51, 52] 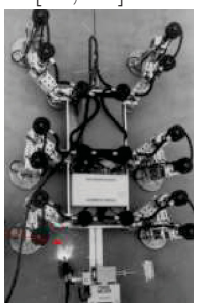	6 legs 18DOF 3DOF per leg	200kg	Floor Incline Vertical Horizontal Inverted Concave Convex	✓ ✓ ✓ ✓	Electro-magnets 100kg payload
ROMA II [53, 54] 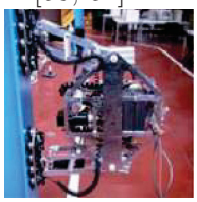	Bipedal 4DOF RzRxRxRz	20kg 1.5m/min	Floor Incline Vertical Horizontal Inverted Concave Convex	✓ ✓ ✓ ✓	Vacuum
NINJA [55, 56] 	Quadruped 12DOF 3DOF per leg	45kg 1.8m long 200mm step size 0.16m/sec vertical	Floor Incline Vertical Horizontal Inverted Concave Convex	✓ ✓ ✓ ✓	Active suction 1500N/leg

Continued on next page

Table 2.1 – continued from previous page

Robot	Type of Locomotion	Details	Climbing & Transition Ability		Adhesion Method
REST2 [51, 52] 	4 legs 12DOF 3DOF per leg	200kg	Floor Incline Vertical Horizontal Inverted Concave Convex	✓ ✓ ✓ ✓ ✓	Electro-magnets 100kg payload
ROWER [51] 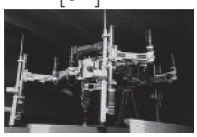	Quadruped 12DOF 3DOF per leg	310kg	Floor Incline Vertical Horizontal Inverted Concave Convex	✓ ✓ ✓ ✓ ✓	Clamping by extension of legs between walls Limited to double bottom cells 130kg payload
Abigaille-II [57] 	Quadruped 18$ActiveDOF$ 18$PassiveDOF$ 6 legs 3DOF per leg	260g 90mm diameter 4.5cm/s horizontal 0.1cm/s vertical	Floor Incline Vertical Horizontal Inverted Concave Convex	✓ ✓ ✓ ✓ ✓	Micro-posts, dry adhesion

Continued on next page

Table 2.1 – continued from previous page

Robot	Type of Locomotion	Details	Climbing & Transition Ability		Adhesion Method
ROBUG II [58] 	Quadruped 12DOF 3DOF per leg	$17kg$ 1m long, 0.7m wide $1m/min$ 200mm step size	Floor Incline Vertical Horizontal Inverted Concave Convex	✓ ✓ ✓ ✓ ✓ 	Vacuum
Waalbot [47, 59] 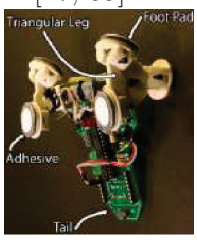	Wheeled-Legged $2DOF$	$100g$ 130mm length $6cm/sec$	Floor Incline Vertical Horizontal Inverted Concave Convex	✓ ✓ ✓ ✓ ✓ 	Synthetic fibrillar dry adhesive, directional
DEXTER [60] 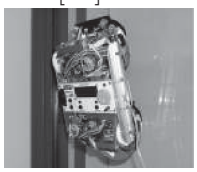	Bipedal 4DOF RzRxRxRz	$3kg$ $370m$ in length	Floor Incline Vertical Horizontal Inverted Concave Convex	✓ ✓ ✓ ✓ ✓ 	Passive Suction Cups

Continued on next page

Table 2.1 – continued from previous page

Robot	Type of Locomotion	Details	Climbing & Transition Ability		Adhesion Method
Inchworm robot [61] 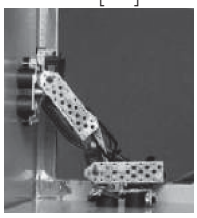	Bipedal 4DOF RzRxRxRx	455g 0.25m/min 252mm in length	Floor Incline Vertical Horizontal Inverted Concave Convex	✓ ✓ ✓ ✓ ✓ 	Electro-magnetic
MRWALL-SPECT III [62, 63] 	Quadruped $12DOF$ $3DOF$ per leg plus 1 passive per ankle 50cm/min		Floor Incline Vertical Horizontal Inverted Concave Convex	✓ ✓ ✓ ✓ ✓ 	Suction pads
MiniBibot-W [64] 	Bipedal 6DOF RzRxRxRxRxRz	800g 8m/min	Floor Incline Vertical Horizontal Inverted Concave Convex	✓ ✓ ✓ ✓ ✓ 	Electro-magnetic

Continued on next page

Table 2.1 – continued from previous page

Robot	Type of Locomotion	Details	Climbing & Transition Ability		Adhesion Method
ROMA I [53] 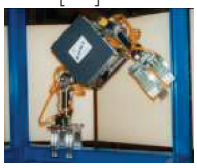	Bipedal 8 DOF RzRxRzPzRxRz +2DOF for grippers	75kg 1m/min	Floor Incline Vertical Horizontal Inverted Concave Convex	✓ ✓ ✓ ✓ ✓ ✓	Mechanical Grippers
3D Climber [65] 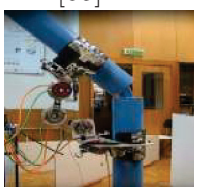	Bipedal 4DOF RzRxRxRx	42kg 1m/min 1m in length	Floor Incline Vertical Horizontal Inverted Concave Convex	✓ ✓ ✓ ✓ ✓ ✓	Mechanical Grippers
MATS 5DOF [66–68] 	Bipedal 5DOF RzRxRxRxRz	11kg 0.2m/sec 1.3m	Floor Incline Vertical Horizontal Inverted Concave Convex	✓ ✓ ✓ ✓ ✓ ✓	Docking stations are required

Continued on next page

Table 2.1 – continued from previous page

Robot	Type of Locomotion	Details	Climbing & Transition Ability		Adhesion Method
ROBIN [69] 	Bipedal 4DOF RzRxRxRx	$20kg$	Floor Incline Vertical Horizontal Inverted Concave Convex Max Angle	✓ ✓ ✓ ✓ ✓ ✓ 90°	Vacuum
Brincadeira [70] 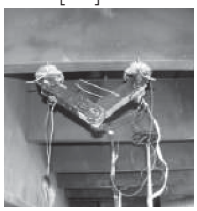	Bipedal 3 DOF RxRxRx No steering ability	$6kg$ 400mm in length No on board camera	Floor Incline Vertical Horizontal Inverted Concave Convex Max Angle	✓ ✓ ✓ ✓ ✓ ✓ ✓ 90°	Electro-magnetic
TREMO [71] 	Bipedal 5DOF (RxRz)Rx(RzRx) (RzRx) have rotations at same origin	800g 500m length 120mm radius footpad	Floor Incline Vertical Horizontal Inverted Concave Convex Max Angle	✓ ✓ ✓ ✓ ✓ ✓ 90°	Permanent Magnetic - Magnetic Switchable Device

Continued on next page

Table 2.1 – continued from previous page

Robot	Type of Locomotion	Details	Climbing & Transition Ability		Adhesion Method
RVC [72, 73] 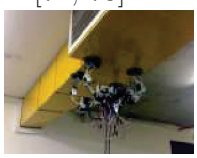	Quadruped 12 Active DOF 12 Passive DOF Per leg: 3 Active DOF, 3 Passive DOF	3kg	Floor Incline Vertical Horizontal Inverted Concave Convex Max Angle	✓ ✓ ✓ ✓ ✓ ✓ ✓ 90°	Peel-able magnetic array Magnostar
W-Climbot [74] 	Bipedal 5DOF RzRxRxRxRz	$22kg$ $1.37m$ Footpad is $350 \times 350 \times 50mm$	Floor Incline Vertical Horizontal Inverted Concave Convex Max Angle	✓ ✓ ✓ ✓ ✓ ✓ ✓ 109°	Vacuum
RAMR 1 [75] 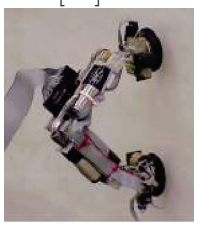	Bipedal 4DOF RzRxRxRx	$355g$ 248mm in length	Floor Incline Vertical Horizontal Inverted Concave Convex Max Angle	✓ ✓ ✓ ✓ ✓ ✓ ✓ 135°	Vacuum

Although no legged climbing robots have been identified with the ability to perform the required 180° thin plane transition, several robots have demonstrated the ability for convex plane transitions, these are RAMR 1, W-Climbot, RVC, Tremo, Brincadeira and ROBIN. It is interesting to note that in general, inchworm type robots have demonstrated superior ability in performing plane transitions, particularly those which are convex.

For RAMR 1 and Tremo, their ability for convex transitions can be realised by having at least 3 revolute, Rx joints; These being at either end of the bodies in close proximity to the surface and also in the middle of the body.

For the RVC robot, the ability for convex plane transitions as seen in Fig 2.4 can be attributed to the numerous DOF incorporated. Each leg includes three active DOF and a passive ankle with three DOF. Between two legs there are 6 active DOF, 4 of which are in the Rx axis. Due to the length of this chain and the number of Rx joints, convex transitions become kinematically easier.

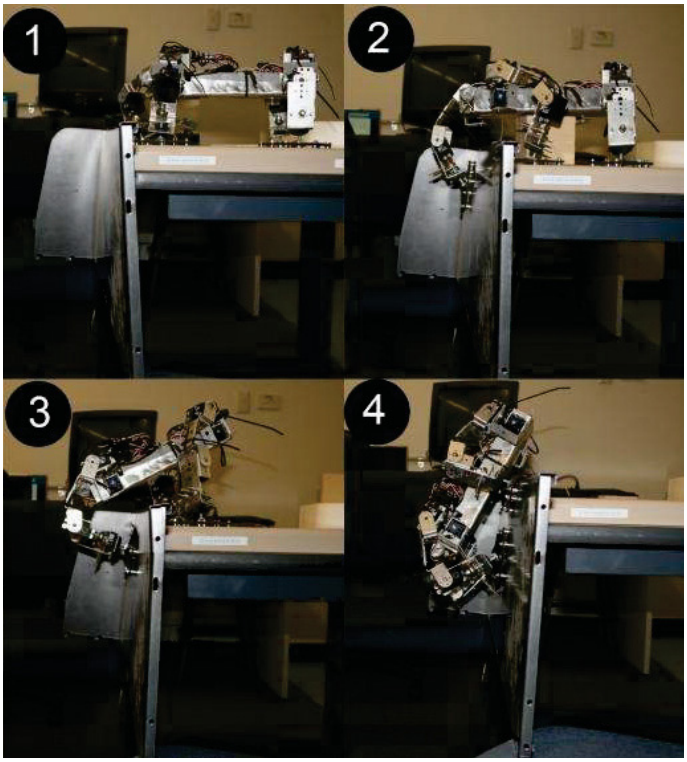

FIGURE 2.4: RVC climbing robot: Performing 90° convex transition from horizontal plane to vertical plane [72].

2.1.4 Summary of Robot Locomotion

It is widely recognised that "one of the major issues for achieving widespread adoption of robots is mobility" [76]. The mobility of climbing robots is determined by the robot locomotion and the number of DOF. The implementation of locomotion and design of the robot configuration is directed by the application scenarios, intended environment and the operational tasks which it must accomplish. While wheeled robots require low control complexity and can achieve high climbing speeds, they typically lack the capability required for complex plane transitions robustly, and the ability to span discontinuous surfaces. Legged robots on the other hand have a distinct advantage in performing plane transitions.

With consideration to the intended application scenarios, legged climbing robots are seen as a necessary step to achieve the required mobility. Of the legged configurations, bipedal or inchworm type robots have demonstrated greatest mobility, with reduced control complexity for performing plane transitions. Many different bipedal configurations with varying DOF have been identified. Whilst DOF directly increases mobility, it also increases control complexity and overall system weight. There are no solutions which meet the mobility requirements for the plane transitions; evidently the design of the climbing robot is not trivial.

2.2 Adhesion

Akin to choosing a suitable locomotion, a suitable means of adhesion must also be determined. This is again, largely constrained by the intended environment and the operational tasks for the climbing robot. A comprehensive literature review on implementations for various adhesion methods for climbing robots is presented, with a focus on analysing methods suitable for deployment in the intended environment and operating tasks. While some forms of adhesion provide numerous advantages, it is ultimately the disadvantages that render an adhesion method unsuitable for a particular task or environment.

Following the review, Table 2.2 summaries the key forms of adhesion identifying their advantages and disadvantages. Table 2.3 analyses the feasibility with respect to performance criteria, environmental conditions, and the operation of a bipedal or inchworm type robot.

2.2.1 Chemical

Methods of chemical adhesion for wheel and tracked type robots have relied on sticky tape, whilst legged robots have relied on Hot Melt Adhesives (HMA). Several bipedal type robots have been demonstrated with HMA [77, 78]; however practical use for inspection and maintenance tasks are limited.

> "the approach has a trade-off between time cost and energy cost. This suggests that self-contained climbing with HMA based technology favours applications where speed is not the priority but payload is more important, such as vertical transportation on rough terrains. Alternatively, due to the long-term bonding effect of HMAs, the robot may be used in tasks where the static period is much longer than its movement period"[77]

The use of a chemical adhesive leaves behind residues and has the potential to damage the surface through detachment. Furthermore, the adhesion is not reliable in harsh environments where the outermost surface layer built up of dirt and paint flakes, is easily peeled from the surface. For most inspection and maintenance task, these are undesirable traits.

2.2.2 Electrostatic

Electrostatic adhesion consists of conductive electrodes with alternating polarities. The electrode panel is separated from the target surface by an insulating layer. When the electrodes are energised, an electric field is generated which induces an opposite field in the target surface, as can be seen in Fig 2.5. The polarising field creates an attractive force between the electrodes and the surface. This clamping force is known as electrostatic adhesion. [79]

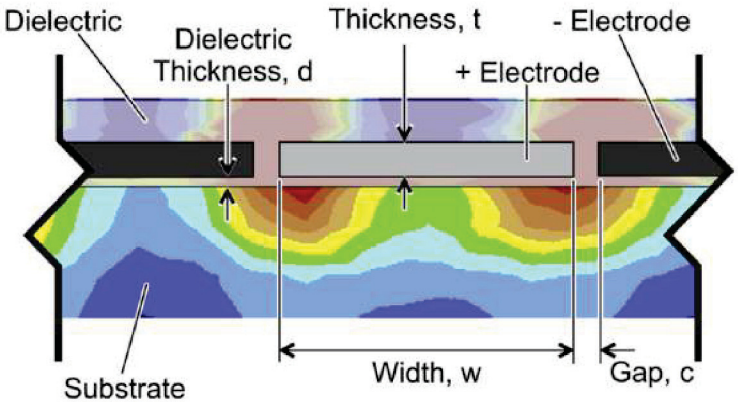

FIGURE 2.5: Cross-section of an electrostatic adhesive pad. [79]

The advantages of electrostatic adhesion include the ability to adhere to a wide range of materials including conductive and non-conductive surfaces, smooth and rough surfaces, high power to weight ratio and low power requirements.

The Stanford Research Institute (SRI) have demonstrated several wall tracked type climbing robots [18, 19]. However the technology is still developing and the researchers are still looking at increasing payload capabilities and the mobility.

2.2.3 Van Der Waals

Another type of electrostatic adhesion is known as Van Der Waals forces; these are weak intermolecular forces which exist between all molecules [80]. Although this force is very weak between two molecules, when millions of intermolecular forces are combined a great adhesion potential is realised. Geckos are examples of this adhesion principle in use. The pad of a Tokay gecko contains approximately 14,400 setae per square millimetre. As can be seen in Fig 2.6, the setae are sub-millimetre hairlike branches which further divide into hundreds of split ends. Each of these split ends provide intermolecular Van Der Waals forces generating up to $200\mu N$ of force per setae [81].

With inspirations from the gecko, adhesive gecko-like skin utilising Van Der Waals forces has been by artificially created by several research organisations. RiSE [83], StickyBot [49], GeckoBot [47]and Waalbot [84] are legged climbing robots which implement Van Der Waals

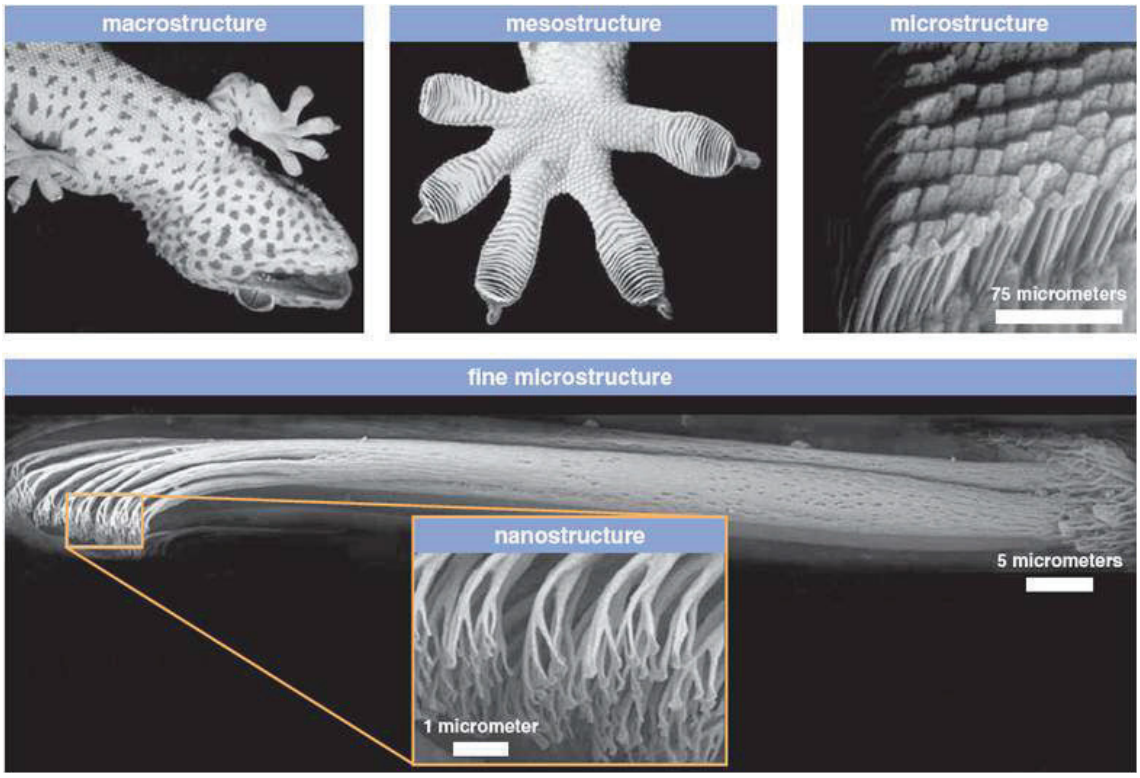

FIGURE 2.6: The structural hierarchy of the gecko adhesive system reveals different features at each scale from macro-structure, down to nano-structure. [82]

principles. The primary advantages for this adhesion type are low power consumption due to its passive nature, high power to weight ratio and adaptability to a broad range of surface materials. However, this adhesion method lacks robustness and reliability due to the fragile construction of the synthetic nano-fibres. This leads to the fibre degradation over time, resulting in lower adhesion forces. Finally, the adhesion is prone to contamination which may also result in adhesion failure.

> "The adhesives used on the feet of the robot gather dust and other contaminants[, as a result] their performance degrades quickly. Therefore, these adhesives are not suitable for dirty outdoor environments, walking across indoor floors, or for long term tasks."[47]

2.2.4 Pneumatic

Pneumatic type adhesion is one of the most common methods for adhesion in climbing robots where there are no features to grasp, or where there are no ferromagnetic surfaces. There are many advantages, in particular the ability to adhere to numerous surfaces materials, and the high payload capacities which can be achieved.

Pneumatic adhesion can be categorised by open or closed suction. Closed suction utilises a cup-shaped elastic material, which expels the internal volume of air when pressed against a surface. A low pressure chamber is formed within the cup. The pressure difference between the outside atmosphere and the internal low pressure holds the cup to the surface. These suction cups are often observed with tracked type robots which utilise many suction cups for redundancy, and require constant motion to prevent failure from leaking air. Closed suction cups can also incorporate active means of suction which provides much greater adhesive by actively vacating the air from within the cup. With the use of compressed air lines, active suction cups provide greater pressure difference, thereby generating stronger adhesive forces, a more reliable seal and better stability. For these reasons, several legged robots have adopted this method [53–56, 58, 69, 74, 75, 85]. There are several disadvantages for closed suction methods. They rely on smooth surface conditions to provide a good seal around the suction cup, and can be compromised easily in dirty environments with rust, dirt, dust, paint. Due to the elastic nature of the suction cups, the adhesion system is compliant which causes robots deflections from a desired robot pose, as seen in Fig 2.7a. This can be reduced using multiple adhesion modules.

Figure 2.7b demonstrates an open suction method, whereby a vacuum chamber allows leakage to occur. The vortex generated within the chamber creates a pressure differential, and hence provides an adhesive force. These are well suited to low height, wheeled based robots as they can provide high speed mobility without a closed seal contacting the surface. On the other hand they requires continuous power, and have less stability when performing tasks. Finally, no open suction method has been identified with the ability to perform plane transitions.

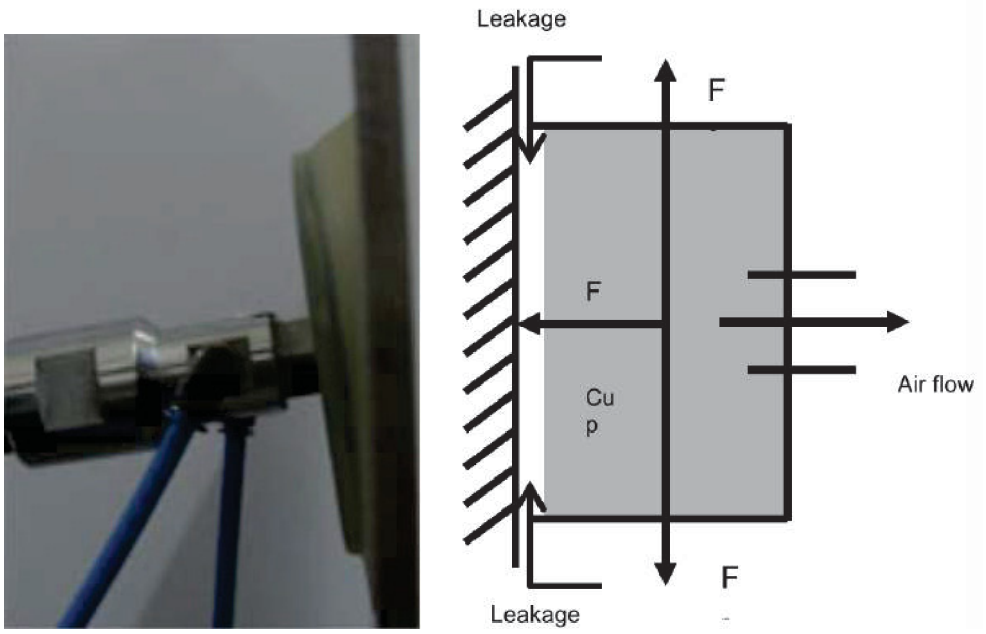

FIGURE 2.7: Pneumatic adhesion techniques. (a) Deformation in elastic suction cup. [74] (b) Thrust generated by open suction vacuum chamber. [86]

2.2.5 Mechanical Adhesion

Mechanical attachment devices exist in many different forms with their design catering for the specific environments. Mechanical adhesion is the most reliable form of adhesion when there are features in the environment that can be secured to. Forms of mechanical adhesion include claws, grasping, clamping or docking.

LEMUR IIB [87] achieves mechanical adhesion through the use of micro spine grippers. Each leg of the quadruped consists of a gripper, with 250 micro-spines. These grippers allow uni-directional adhesion to environments with cm-scale roughness. This technology has also been demonstrated down to the mm-scale roughness with the RiSE robot. Different environment surfaces can be accommodated through interchangeable micro-spine designs, as shown in Fig 2.8. Clawing adhesion is not suitable for smooth surfaces, and it is difficult to ensure adhesion reliability.

"the dactyl foot is used to climb carpet, trees, chain link, wood planks, and in the preliminary brick gaits. The walking foot is used for all horizontal

mobility tests. The spiny foot is being used to climb vertical stucco. And finally the lamellar structured sticky foot is used on hard smooth surfaces such as acrylic and glass."[83]

FIGURE 2.8: Four different feet variants used by the RiSE climbing robot. [83]

Several bipedal climbing robots with mechanical grasping grippers [51, 53, 54] for steel girders and poles [65] have been identified. Mechanical grasping grippers are advantageous because they can provide reliable, power-fail safe adhesion, with strong adhesive forces and high stability. However their greatest disadvantage is the lack of support for flat and featureless surfaces.

Another mechanical means of adhesion is through docking stations. The MATS robot [66–68] requires the installation of docking stations in the intended environment; each docking station provides the robot with power and means for control. The use of docking stations reduces the weight of the robot, by relocating the grippers, power system and control system of the robot.

In environments where there are features to grasp, mechanical adhesion is ideal. However, as the intended environment has very limited features and installing features or docking stations is not possible, the use of mechanical adhesion is limited.

2.2.6 Magnetic Adhesion

Other than mechanical grippers, non-magnetic forms of adhesion, such as pneumatic, electrostatic, or biologically inspired adhesion rely on adhesion to the outermost layers of the surface of the structure. The surfaces of real world inspection locations are often porous and contaminated with dirts, oils, rust, paint and other irregularities.

Magnetic adhesion has the advantage that it does not necessarily adhere directly to the outermost surface of the steel structure; rather it adheres to the underlying steel structure beneath exterior layers of paint, dirt and rust. The primary disadvantage of magnetic adhesion is that layers of paint, dirt and rust reduce the holding force at a significant rate. The rate at which the holding force decreases depends on the magnetic configuration.

Magnetic adhesion can be split into two types; these are electromagnetic and permanent magnetic adhesion. This research classifies electromagnetic to be all forms of magnetic adhesion which require continuous power to remain in a state where adhesion can be sustained; when power is not supplied the adhesion is no longer active.

2.2.6.1 Electromagnetic

Where the inspection of ferromagnetic structures is required, many researchers have adopted electromagnetic adhesion for their climbing robots [51, 52, 61, 64, 70, 88–90].

The primary advantage in adopting electromagnetic adhesion is that it can be deactivated very simply and quickly, without any moving parts, by switching off the energising current which induces a magnetic field within the electromagnetic coils. Other advantages for electromagnetic adhesion include high adhesion strength and the ability to work without direct contact with the surface. The primary disadvantage with electromagnetic adhesion is that when the power turns off, so does the adhesion, hence it is not power-fail safe.

2.2.6.2 Permanent Magnetic Adhesion

Permanent magnets are able to retain their magnetic state in the absence of an energising current. The primary advantage over electromagnetic adhesion is lower power consumption while attached and power-fail safe adhesion.

As permanent magnets retain their magnetic properties, this means they require a mechanism in order to disengage the magnet from the ferromagnetic surface. For this reason, permanent magnetic adhesion has predominantly been adopted by wheeled climbing robots.

However, several means of detachment for legged robots have been identified; these include peel-able magnetic adhesion, electro-permanent magnetic devices and mechanically switch-able devices.

2.2.6.3 Peel-able Magnetic Adhesion

Peel-able magnetic adhesion has been demonstrated with the MagnoStar on RVC [72]. This attachment mechanism had a maximum holding force of 105.95N using a total of 28 rare-earth pot magnets (a cylindrical magnet contained in a steel housing). The detachment was generated through a linear actuator to initiate a peeling effect, further decreasing the holding force as each magnet releases. This method is suited to multi-legged robots, where multiple feet are in contact with the surface at any one time. However, this method showed stability issues and is not suitable for bipedal robots, where only one foot would be in contact at a time.

2.2.6.4 Permanent Electro Magnetic Adhesion

Permanent Electro Magnets (PEM), use a rare-earth magnet in the core of the device to provide the adhesive force in the 'on' state. To switch the magnet to the 'off' state, a current is applied to a coil wrapped around the magnet. The magnetic field generated must be sufficient to provided an equal and opposing field, in order to counteract the magnetic field from the rare-earth magnetic core. The opposing field is only required to be powered long enough to remove the magnet from the surface. When the power is removed the full adhesive force of the magnet returns. Due to the configuration of these devices, they require direct contact with smooth ferromagnetic surfaces to work effectively. On a power to weight ratio, these devices are half as effective as using electromagnets. A 12W, 900g electromagnet has a maximum pull force capacity of 1500N, while a PEM of 13.3W and 900g has a pull force capacity of 720N [91]. This can be explained, as electromagnets can allocate the entire weight of the device to generating a large field. The PEM uses half of the system weight to generate the magnetic field in one direction, and the remaining half of the system weight to generate an opposing field when required. Some devices allow control on the direction of the electromagnetic field, allowing the PEM to align both magnetic

fields and increase overall adhesion. However, if relied upon, the device would no longer be power-fail safe.

2.2.6.5 Electro-Permanent Magnetic Adhesion

Electro Permanent Magnetic adhesion (EPM) has been demonstrated with a 6 mm, 200 mg device used as a latch for a millimetre-scale modular robotic system; the device was measured to reach a maximum holding force of 4.4 Newtons [92]. The EPM consists of two magnetic cores, where one of the magnetic cores must be a rare-earth magnet, in which the magnetic polarity remains in a constant state. The second magnet is referred to as the switching magnet, whose magnetic polarity is switch-able due to a much lower coercivity. The two magnetic cores sit side by side and are wrapped in the coil. The assembly uses two soft iron poles, at each end of the assembly. The soft iron poles provide a path for the magnetic field between the poles of the magnets and the surface whilst in the 'on' state, or between the two magnetic poles in the 'off' state, as can be seen in Fig 2.9.

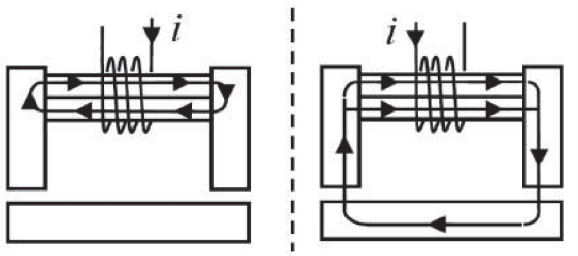

FIGURE 2.9: Operation of the Electro Permanent Magnet, 'off'state (left) and the 'on'state (right). [93]

In the on state the magnets have the same polarity and the same residual magnetisation. To switch from the on state to the off state, a high current momentarily energises the coil inducing a magnetic field around the magnetic cores and reversing the magnetic polarisation of the switching magnet, with the lower coercivity. With the magnetic cores having opposing polarity, the magnetic field is then contained within the pole. In this state there is no adhesion force experienced. Each magnetic state is preserved with no further power and hence this is also a power-fail safe solution.

This solution was investigated in previous work [94, 95] scaling the original 0.2g EPM to a 96g EPM for use at high adhesive forces as an adhesion mechanism in the climbing robot. The research demonstrated that the EPM was scalable, however the weight of the optimised device did not scale proportionally with the adhesion strength. The EPM adhesion strength to weight ratio is similar to that of the PEM; this can be linked to the issue regarding added system weight from the energising coils which does not provide any increase in adhesion strength. One proposal is that the coil could remain active to increase adhesion. However, this has the same issue with the PEM, meaning the system would no longer be power-fail safe.

2.2.6.6 Magnetic Switch-able Device

Magnetic Switch-able Devices (MSD) seen in Fig 2.10 use mechanical motion to alter the direction of magnetic fields within the mechanism through rotation of a magnet [96]. Akin to the EPM device, two magnetic cores are used. In this instance, both cores are strong rare earth magnets. Instead of re-polarising one of the magnetic cores, a motor can be employed to physically rotate the magnet. This has been demonstrated with the inchworm robot Tremo [71]. The adhesion system uses three MSD to achieve a holding force of 90N at a weight of 108 grams, consuming 187.5mJ of energy to change state. The adhesion strength to weight ratio is again similar to that of the PEM and EPM devices; this is because the motor used to rotate the magnet is of similar weight to the coils required to re-polarise the magnet.

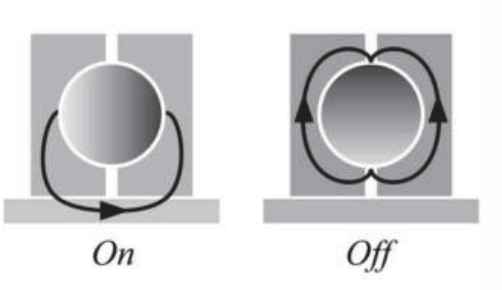

FIGURE 2.10: Operation of the Magnetic Switchable Device, On state (left) and Off state (right). [96]

2.2.7 Summary of Adhesion Methods

It is widely agreed that the type of adhesion implemented on a climbing robot is largely dependent on the intended operating environment and the required tasks. No single adhesion method is idea for all scenarios. When climbing robots are used on flat and smooth surfaces such as glass, pneumatic type adhesion is used most often. When structures consist of numerous features such as trusses or poles, mechanical grippers are best suited. On ferromagnetic surfaces, magnetic adhesion is the preferred option. Table 2.2 summarises the various forms of adhesion, highlighting their major advantages and disadvantages.

Table 2.2: Summary of the advantages and disadvantages for each adhesion method

Type of Adhesion	**Advantages**	**Disadvantages**
Biologically Inspired	-Can be used on various surfaces types -Power-fail safe	-Susceptible to peeling -Not suited for large moments -May peel surface exterior
Chemical	-Power-fail safe -Conforms to surface irregularities	–May leave residues -Attaches to exterior surface -Not suited for large moments -Slow activation/ deactivation times
Electrostatic	-Low power consumption -Fast attachment detachment times -High adhesion to weight ratio	-Attaches to exterior surface -Not suited for large moments
Grasping	-Provides high torque -Reliable -Power-fail safe -Stable	-No features to grasp -Heavy

Continued on next page

Table 2.2 – continued from previous page

Type of Adhesion	Advantages	Disadvantages
Pneumatic (Suction & Vacuum)	-Provides large moments -Can be used on various structural materials, i.e. concrete, steel, glass -To some extent, power-fail safe	-Can not guarantee power-fail safety -Not suited to rough surfaces, riveted surfaces, performing plane transitions -May peel surface exterior
Electro-Magnetic	-Adhesion to underlying structure rather than outer surface layers - Can provide strong holding force - May be turned on and off - something good	- Can only use on ferromagnetic structures -May collect ferromagnetic dust -Adhesion drops rapidly with air gaps
Permanent-Magnetic	-Adhesion to underlying structure rather than outer surface layers -Provides strong force -High adhesion to weight ratio -Power-fail safe	-Can only use on ferromagnetic structures -May collect ferromagnetic dust -Adhesion drops rapidly with air gaps

Whilst each of the methods provide a range of advantages and disadvantages to their respective environments, as noted earlier, it is typically the disadvantages that will determine the feasibility for a particular adhesion method. With consideration to the application scenario, environment, and operational tasks, Table 2.3 provides an overview of the feasibility for the adhesion methods discussed.

In evaluating the various adhesion methods, the following performance criteria are considered:

Inchworm Compatibility: whether or not the system can support a bipedal / inchworm type robot with high mobility.

Surface Material: The adhesion system must be capable of handling the painted steel surfaces within the archways of the Sydney Harbour Bridge. Within these sections there are very limited features.

Payload Capacity: The adhesion system must be capable of supporting the robot in all orientations with respect to gravity, with consideration to the worst case scenario for the robot.

Speed: The speed of activation and deactivation of the adhesion system should not severely limit the operation of the robot such that it is not practical for real world deployment.

Reliability: The reliability of the system depends on whether there is capability for feedback of the adhesion, and the ability to maintain reliable adhesion without destruction or peeling of the outermost surface layers on the structure.

Power-fail Safety: The adhesion system must not deactivate in the event of a momentarily or complete loss in the robots power supply. Passive adhesion principles are preferred.

Stability: The adhesion system must provide sufficient stability for the inchworm robot, in order to carry out tasks with sufficient accuracy which includes inspection and maintenance tasks.

Durability: The adhesion system must be durable, such that containments from the environment will not cause the adhesion to fail over time.

With respect to these performance criteria and the intended environment and operational tasks, permanent magnetic adhesion is considered the most feasible adhesion method.

TABLE 2.3: Specific performance ratings for each adhesion methods with consideration to application scenario, environment, and operational tasks of the climbing robot.

Adhesion	Performance Criteria: Inchworm Compatibility	Surface Type	Payload Capacity	Speed	Reliability	Power-fail Safety	Stability	Durability
Electrostatic	✘	✓	✘	✓	✘	✘	✘	✘
Van Der Waals	✘	✓	✘	✓	✘	✓	✘	✘
Pneumatic	✓	✓	✓	✓	✘	✘	✓	✓
Mechanical	✓	✘	✓	✓	✓	✓	✓	✓
Electromagnetic	✓	✓	✓	✓	✓	✘	✓	✓
Permanent Magnetic	✓	✓	✓	✓	✓	✓	✓	✓

Chapter 3

Design of a Biologically Inspired Inchworm Robot

This chapter presents the design of an inchworm inspired climbing robot in order to meet the mobility requirements of the intended application scenarios. The chapter first studies inchworm caterpillars for inspiration in view of their ability to perform complex manoeuvres and plane transitions.

3.1 Biological Inspiration

Analysing biological systems is key to understanding the principles in which these animals can navigate through complex environments. Chapter 2 has highlighted the capability of climbing robots inspired by animals such as snakes, geckos, ants, spiders, monkeys and caterpillars.

In performing plane transitions inchworm inspired robots have demonstrated more robust and reliable techniques in comparison with other legged robots. With many degrees of freedom in a serial chain, they are capable of a high degree of mobility. Despite their mobility, overall, they contain less DOF than other multi-legged robots. This reduces overall control complexity in overcoming complex obstacles. For these reasons inchworm inspired robots are often considered by researchers.

However, as discussed in the literature review, no solution has been identified which is suitable for the intended application scenarios. To understand why, this chapter looks for inspiration from the biological inchworm. Several traits have been identified. These are summarised as follows:

- **Body Structure:** The inchworm caterpillar is predominately associated with the Geometriade family of the insect order Lepidoptera. The Geometriade caterpillar differs from others in that it only has one set of the anterior prolegs in its abdominal section, as see in Fig 3.1. At the head of the caterpillar are its thoracic legs which transform into the adult legs during metamorphosis. The abdomen of the inchworm consists of 8 segments each having several degrees of freedom. There are approximately 70 muscles per body segment.

- **Primary Gait:** With only one set of anterior prolegs, and one pair of anal claspers, the primary looping gait of the caterpillar is of an Ω appearance, which is more pronounced in comparison to other caterpillar families. With the prolegs firmly gripped to the surface, the body extends forward as far as possible. The thoracic legs grip onto the surface, followed by the prolegs and anal claspers releasing. The body is brought forward to the front legs, and the prolegs grip once again. This process repeats, and produces a looping appearance.

- **Step size and speed:** The inchworm maximises it mobility through large steps. To maximise step size, the robot is able to fold its body flat and parallel to the surface. With a large step size the inchworm is able to step over obstacles and reach remote surfaces. Studies have also shown that there is negligible effect on mobility (step size and speed) of the inchworm in any direction with respect to gravity [97]

- **Overcoming Obstacles:** The hyper redundancy in the body provides inchworms with high manoeuvrability in order to explore their environment (Fig 3.2a), and the ability to perform the required 180° plane transition as seen in Fig 3.2a and 3.2b.

- **Sensory and Exploration:** The main form of sensory input for the inchworm is through highly sensitive directional hairs, in various lengths throughout their body. This provides the inchworms with a sense of touch to feel the environment

around them, and the ability to measure and distinguish vibrations from prey or predators [97]. Furthermore, the head of the inchworm contains 6 eyelets, referred to as Stemmata or Lateral Ocelli, on each side of their head. These are light-sensitive organs which are thought to enable the detection of outlines and track movements by constructing coarse light intensity mosaics [98]. It has also been speculated, that by panning their head from side to side, they are able to judge distance to objects through means such as optical flow [99].

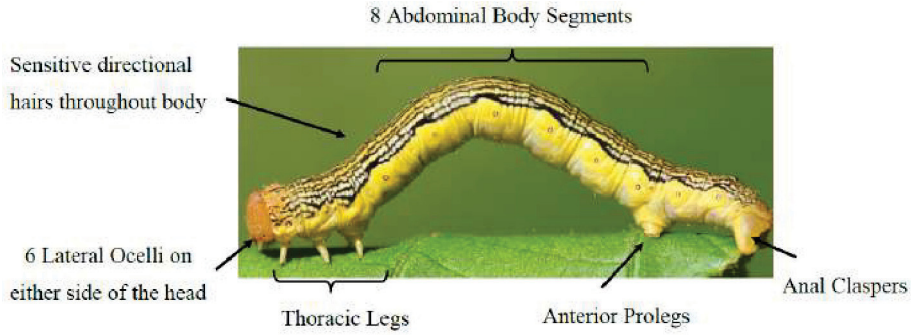

FIGURE 3.1: Commonly referred to as the inchworm or looper, the Geometriade family of Lepidoptera contain only one pair of anterior prolegs. The Geometriade, meaning 'measure the earth'walk in a looping fashion as if measuring the ground as it crawls. The head of the inchworm is on the thorax, with 3 pairs of thoracic legs. At the rear of the inchworm is a pair of prolegs and a pair of anal claspers. [100]

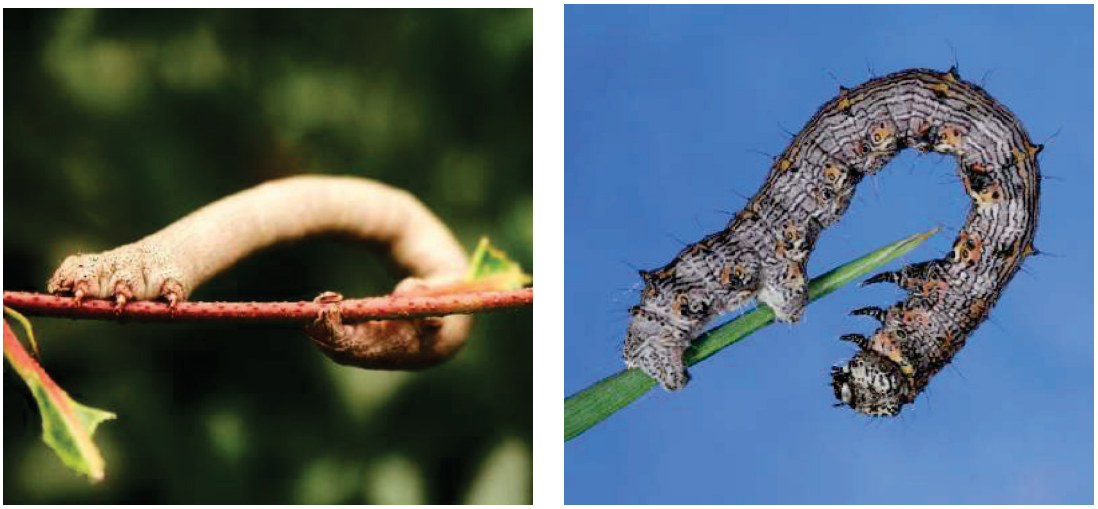

(a) (b)

FIGURE 3.2: Examples of Geomtriade caterpillars performing a 180° wrap. [100]

3.2 Design Considerations

To meet the mobility requirements in overcoming complex obstacles in the intended environment, this research learns from the current state of the art and draws inspiration from the traits of the inchworm caterpillar.

The primary consideration in designing the inchworm inspired climbing robot is identifying a suitable robot configuration and kinematic design which can perform complex plane transitions, including the 180° plane transition.

Symmetry in the robot configuration is considered important. Unlike the biological inchworm, a symmetrical climbing robot will enable movements in either direction, irrespective of whether the rear or the head is attached to the surface. This will also simplify control and path planning complexity as it does not need to consider the choice between placing the rear or the head in order to perform complex motions and plane transitions.

In defining the type of joints used in the robot configuration, Fig 3.3 shows the rotational R type, and the twisting T type. Each joint provides one degree of freedom. Other joint types such as prismatic and spherical have not considered in the design of the inchworm robot.

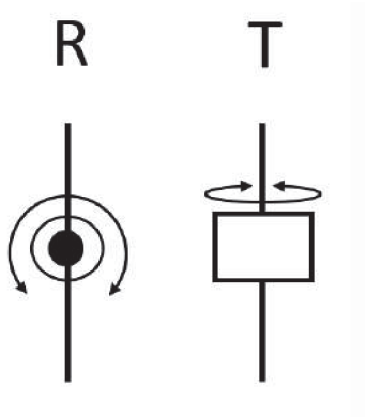

FIGURE 3.3: Joint conventions used for the inchworm robot configuration. Rotational joints represented by R, twisting joints represented by T. Each joint type is constrained to movements in 1DOF.

3.3 Robot Configuration, Kinematic Design and Evaluation

The design of the robot configuration is achieved primarily through an analytical approach, supported empirically. Through observation of the application scenario and required manoeuvrability the robot configuration has been determined and verified.

In order to maximise reach capability and step size, rotational joints are required at either end of the robot. In the simplest form this would be a 2DOF RR robot capable of a 'flip step'motion, seen in Fig 3.4a.

In order to achieve the required 180° plane transition, an extra R type joint is required as shown in Fig 3.4b. The 3DOF RRR configuration allows the end of the robot, referred to as the end effector, to be with 3DOF in space. This means the end effector has the ability to translate up/down, left/right, and change its orientation with respect to the base. With this capability, it is the minimum number of DOF required to perform the 180° plane transition.

However, the required joint angles necessary to perform the plane transition are not or practically achieved by typically actuators. This is largely due to the physical requirement that the sum of the joint angles must total 360°. In most robot designs, the R type joints are limited to ±90° from its zero position. Assuming this limitation, the robot would be capable of up to 270° rotation, permitting no more than a 90° convex plane transition. Assuming each of the R type joints were capable of up to ±120° to meet the requirement, this also assumes the plane has no thickness. As the plane thickness increases the joint limits for first and last joint must also increase, or alternatively the link lengths must increase.

It should be noted that nine of thirteen inchworm type robots identified in Table 2.1, use at least 3 R type joints, however not one can perform a 180° plane transition. Five of the nine climbing robots (Brincadeira, Tremo, RAMR1, W-Climbot and MATS) are able to perform 90° convex plane transitions. This can be attributed to the use of 3 R type joints, each limited to ±90°.

A well designed configuration with large joint limits and link lengths could be developed to achieve the required 180° transition; however for more versatile ability in performing the 180° transition, a fourth R joint can be added. Figure 3.4c highlights how the addition of the fourth R joint reduces the required joint limits to within typically actuated joint limits of ±90°.

Whilst the constraints in performing the plane transitions have been reduced, there are still limitations to the thickness of the plane. These are determined by the link lengths and the joint limits, as seen in Fig 3.4d.

The RRRR configuration could be considered the minimum required DOF in order to robustly perform the 180° transition. However with all joints limited to motion in the same axis of rotation, 3D mobility is not possible. Therefore additional DOFs are required to permit motion out of the plane.

It should also be noted that despite the addition of the fourth DOF in the robot configuration, the end effector has no additional total DOF in space. That is, there are no added translations or rotations possible as a result of adding the fourth DOF, in comparison to the 3DOF configuration. Therefore this joint can be considered redundant and simply increases the manipulability of the robot, particularly in performing the 180° transition.

For robust operation and ability to position the robot's end effector, the end effector requires a total of 6DOF of movement in space, thereby allowing translations and rotations in each of the x,y,z axes. If it is assumed one of the 4DOFs in the Fig 3.4c robot configuration is added simply to improve the manipulability of the robot in the 180° transition pose, then this would require an additional 3DOFs in order to acheive the require 6DOF of movement at the end effector. Figure 3.4e shows the proposed 7DOF robot configuration capable of 6DOF positioning of the end effector in space. The redundancy provides robustness in performing the 180° plane transition, meaning there may be multiple solutions in performing the plane transition. Furthermore, it is capable of positioning itself with offsets in translation and orientation, which may result from surface irregularities and obstacles.

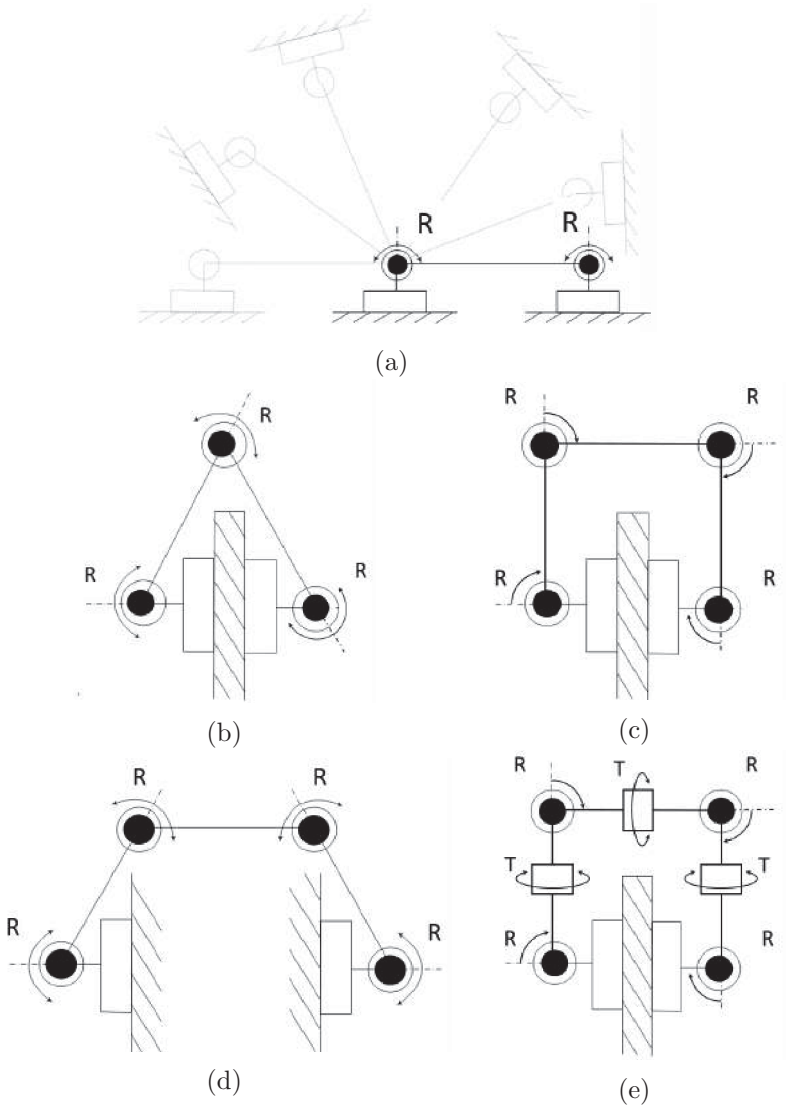

FIGURE 3.4: Evaluating different robot configurations in order to achieve high mobility and manoeuvrability. (a) Maximising step size with RR configuration. (b) RRR configuration has minimum number of DOF for 180° plane transition. (c) RRRR increases robustness in performing 180° plane transition with a redundant degree of freedom. (d) 4DOF configuration is more robust and capable of larger plane thickness, however constraints on joint limits and link lengths still exist. (e) Proposed redundant 7DOF robot configuration, RTRTRTR, provides high versatility in performing complex 3D plane transitions. This allows for positioning of the end effector in 6DOF in space to cater for surface irregularities.

3.4 System Scalability

Robots are complex systems with many subsystems such as actuators, structural brackets, adhesion modules, power supplies, computing hardware, wiring, and many other electronic

components. Therefore more often than not, they do not scale. This is often due to a conflict in the way the different subsystems scale. For example, the way in which the size and mass of an actuator scales, may be very different to the way in which performance characteristics such as torque and speed scale.

In determining a suitable actuator it is useful to consider the ways in which the many subsystems of the robot scale. If all subsystems of the robot are scalable, then it is feasible to build the robot in many different sizes relative to some dimension. If the robot is not scalable then there is only one size that is feasible for the given characteristic of that system.

By understanding the way in which the subsystems of the robot scale the understanding of the entire system greatly increases, and conclusions can be drawn on the effectiveness of design decisions, and their possible repercussions. This then allows the designer to compare the effectiveness of a particular subsystem, such as an actuator or adhesion system, and consider replacing with a system that may scale better.

> "Consider the relationship between scaling laws and detailed formal analysis. Neither is a substitute for the other; rather, they reinforce each other. The scaling law may sometimes tell you the answer you need, but even if it doesn't, it suggests how to do the analysis. The analysis, in turn, may reveal additional scaling laws."[101]

The study of scaling laws between the size of a body and its shape, is known as allometry, and is often used in the study of biological systems. For example, one may expect that as an animal grows, its body will grow in proportion to its size. When a directly proportional relationship is preserved with increases in size, this is referred to as isometric scaling. In this instance the two bodies will be of the same shape, and they are said to be geometrically similar. It should also be noted that isometric scaling is governed by the square-cube law [102].

Given l_1 the original length, and l_2 the new length, the isometric scaling, or square-cube law is

$$A_2 = A_1 \times \left(\frac{l_2}{l_1}\right)^2 \tag{3.1}$$

where A_1 is the original surface area and A_2 is the new surface area, and

$$V_2 = V_1 \times \left(\frac{A_2}{A_1}\right)^3 \tag{3.2}$$

where V_1 is the original volume and V_2 is the new volume. This thereby demonstrates that as the object increases in length, the area increases by the square power of the length, and the volume increases by the cube power the length. It should also be noted that the mass of the system is directly proportional to the volume of the system and the cube power of the length.

If an object scaled by its length is not geometrically similar to its original shape, then it does not scale isometrically, and it is referred to as differential allometric scaling. Whether a system scales isometrically, with positive allometry, or with negative allometry can be determined by collecting data for the system characteristics whilst scaling one characteristic such as length. Then by comparing other system characteristics to the length, scaling laws may be observed.

It is also important to hypothesis the scaling law to understand whether the system scales isometrically or not. For example, it can be hypothesised that the diameter of the inchworm scales proportionally to the length of the inchworm. By collecting data for the diameter and lengths of inchworms, a scaling law may be established, and the system may be better understand. Figure 3.5 shows the directly proportional relationship between the diameter of the inchworm and its length for numerous inchworms.

Measurements have been taken from photographs of inchworm caterpillars. The collection of measurements assume aspect ratios for the images are correct, sufficient range of inchworm sizes were measured throughout the growth of an inchworm, and the photographs

used show the robot directly side on in an outstretched position. It can therefore be asserted that inchworms scale isometrically, and those that were measured have geometric similarity. This also implies that their mass is proportional to the cube of their length.

It should be noted that number of samples in the analysis should be statistically significant; however with 17 data sets the diameter is approximately proportional to the length. To ascertain this relationship one would perform measurements on real inchworm caterpillars.

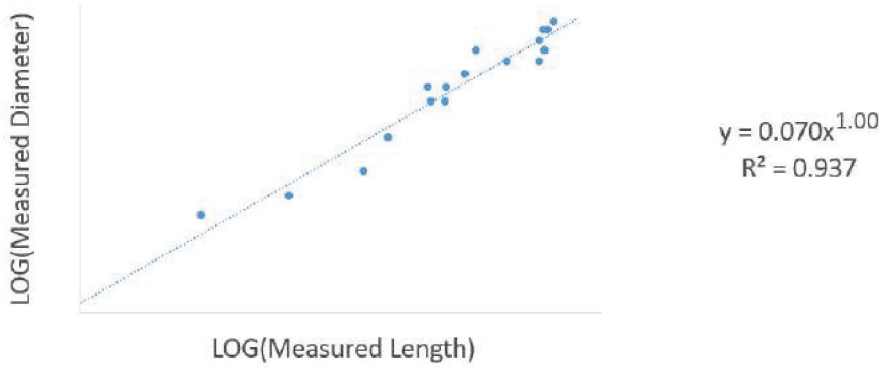

FIGURE 3.5: A directly proportional relationship can be observed between the diameter of the inchworm and its length, therefore it can be said that inchworms scale isometrically and have geometric similarity.

In scaling an inchworm-inspired robot, the following characteristics are considered important.

- R_r – Radius or transverse length of robot
- L_r – Length of robot
- M_r – Mass of robot
- T_L – Total load due to external forces and the robot weight in a cantilevered pose

If it is assumed that an inchworm-inspired robot also follows geometric similarity, as observed with the biological inchworm, the following can be deduced, noting that the robot is assumed to be a rigid beam like structure in cantilever.

$$R_r \propto L_r \tag{3.3}$$

$$M_r \propto L_r \times R_r^2 \tag{3.4}$$

$$M_r \propto L_r^3 \tag{3.5}$$

and the load of the system by isometric scaling is

$$T_L \propto M_r \times L_r \tag{3.6}$$

$$T_L \propto L_r^3 \times L_r \tag{3.7}$$

$$T_L \propto L_r^4 \, . \tag{3.8}$$

Table 3.1 shows the effect of increases in DOF to increases in length of the robot, radius of the robot, length of the actuator and radius of the actuator. Two assumptions have been made.

The first is that the length of the robot L_r is directly proportional to the number of DOF times the length of an actuator, that is, $L_r \propto DOF \times l_a$. That is to say that for every additional degree of freedom, there is an additional actuator (or joint) added to the end of the kinematic chain, with each additional actuator having the same associated length as the rest of actuators. Although there would be additional link lengths or brackets to support the actuators, these would add a constant offset, thereby not effecting the proportionality law assumed.

It is not logical to assume that the length of the actuators is fixed for all increases of the robots length and weight. Therefore another assumption is made, such that, for any increase in the length of the robot, there is a directly proportional relationship to the length of the actuators, i.e. $l_a \propto DOF$.

TABLE 3.1: Characteristics for an inchworm-inspired robot with isometric scaling. It is evident that $DOF^2 \propto L_r \propto R_r \propto l_a^2 \propto r_a$.

DOF	L_r	R_r	l_a	r_a
1	1	1	1	1
2	4	4	2	4
3	9	9	3	9
4	16	16	4	16
5	25	25	5	25

The scaling relationships with increases in DOF, as observed in Tab. 3.1 are $DOF^2 \propto L_r \propto R_r \propto l_a^2 \propto r_a$. It should be noted that the actuators do not observe isometric scaling.

To represent this visually, the changes in the inchworm shape and dimensions can be observed in Fig 3.6a. Each new colour represents a new inchworm type robot with an additional degree of freedom, or actuator. Geometric similarity can be observed for each new inchworm robot.

In order to visually illustrate the geometric similarity of the inchworm robot with the biological inchworm, a proportionality constant k can be applied, where $k = \frac{R_r}{L_r^2}$. Figure 3.6b uses $k = 0.2$ to demonstrate how a proportionality constant can be applied, whilst maintaining a scaling law. In the case of the biological inchworm $k \approx 0.07$, as determined by the data set Fig 3.5. The proportionality constant does not affect geometric similarity, as highlighted by the linear line passing through each geometrically similar body.

The scaling of robotic mechanisms is often overlooked in the initial design of climbing robots; however it has been discussed in detail by [103] as an important step for initial configuration of new designs. The article investigates the mechanics behind the scaling for several robotic mechanisms, such as strength, deflections, kinematics and actuator performance. In particular the article presents a principle in which structural strength can be maintained and deflections can be avoided through scaling, if the cross section of a rigid system scales to the square power of the length, i.e. $r \propto l^2$.

Considering the biological inchworm body as a rigid beam, with a scaling law of $r \propto l$, suggests that the body will be subject to deflection through increases in l. The biological inchworm has built-in robustness and a compliant body structure which can handle this.

For the inchworm robot on the other hand, whilst it may be possible to design a body structure and actuators with such compliance, there would be increased control complexity if precise movements were required. For an ideal manipulator or inchworm type robot, designers seek high structural rigidity to prevent deflections in the robot kinematic chain, to enable precise movements.

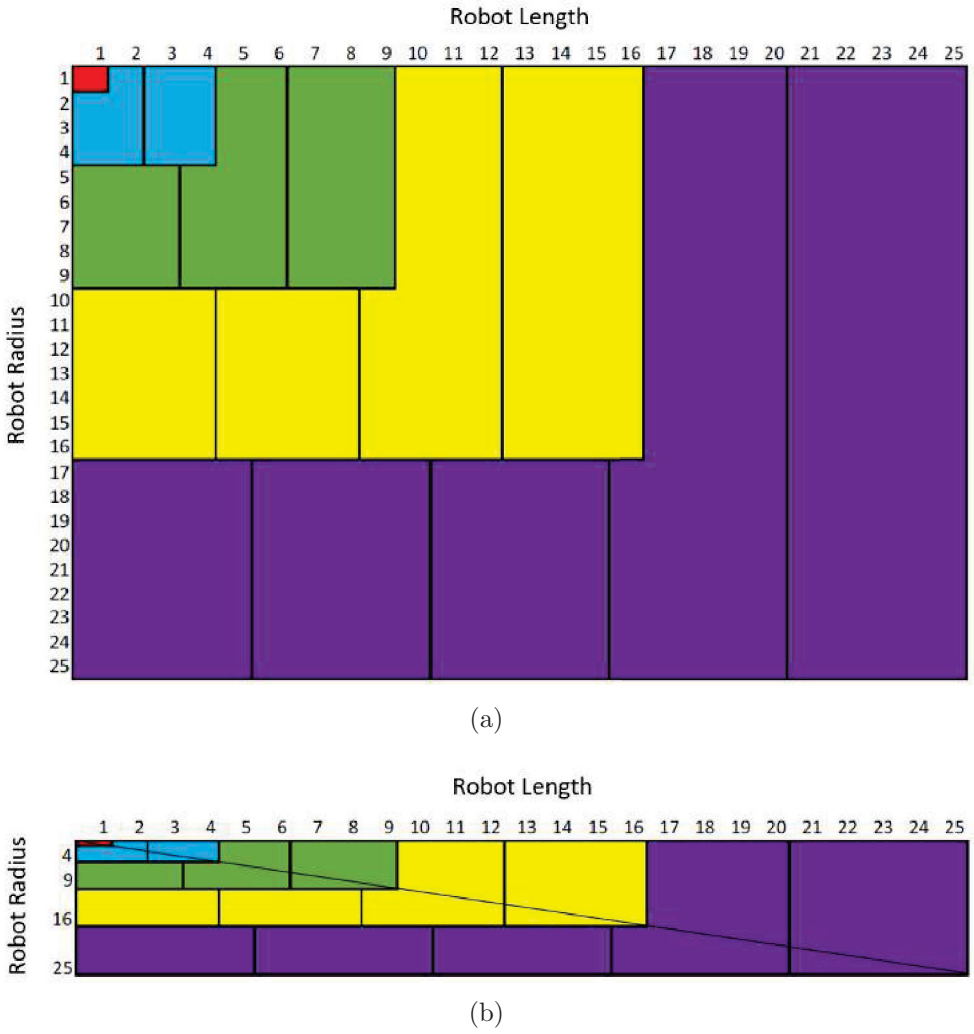

FIGURE 3.6: Isometric scaling of an inchworm-inspired robot. (a) The radius of the inchworm body is proportional to the length of the inchworm. (b) A constant scaling factor has been used to approximate shape of inchworm body; isometric proportionality remains.

Re-evaluating the design of the inchworm robot to scale by differential similarity, such that the structural strength is preserved, $R_r \propto L_r^2$ must be used as noted by [103]. The expected mass of the system then scales as

$$M_r \propto L_r \times R_r^2 \tag{3.9}$$

$$M_r \propto L_r \times \left(L_r^2\right)^2 \tag{3.10}$$

$$M_r \propto L_r \times L_r^4 \tag{3.11}$$

$$M_r \propto L_r^5 \tag{3.12}$$

and the load of the system scales as

$$T_L \propto M_r \times L_r \tag{3.13}$$

$$T_L \propto L_r^5 \times L_r \tag{3.14}$$

$$T_L \propto L_r^6 \, . \tag{3.15}$$

It is clear that the mass of the inchworm-inspired robot and the load torque increases much faster than the robot's length in comparison to isometric scaling. The relationships for increases in DOF can be observed in Table 3.2. It can now be seen that the scaling rate between the actuator radius and the actuator length, in order to maintain structural integrity for the robot body, is $r_a \propto l_a^4$. The radius for the actuator clearly must increase much faster than the length of the actuator to maintain structural integrity for the robot.

TABLE 3.2: Table of scaling characteristics extracted from visual representation of the inchworm-inspired robot with differential scaling to maintain strength.

DOF	L_r	R_r	l_a	r_a
1	1	1	1	1
2	4	16	2	16
3	9	81	3	81
4	16	256	4	256
5	25	625	5	625

This can be visually observed in Fig 3.7. A constant scaling factor has been applied to the radius of the inchworm, where $k = \dfrac{R_r}{L_r^4}$ and $0 < k \ll 0$. It is clear that the shape of the robot is not maintained with scaling.

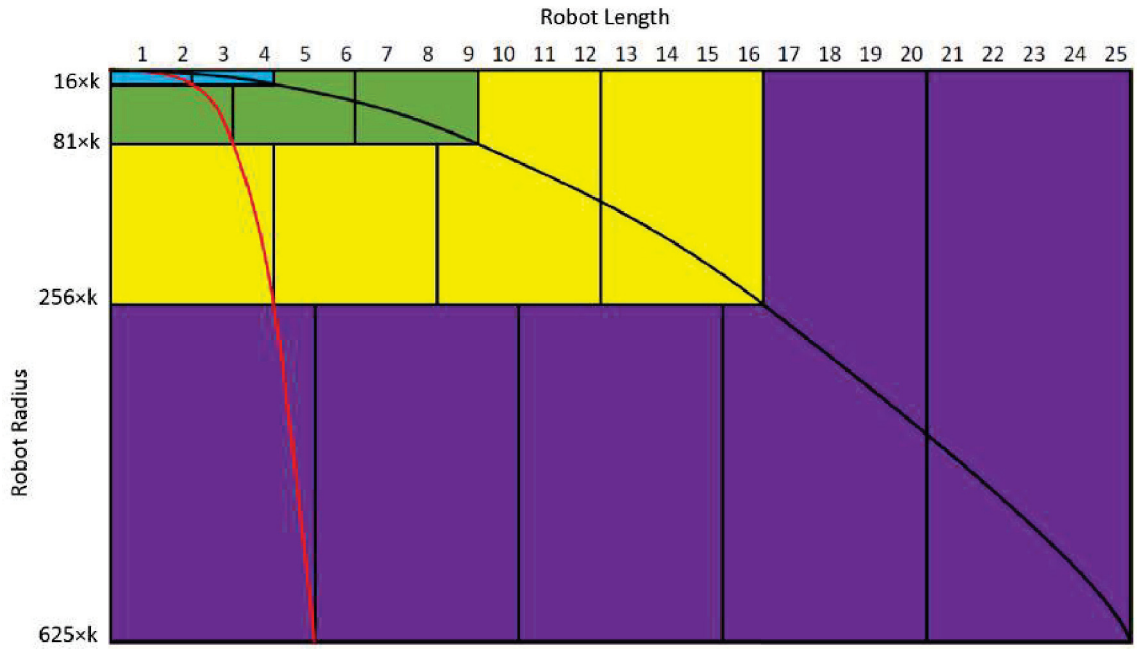

FIGURE 3.7: Differential scaling used in the body of an inchworm-inspired robot to maintain structural strength and avoid deflections. Visual representation in scaling the inchworm-inspired robot. The black line between corners of each coloured inchworm body highlight how the robot radius is now proportional the square of its length, $R_r \propto L_r^2$. Whilst the red line between the corners of the actuators illustrate that the radius of the actuators now scale to the 4 power of the length, $r_a \propto l_a^4$.

To evaluate the effect on the actuator characteristics for $r_a \propto l_a^4$, the scaling of the actuator mass scales becomes

$$m_a \propto l_a \times r_a^2 \tag{3.16}$$

$$m_a \propto l_a \times \left(l_a^4\right)^2 \tag{3.17}$$

$$m_a \propto l_a \times l_a^8 \tag{3.18}$$

$$m_a \propto l_a^9 \tag{3.19}$$

and as the required motor torque is proportional to the robot's load torque, from Eqn 3.15 , the relationship between the required actuator torque to actuator length becomes

$$T_a \propto T_L \propto L_r^6 \qquad where, \quad L_r \propto l_a^2 \tag{3.20}$$

$$T_a \propto (l_a^6)^2 \tag{3.21}$$

$$T_a \propto l_a^{12} \ . \tag{3.22}$$

Given 3.19 and 3.22, the actuator torque scales to its mass as

$$T_a \propto (\sqrt[9]{m_a})^{12} \tag{3.23}$$

$$T_a \propto m_a^{\frac{4}{3}} \ . \tag{3.24}$$

This section has looked at the effect of scaling various subsystems of an inchworm type robot. It has illustrated that the inchworm robot does not scale isometrically with increases in number of DOF. The understanding gained in the scalability for the various subsystems of an inchworm type robot is valuable in the design and component selection of the robot. The required scaling laws for the robot dimensions have been determined such that structural integrity can be preserved. Furthermore, the expected relationships and required scaling laws for the actuators have been determined. In selecting a suitable actuator, it is now known that the power to weight ratio is not the only important characteristic, other characteristics such as the radius and length also play a role in the robots feasibility.

3.5 Actuator Selection

There are many types of actuators which have been employed in inchworm-inspired climbing robots. Some of these include electromechanical servo motors, pneumatic cylinders, soft pneumatics, and Shape Memory Alloys. This research has only considered an inchworm-inspired robot consisting of DC servo motors in a serial kinematic chain. These electromechanical actuators consist of an electric motor, gear stages, and typically include on-board controllers for position, speed and torque control. They are widely used in industry and

robotics, providing a wide range of configurable performance specifications such as speed and torque, and for their ability to achieve high positional accuracy, ease of control complexity, and structural rigidity.

Electromechanical actuators have many specifications to consider including torque, weight, speed, dimensions, power usage, braking ability, control and communication methods, reliability, serviceability, and modularity to name a few. Whilst all of these factors are important, the most critical specifications in the design of inchworm-inspired robots come down to the size, weight, torque and speed. In selecting an actuator, an investigation into different electromechanical actuator designs was considered. Most manufacturers differ in their design and hence the scalability of the motors may differ between brands and even models. The scalability of these actuators comes down to many parameters such as its gearbox type and material, housing construction material, motor type, motor orientation, motor power, winding configurations, extra features. Therefore generalisations may be misleading; however it has been proposed that the there is considerable similarity in scaling behaviour [103].

Several actuators were studied to determine their feasibility in scaling within the inchworm-inspired robot. The specifications of the actuators, including torque, speed, mass and dimensions are recorded in Table 3.3. The relationship between continuous torque to actuator length, mass to actuator length, and radius to actuator length are plotted on log-log graphs. The log-log graph is used so that any relationship in the form of $y = k\,x^a$ appear as a straight line. This is an easy way of visually comparing the relationship between the system characteristics. The gradient of this line is the exponent a, and k is the intercept of $x = 1$

Obtaining the exponents for each scaling law, Table 3.4 compares them to the expected exponents, as calculated in Eqn 3.19 , 3.22 and 3.24. It is clear that the actuators do not scale with the required exponents to maintain structural strength, and hence deflections are to be expected for any inchworm-inspired robot which uses these actuators. The

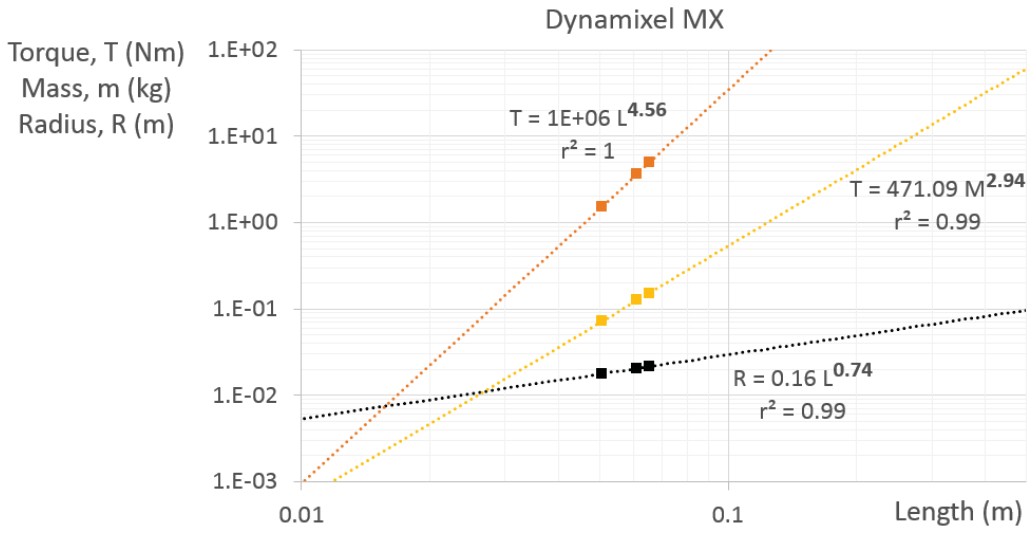

(a)

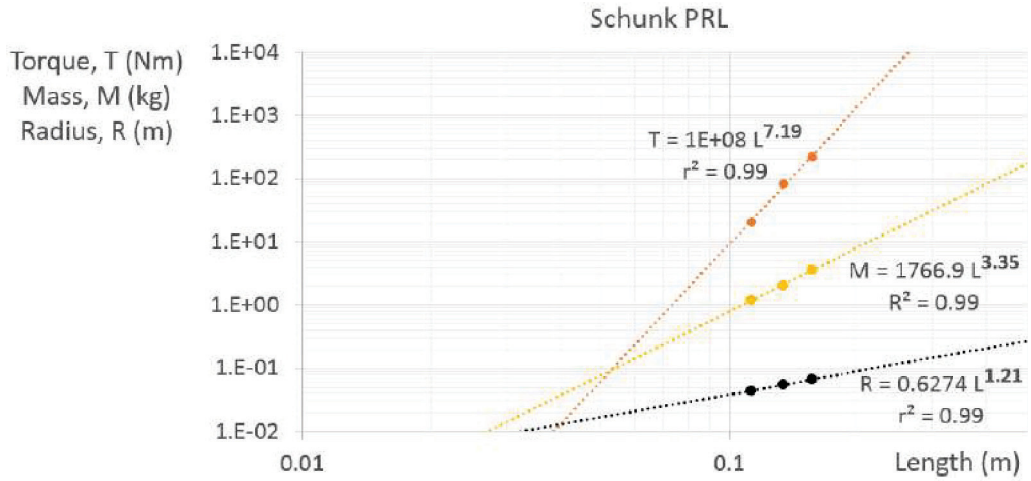

(b)

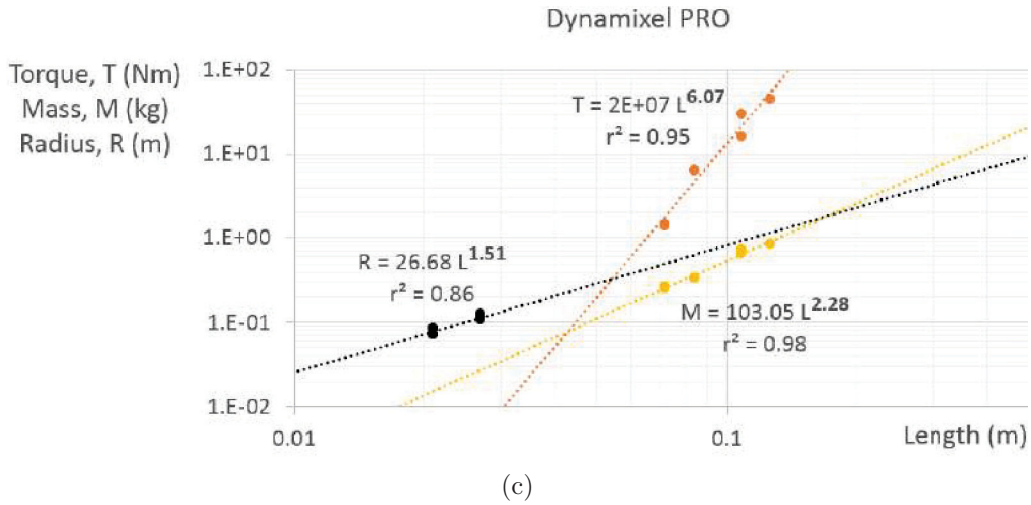

(c)

FIGURE 3.8: Log-log plots for scaling relationship to increases in length for several actuator characteristics including torque, mass, and radius. (a) Dynamixel MX. (b) Schunk PRL (c) Dynamixel PRO.

Table 3.3: Comparison of actuator specifications.

Motors	Performance Criteria						
	Continuous Torque (Nm)	Peak Torque (Nm)	Mass (kg)	Speed (rpm)	Torque to Weight Ratio	Length (mm)	Width/Diameter (mm)
Dynamixel MX28	˜1.2	3.1	0.045	67	26.7	50.6	35.6
Dynamixel MX64	˜3.5	7.3	0.126	78	27.7	61.1	41
Dynamixel MX106	˜4.7	10.0	0.153	55	30.7	65.1	46
Schunk PRL60	4.5	9.6	1.0	8.3	4.5	102	75
Schunk PRL80	20.7	41.4	1.2	4.2	17.25	112.5	89
Schunk PRL100	81.5	176	2.0	4.0	40.75	134	112
Schunk PRL120	216	372	3.6	4.2	60	156	132
Dynamixel PRO H42-20	6.3	-	0.34	29.8	18.5	84	42
Dynamixel PRO H42-100	30.1	-	0.732	24.8	41.2	108	54
Dynamixel PRO H42-200	44.2	-	0.855	27.9	51.7	126	54

primary reason for the deflections can be related to the scaling law between the actuator radius and length.

The difference in scaling rates can be interpreted more easily after normalising the exponents by the required exponent, as seen in Table 3.5. A normalised exponent greater than one indicates positive allometry (increasing faster than expected), and an exponent less than one indicates negative allometry (increasing slower than expected), and an exponent of 1 is scaling as expected.

As mentioned, the most significant difference in scaling relationships can be observed between the actuator radius to its length for the Dynamixel MX and Schunk PRL actuators. For the Dynamxiel Pro this is seen in the scaling law between the mass and the

TABLE 3.4: Comparison in scaling factors for three different motor designs against expected scaling exponents for actuators of an inchworm-inspired robot. Required scaling rates are for an inchworm type robot which maintains structural integrity, as determined by Eqn 3.19 , 3.22 and 3.24 . Scaling looks at torque to weight, torque to mass, and mass to length.

	Exponent x			
	Required	Dynamixel MX	Schunk PRL	Dynamixel Pro
$Torque \propto Length^x$	12	4.56	7.19	6.07
$Mass \propto Length^x$	9	2.94	3.35	2.28
$Radius \propto Length^x$	4	0.74	1.21	1.51
$Torque \propto Mass^x$	$4/3 = 1.33$	1.55	2.12	2.60

TABLE 3.5: Comparison of normalised scaling factors for three different motor designs.

	Normalised Exponent, Norm(x)			
	Required	Dynamixel MX	Schunk PRL	Dynamixel Pro
$Torque \propto Length^x$	1	0.38	0.60	0.50
$Mass \propto Length^x$	1	0.33	0.37	0.25
$Radius \propto Length^x$	1	0.18	0.30	0.38
$Torque \propto Mass^x$	1	1.16	1.59	1.96

length. There are several ways in which these scaling laws can be improved. Firstly, it should be noted that the orientation of the actuators are assumed to be in a fixed direction relative to the length, however in practice the orientation may change as noted in the robot configuration proposed in Section 3.3. Changing the orientation such that the length becomes the radius, shows some improvement for the scaling of the Dynamixel MX actuators.

The radius of the actuators may also be increased using a structural housing around the motor; this would possibly increase the mass of the system beyond what can be afforded in terms of scaling the torque to the weight.

Ideally, two designs of actuators should be used, one design for R type joints, and another for T type joints. Each configuration should have the same scaling laws, in particular ensuring that the actuator radius is proportional to the 4 power of the actuator length. However, this is not so simple if one were to consider the practical design of an actuator. Figure 3.5 depicts the two configurations. It is clear the T type actuator can satisfy $r \propto l^4$. However, it can also be observed that the R type joint can only scale as $r \propto l$.

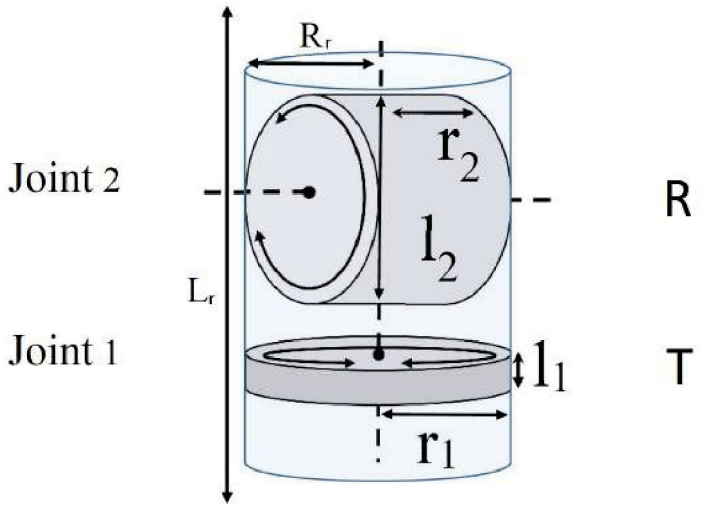

FIGURE 3.9: Figure depicts two joint configurations and observes limitations in scalability. Joint 1, a T type actuator is able to scale with $r_1 \propto l_1^4$ in order to maintain structural integrity. Joint 2, a R type actuator is characterised by $r_2 \propto l_2$ to maintain symmetry in shape.

It can be concluded that the design of a rigid inchworm type robot is not easily scalable. This means that each inchworm design will be its own unique solution, carefully constructed with detailed analysis. The design of inchworm type robots should focus on maximising characteristics such as torque to weight of the actuators and strength to density of the body structure.

In concluding this discussion on scalability, it should also be noted that other subsystems were not considered, most importantly the adhesion system and the required inspection equipment. The adhesion system and inspection equipment again face additional and varying scaling laws. The adhesion itself consists of its own subsystems and characteristics such as radius, length, weight, magnet size, and magnetic adhesion strength. Inspection equipment is expected to be invariant of system, which is advantageous in scaling up, and disadvantageous in scaling down.

Finally the design, scalability and feasibility of the robot must take into account other variables such as technological limits, cost, and lead time. One must consider whether these parameters also scale and what how they may limit the design.

3.6 Static Model and Analysis for Robot

In considering a suitable actuator for the intended application scenario, the Dynamixel MX motors were decided on to be used in proof of concept prototype.

Although not the most suitable option, the Dynamixel MX actuators were cost effective and readily available solution for the prototype inchworm robot. With reduced length and weight the ability to pass through the confined spaces and manholes were predicted to be easier; on the other hand it was noted that the robot may pose challenges in carrying the required inspection equipment.

The robot configuration with the selected actuators were modelled in 3D to determine the necessary link lengths to perform the 180° plane transition and such that the load torque on the motors and links is reduced. The 3D kinematic chain of the 7DOF inchworm robot can be in Fig 3.10 . The ability to perform the 180° plane transition is verified in Fig 3.10a, with the plane thickness varying from 0mm up to 65mm. The maximum plane thickness is limited by the joint angles, radius of the adhesion system, and the link lengths.

The 7DOF configuration demonstrates adequate manoeuvrability, permitting numerous poses and foot placements whilst performing the 180° plane transition, as seen in Fig 3.10b. A radius of 150mm and a height of 40mm has been assumed for the adhesion system, being the maximum foot pad radius that can pass through the intended manholes. With this constraint, joints 1 and 7 are limited to 133° from their zero position, whilst joints 3 and 5 reach 47° each. These constraints still permit high dexterity for the robot.

Having confirmed the robot configuration, actuators and link lengths, a static load analysis for the entire system was conducted to validate the feasibility of the actuators. A worst-case scenario approach has been conducted for the robot, being the fully cantilevered pose whilst attached to a vertical plane. This assumes the operation of the robot will be sufficiently slow.

The static loads are first calculated without an assigned footpad weight, by summing of the moments for each component of the robot and comparing the total moment to the available motor torque. To prevent the first motor exceeding the rated stall torque, the foot pad

weight must not exceed $1.2kg$ assuming a 40mm height; see Appendix A for spreadsheet of static analysis. Reaching stall torque is not desirable, particularly as dynamic loads are not included. Therefore, the maximum foot pad weight has been limited to $0.6kg$ so that the first actuator would be loaded to $6.8Nm$ in a worst-case scenario. With the assumptions made, the actuators are feasible from a torque rating point of view. The resulting constraints for the adhesion system, include a 0.6kg weight limit, and a $40mm$ footpad height.

In the intended deign scenarios, plane transitions are not expected to be greater than 20mm in thickness. Therefore this robot configuration has been designed for the given actuators with minimal weight, actuator length and overall robot length, whilst providing a high level of robustness in performing the 180° transition.

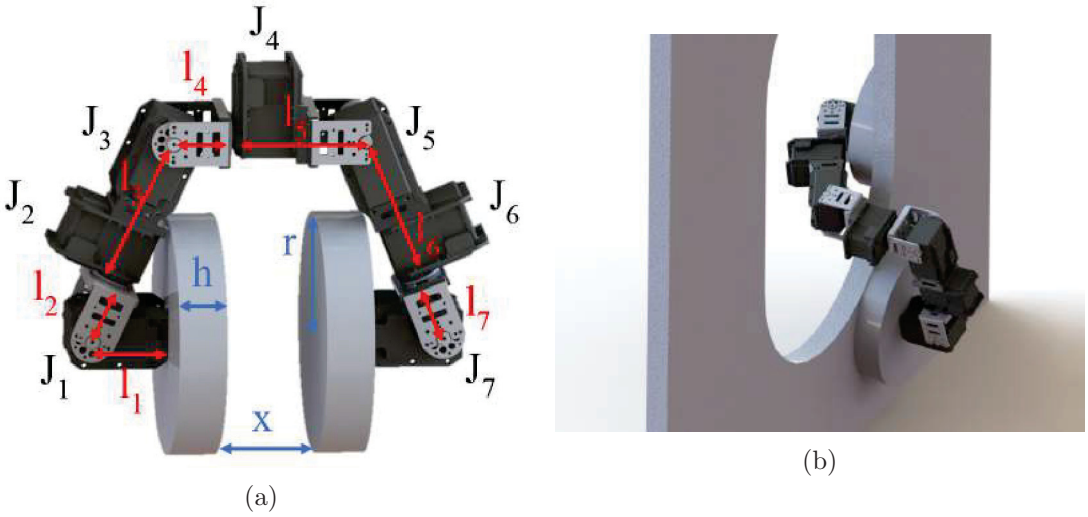

(a) (b)

FIGURE 3.10: Proposed 7DOF inchworm robot configuration. (a) Maximum separation of feet x, in performing 180° transition, being limited by link lengths l_3 and l_5, footpad radius r, and footpad height h. (b) Example of complex plane transition through a manhole.

3.7 Construction and Validation

The 7DOF inchworm inspired robot is assembled using the selected actuators and minimum link lengths. The robot can be seen in Fig 3.11. The robot has validated the physical capability for various step sizes between 0 to 65mm, including the expected on site plate size seen in Fig 3.11a.

The robot has also verified its capability to support itself in cantilever (Fig 3.11b) verifying the static model and torque capabilities of the actuators. The robot is also able to move through this pose irrespective of gravity.

The mobility of the robot is verified in Chapter 5.

3.8 Discussion and Conclusions

This chapter has analysed the inchworm caterpillar to gain insight into its ability to perform complex plane transitions. A study on the scalability of inchworm caterpillars and inchworm robots has been presented to demonstrate the challenges presented in the design of inchworm type robots.

A robot configuration with high robustness in performing the 180° plane transition is presented. A discussion of actuator selection presents the limitations in current technological advancements. A prototype inchworm robot is constructed and tested in a replica structure of the Sydney Harbour Bridge, validating it's ability to inspect the required application scenarios.

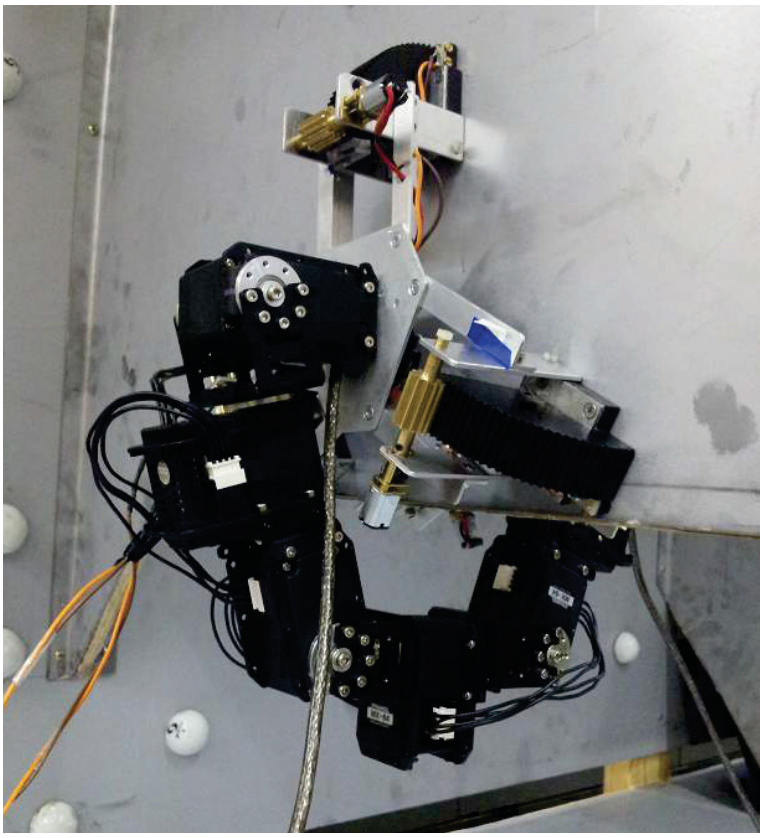

(a)

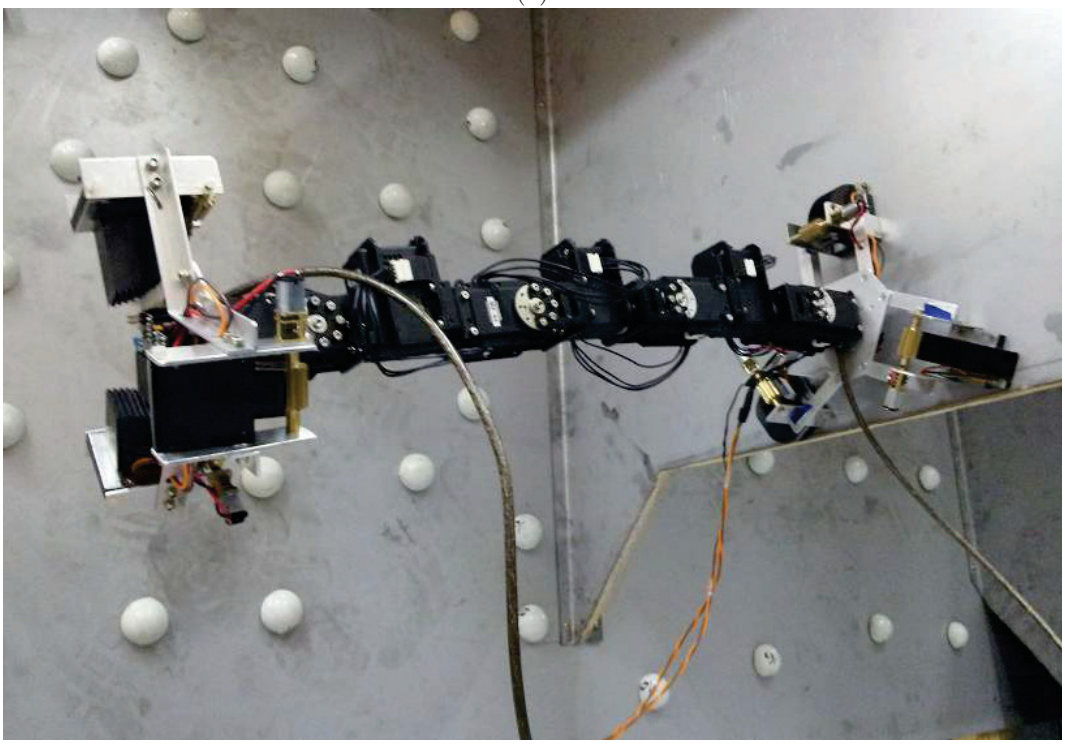

(b)

FIGURE 3.11: (a) Verification of geometric constraints in 180° plate transition. (b) Complete inchworm climbing robot in cantilever.

Chapter 4

Design of a Magnetic Adhesion System

The previous chapter presented the challenges in identifying a suitable robot configuration, the challenges faced when subsystems scale differently and the difficulty in identifying existing hardware limited by technological advancements which meet the desired requirements for the climbing robot. The adhesion system faces the same issues, in addition to being constrained by the robot configuration, and more so by the environment and operating constraints.

Whilst weight is a concern for all climbing robots, in an inchworm type robot, this is true even more so. The adhesion mechanisms are located at the extremities, on either end of the robot. In one instance this means one of the adhesion systems must support the maximum load of the robot. In another instance the same footpad will be at the other end of the body, thereby potentially producing the largest moment of any component on the body. In the first instance the adhesion system must support the greatest torque load in the system, and in the other instance the adhesion system should be the lightest element of the system.

Furthermore, there are operational goals which must be satisfied. In order to achieve the power-fail safety requirement, a permanent magnetic adhesion solution is the only feasible option, as discussed in Chapter 2.2.7.

The design process is broken into several steps, in order to achieve these requirements:

- A study on the inchworm
- Analysis of the modes of failure for the adhesion system
- Determination of the most suitable magnetic configuration
- Design of an attachment and detachment mechanism
- Design model for the adhesion system
- Testing and evaluation

4.1 Biological Inspiration

In order to minimise the weight and maximise the adhesion capacity, there are several biological traits that can be used for inspiration in the design process.

Through evolution, the inchworm caterpillar has been optimised to support the bending moment required whilst crawling forwards. In Fig 4.1a and 4.1b it can be observed that the anal claspers are significantly larger than the other pair of prolegs. This provides greater contact surface area for the adhesion and better stability whilst exploring in a forward fashion. As the inchworm does not need to explore behind itself or take large steps backwards, the inchworm has optimised its adhesion in this manner such that can provide large reach capability whilst minimising the required weight. The anal claspers contain crotches, which are hook-like structures arranged in rows or circles, and provide strong grip strength [104]. In order to support their body in cantilevered poses, the anal claspers are positioned as far back as possible from the proceeding prolegs. The prolegs are a pivotal point in which the moments M_a and M_b must be balanced, as shown in Fig 4.1c. Furthermore the crotchets are also located at the extremities of the anal claspers to increase the circumference of the foot.

When attaching to rough surfaces with possible loose debris, the inchworm tests its grip by pulling at the surface. An array of sensors in the feet and hairs surrounding the proleg

(a)

(b)

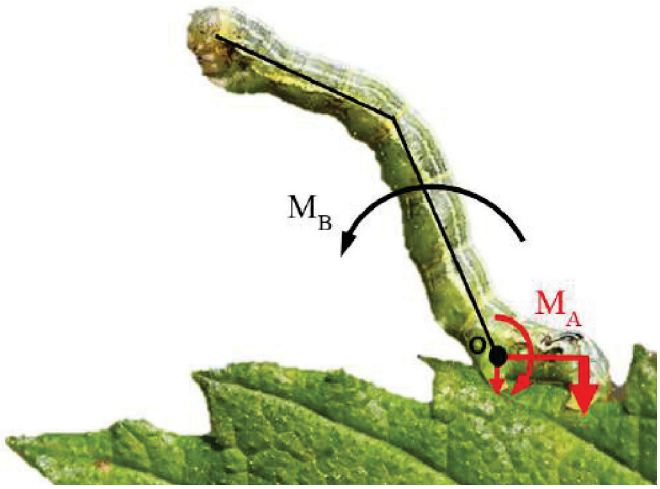

(c)

FIGURE 4.1: Biological inspiration from the inchworm caterpillar. (a) Anal claspers are notably larger than proceeding prolegs. Anal claspers have the compliance to wrap around branch. [105] (b) Rear claspers are significantly larger than proceeding prolegs. Anal claspers have compliance to flat surface with irregularities. Anal claspers are fanned out slightly to improve stability whilst exploring environment by panning left and right. (c) Anal claspers provide strong grip to a branch, preventing tipping around the pivot point noted by 'O'. Adhesive moment from the anal clasper is sufficient to overcome the moments due to body in a cantilevered position. [100]

determine whether the grip is secure. Whilst there are other methods of adhesion testing, this trait inspires a method for providing feedback on the adhesive strength.

Inspired from the inchworm, the adhesion system of the robot was assumed to consist of multiple adhesion modules at the extremities of the foot, akin to the anal claspers of an inchworm caterpillar seen in Fig 4.1. This provides the greatest adhesive moment with the least weight. Several assumptions were made for the adhesion system, which differs from that of the biological inchworm. The front and back feet of the robot should be the same so that the robot can perform any transitions with either foot. This also allows the

robot to precisely retrace its steps, which is not possible for the inchworm caterpillar. The adhesion system should be symmetrical where possible so that the orientation of the foot is arbitrary for any transition performed. Furthermore, all adhesion modules should be located at the same radius from the footpad centre and should be equally spaced around the circumference of the footpad.

4.2 Modes of Failure

The performance of a footpad design can be determined by the five modes of failure as identified in Fig 4.2. The modes include failure through excessive pull force F_p, slip force F_s, bending moments M_x and M_y, and torsion M_z due to the load imposed by the robot and payload.

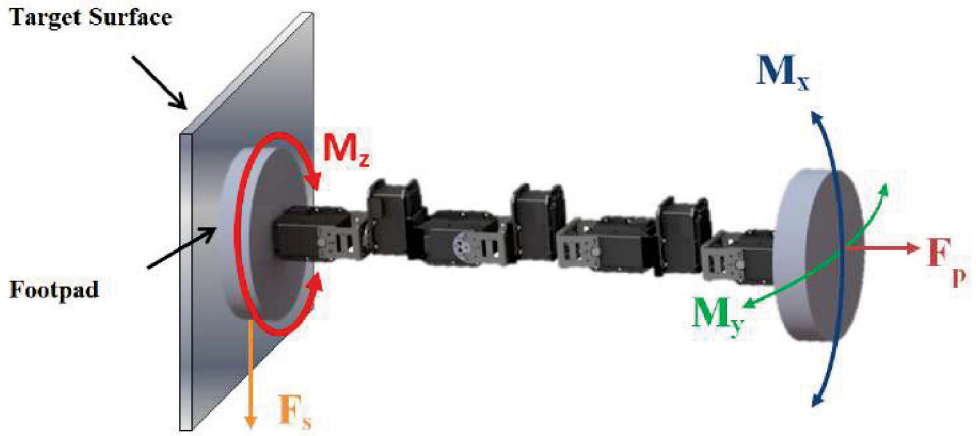

FIGURE 4.2: Loads imposed by climbing robot on footpad in worst case scenario. *Mx* - Bending moment in x direction; *My* - Bending moment in y direction; *Mz* - Torsion in z direction; *Fp* - Pull force, being the weight of the robot; *Fs* - Slip force between adhesion system and surface.

4.3 Optimal Design Model for Adhesion System

This research presents an optimal design model for an adhesion system such that the design variables for a footpad can be optimised in order to maximise performance criteria.

The performance criteria of the adhesion system that should be maximised in order to prevent failure in adhesion are then defined as follows:

$F_p =$ The maximum pull force of the adhesion system normal to the surface

$F_s =$ The maximum slip force that can be sustained by the adhesion system on a vertical wall

$M_x =$ The maximum bending moment that the adhesion system can sustain about its the x axis

$M_y =$ The maximum bending moment that the adhesion system can sustain about its y axis

$M_z =$ The maximum torsion that the adhesion system can sustain about the z axis

Although the performance criteria should be maximised, a design problem exists where there must be a trade off between the performance and weight of the adhesion system. Therefore minimising the weight of the adhesion W_{pad}, is another criterion which is incorporated in the objective function.

Before formulating the objective function, each of the criteria are normalised. The performance criteria are normalised by the required performance of the system in a worst case scenario.

For example, the measured pull force of the adhesion system is divided by the force required to support the robot in a worst case scenario; this is inverted whilst support the entire weight of the robot.

$$N_{F_p} = \frac{F_p}{F_{p\ required}} \tag{4.1}$$

Where $F_{p\ required}$, can typically be considered to be the weight of the robot due to gravity. In other circumstances $F_{p\ required}$ may also include external forces and/or a factor of safety.

The advantage of normalising the performance criteria in this manner, is that the resulting normalised performance criteria also represent the FOS in performance for each criteria of the adhesion system. As a result, these can be extracted and used to validate the overall safety of the adhesion system with respect to each of the performance criteria.

That is to say, N_{F_p} is the FOS for the pull force criterion of the system. Values of N_{F_p} greater than 1 are associated with safer performance levels, and therefore should favour the objective function.

To normalise the slip force of the adhesion system N_{F_s}, the required force to prevent the robot from slipping in a worst case scenario $F_{s\ required}$ is considered. Typically this is the weight of the robot multiplied by the static coefficient of friction for the intended surface.

$$N_{F_s} = \frac{F_s}{F_{s\ required}} \tag{4.2}$$

Where, $F_{s\ required}$ is the force required to prevent the adhesion system from sliding down the wall in a worst case scenario.

The moments of the adhesion system are normalised in the same manner, with respect to the worst case scenario for each criterion.

$$N_{M_x} = \frac{M_x}{M_{x\ required}} \tag{4.3}$$

Where, $M_{x\ required}$ is the required bending moment due to the weight of the robot in a worst case scenario.

$$N_{M_y} = \frac{M_y}{M_{y\ required}} \tag{4.4}$$

Where $M_{y\ required}$ is the required bending moment due to the weight of the robot in a worst case scenario.

$$N_{M_z} = \frac{M_z}{M_{z\ required}} \tag{4.5}$$

Where $M_{y\ required}$ is the required torsion due to the weight of the robot in a worst case scenario.

In order to minimise the weight of the adhesion system, the minimum possible weight $W_{pad\ min}$ is divided by the resulting weight of the adhesion system. In most systems there will be a minimum associated weight of the adhesion system, for example the weight of sensors, electronics, cameras, and circuit boards which, for the most part, are invariant to changes in the design of the adhesion system.

$$N_{W_{pad}} = \frac{W_{p\ min}}{W_p ad} \tag{4.6}$$

In this regard, as W_{pad} approaches $W_{p\ min}$, $N_{W_{pad}}$ increases up to a maximum of 1; thereby any minimisation in weight should favour the objective function.

Having identified the performance criteria, the design variables for the adhesion system must be identified. Most inchworm type adhesion systems can be considered to consist of only four primary design variables; these are the footpad radius R_{pad}, radius of the adhesion module r_{am}, the length of the adhesion module l_{am} and the number of adhesion modules used n, as illustrated in Fig 4.3.

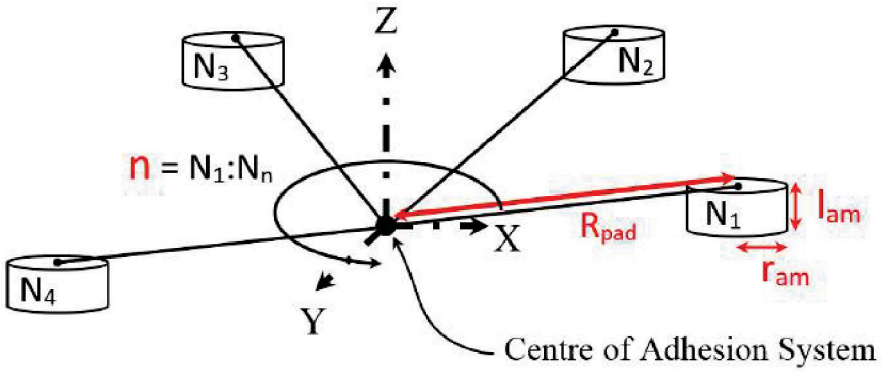

FIGURE 4.3: Design variables for an adhesion system consisting of n adhesion modules. Each adhesion module, situated at the radius of the footpad R_{pad}, has a radius r_{am} and length l_{am}.

The advantage of breaking down the adhesion system into subsystems of adhesion modules, is that scaling laws can be derived for the adhesion module and used in the optimisation solution. For example, the way in which the adhesive force or weight of the module scales with r_{am} and l_{am} can be directly used by the optimisation model in determining the performance or design characteristics such as weight.

Having identified the performance criteria and design variable, the objective function is constructed as follows:

$$\underset{R_{pad},r_{am},l_{am},n}{\text{Minimise:}} \quad -\left(N_{F_p} \times N_{F_s} \times N_{M_x} \times N_{M_y} \times N_{M_z} \times N_{W_{pad}}\right) \tag{4.7}$$

To put this optimisation model into practice, this research presents the design of an adhesion module and then optimises an adhesion system with respect to its design variables. In designing the adhesion module, permanent magnetic configurations are analysed, and a peeling mechanism is developed.

4.4 Magnetic Configuration

The literature reviewed has highlighted the current state-of-the-art methods for permanent magnetic solutions. However, the greatest issue observed with the methods of magnetic adhesion pertains to the rapid decrease of force with increasing air gaps; this being a fundamental characteristic of magnetism. The following sections will demonstrate the significance in which the magnetic configuration effects the force with increasing air gaps. There are many types of magnetic configurations which can be realised, each with advantages and disadvantages for different applications. By studying several different magnetic configurations the most suitable magnetic configuration for a particular application can been identified.

When comparing different magnet configurations, particular parameters should be fixed to prevent bias in the comparison. A comparison between different magnetic configurations with the same weight and volume would demonstrate the best configuration for the intended application. For a given weight and volume, the best configuration for the intended application would demonstrate the greatest adhesion performance over a range of air gaps up to 5 mm. The pull force F, for a magnet (Eqn 4.8), being the stress per unit of area in the normal direction, should be maximised for this air gap. Equation 4.8 shows that in the general case for a magnet, the pull force is strongly related to the residual magnetic flux density B, and also the magnetic pole area, A.

$$F = \frac{B^2 A}{2\mu_0} \tag{4.8}$$

While the weight and volume for different magnetic configurations may be the same, the magnetic flux density at the pole, and area of the pole, may be altered through simple changes in the magnetic configuration. Changes in the magnet configuration will have direct changes in the magnetic field path, yielding advantages and disadvantages depending on the intended application. For example, a magnetic configuration may increase the pull force at the cost of decaying much faster with increased air gaps, the opposite may also be true. Furthermore, this equation assumes no air gaps or magnetic flux leakage are present. For each magnetic configuration, an equation can be derived which relates the magnetic flux density to the distance from the steel surface. This, however, is very difficult to derive and tends not to accurately reflect reality. The best method to determine the force with air gaps is through Magnetic Static Finite Element Analysis (MFEA) and experimental results. Using MFEA, and verified by experimental testing, Tab 4.1 summaries several different magnet configurations. Each magnet configuration has been chosen such that they have the same residual magnet flux density (Grade N42), and each configuration has approximately the same dimensions.

By considering an array of magnets with the magnetic pole orientations in the same direction, that is all North Poles facing up as in Fig 4.4a, it can be observed that the magnetic field extends some distance away from the surface of the magnet. This is comparable to using a single magnet. A pull test of this magnetic configuration determines the magnetic force to a steel plate is 343N. It can also be observed that the magnetic field extends some distance away from the magnets surface. If each alternate magnet is rotated by 180°, as in Fig 4.4b, the adhesion force to a steel plate increases to 392N. However, the magnetic field in the alternating magnet configuration does not extend far from the magnet's surface and hence, the holding force decays rapidly with increased air gaps.

In a Halbach Array, each adjacent magnet is offset by 90°, which redirects the magnetic flux to one surface of the magnet configuration, as seen in Fig 4.4c. Although a lower magnetic force of 334N is achieved, the magnetic field extends further from the magnets surface and caters for a larger range of air gaps.

Table 4.1: Comparison of several different magnet configurations

	Length (mm)	Width / Diameter (mm)	Height (mm)	Pole Area (mm^2)	Volume (mm^3)	Force (N)
Same polarity (Fig 4.4a)	60.9	12.7	12.7	773	9823	343
Alternating polarity (Fig 4.4b)	60.9	12.7	12.7	773	9822.6	392
Halbach Array (Fig 4.4c)	60.9	12.7	12.7	773	9823	320
Rectangular mounting magnet	63.5	19.0	9.5	1209	11462	375
Disc magnet (Fig 4.4d)	-	31.4	12.7	774	9835	271
Disc magnet with steel housing (Fig 4.4e)	-	31.4	12.7	517	9835	458
Disc magnet with steel backplate (Fig 4.4f)	-	31.4	12.7	774	9835	394

The most common magnetic configuration is the holding-magnet which use a steel housing around the magnet. The common holding-magnet configuration increases the magnetic force to 458N for the same volume as previous configurations. However, while this force is very high with direct contact on an ideal surface, the magnetic force decays very quickly with increased air gaps. This can be understood by analysing Fig 4.4e. Even with very small air gaps the flux tends to flow directly from the steel housing to the magnet without passing through the surface.

To reduce this effect the housing can be replaced with a flat steel back plate. This configuration is shown to yield both a high adhesion force of 394N and a greater magnetic field range as seen in Fig 4.4f.

The benefits of this configuration are further realised when studying the magnetic force with an air gap. Figure 4.6a compares the magnetic force with increasing air gaps for

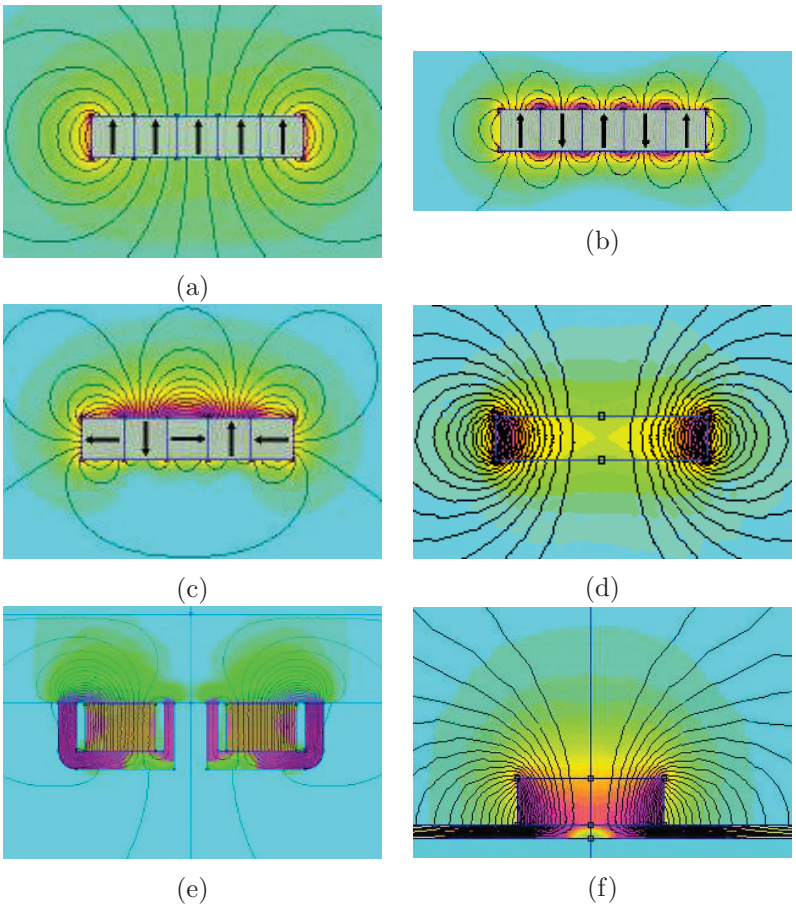

FIGURE 4.4: Magnetic fields for different magnetic configurations. (a) Magnets with same polarity. (b) Magnets with alternating polarity. (c) Halbach Array. (d) Disc Magnet. (e) Disc magnet with steel housing. (f) Disc magnet with steel backplate.

a 1.25" disc magnet and a 1.25" disc magnet with and without a steel back plate. The height of the magnet without the steel back plate is 9.35mm. The magnet with the steel back plate is 6.35mm, and the steel plate is 3 mm. Although the magnet with steel plate has a smaller magnet, Fig 4.6a shows that the use of the steel plate achieves twice the adhesion force with better performance at increased air gaps. Furthermore, Fig 4.6b shows that the performance with increased air gaps is proportional to the height of the magnet. However, with increased thickness in magnet, there is increased weight in the adhesion system. Thus, the optimal thickness must be determined in order to achieve the required adhesion with minimal weight. This requires an accurate force model for this particular magnetic configuration.

Finally the dimensions of the steel back plate must also be designed to maximise the

adhesion force and minimise the weight of this magnetic configuration. If the thickness of the steel back plate is too thin, it will decrease the effective holding force through saturation and hence flux leakage as seen in Fig 4.5a. If the plate is too thick, the weight of the system is increased unnecessarily. Figure 4.5b shows the optimal plate thickness to minimise flux leakage and weight. Figure 4.5c shows the relationship between a steel sheet thickness and the holding force; it can be observed that a steel plate thickness greater than 2.93mm will yield no further increases in the adhesion force.

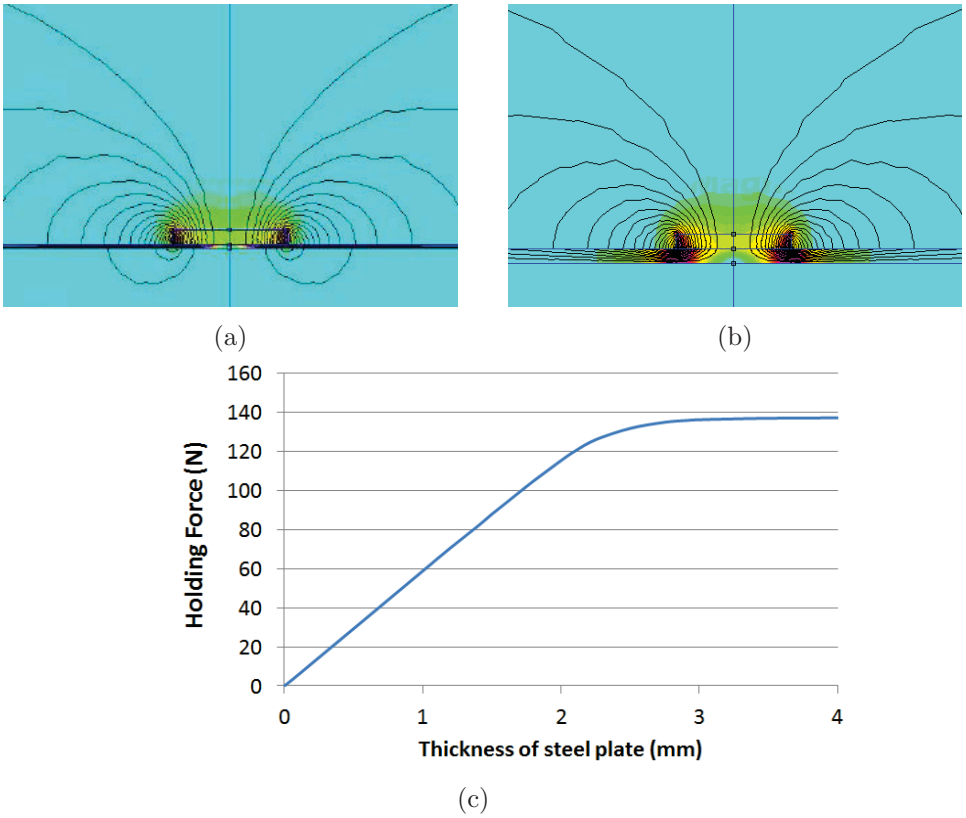

FIGURE 4.5: MFEA for magnet diameter of 31.75mm, thickness of 6.35mm (a) Magnetic flux leakage occurs due to 1mm thickness of steel plate (b) Optimal steel plate thickness to minimise flux leakage and weight of system. (c) Curve relating holding force to thickness of steel backplate with consideration to magnetic flux.

The model for the pull force of the magnet, F_m, is determined by the magnet diameter, D_m, magnet thickness T_m, and the air gap between magnet and ferromagnetic surface, x. The magnetic solution will require a protective layer between the magnet and the surface, this is assumed to be 2mm. Taking into account the expected air gaps due to dirt, roughness and paint in the intended environment, the footpad is designed for a worst case scenario

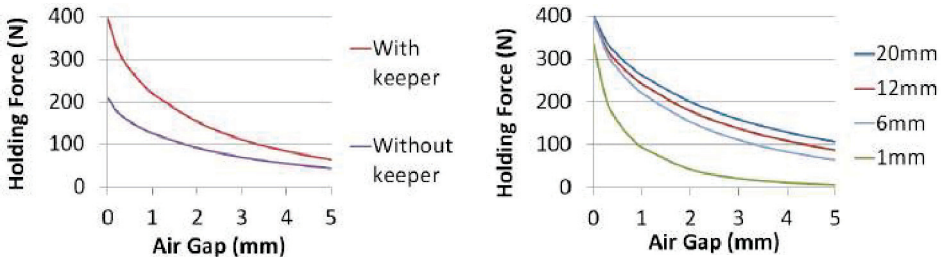

(a) (b)

FIGURE 4.6: Performance of disc magnet with variations in configuration. (a) Comparison of holding force with and without steel back plate. (b) Comparison of holding force performance for different magnet thicknesses (1, 6, 12, 20 mm), using steel back plate.

with a 5mm air gap. Figure 4.7 shows the force model for an N52 Neodymium magnet at a 5mm air gap, where the magnet diameter and magnet thickness range between 0 to 50mm.

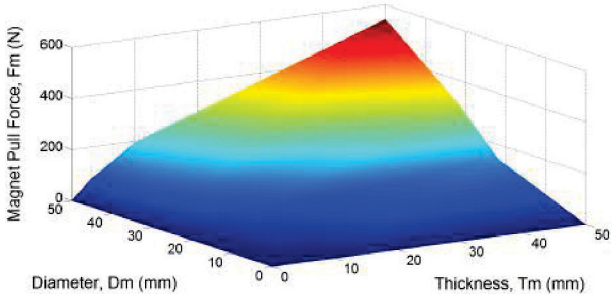

FIGURE 4.7: Force model $F_m(D_m, T_m)$, for rare earth N52 NdFeB disc magnet with 5mm air gap.

4.5 Peeling Mechanism

Having identified a magnetic configuration and obtained the force model for a 5mm air gap, a method to attach and detach the magnetic configuration from the surface must be considered. The most difficult method to remove a magnet from a surface is through lifting perpendicular to the surface. Even very large magnets can easily be removed from surfaces given that sufficient bending moment is applied. It is assumed that the magnetic force F_m, is applied through the centre of a magnet with a radius $D_m/2$. The required torque to peel the magnet M_m is,

$$M_m = \frac{D_m}{2} \times F_m \ . \tag{4.9}$$

A magnet that is peeled from the surface will follow the arch of a semi-circle, with the centre of the arch being at the rotation axis for the magnet. A solution that provides mechanical advantage through both leverage and gear ratios is realised by fixing a quarter gear segment to the magnet, with the centre of the gear located at the rotation axis for the magnet. The conceptualised idea, components and variables for the adhesion module can be seen in Fig 4.8.

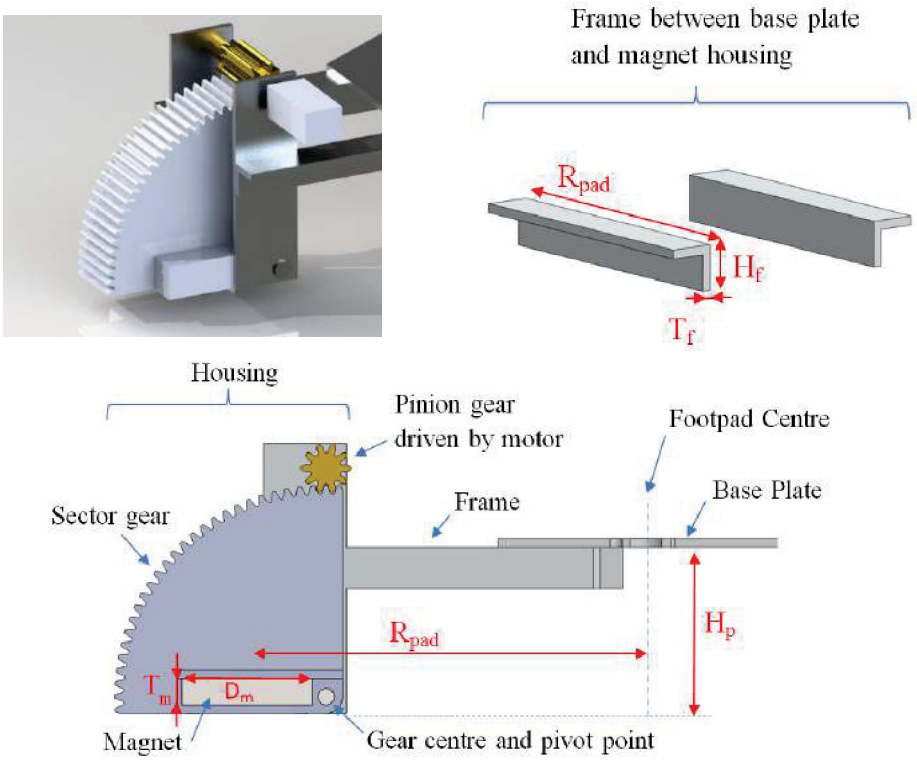

FIGURE 4.8: Components and variables of the adhesion module; Radius from foot pad centre to magnet centre, R_{pad}; Height of frame H_f; Thickness of frame, T_f; Height from surface to first actuator, H_p; Thickness of magnet, T_m; Diameter of magnet, D_m.

The design parameters for this adhesion module seen in Fig 4.8 include the height of footpad H_p, the height of the frame H_f, the thickness of the frame T_f, the density of aluminium ρ_{Alum}, the density of N52 grade Neodymium ρ_{NdFeB}, the length of the robot L_r, the weight of the robot W_r, and the coefficient of static friction μ_s, the weight of the

peeling mechanism W_h. The weight of the peeling mechanism includes the weight of the pinion gear, sector gear, motor and axle. These parameters can be predetermined based on choice and availability of materials or are inherited through the design of other components. The remaining parameters are functions of the design variables. These include the weight of the magnet $W_m(D_m, T_m)$, the weight of the steel back plate $W_{keeper}(D_m, T_m)$, the weight of the peeling module $W_{pm}(F_m(D_m, T_m))$, the weight of the frame $W_f(R_{pad})$, the weight of the footpad $W_{pad}(R_{pad}, W_m, W_f)$ and the pull force of the magnet $F_m(D_m, T_m)$.

Assuming a disc magnet is used, the weight of the magnet is defined by

$$W_m(D_m, T_m) = \pi \times (D_m/2)^2 \times T_m \times \rho_m \ . \tag{4.10}$$

Noting that the steel plate should be 1.5× larger than the magnets diameter, the weight of the steel back plate for the disc magnet can be approximated by

$$W_{keeper}(D_m, T_m) = (\pi \times ((1.5 \times D_m)/2)^2 \times T_s) \times \rho_{steel} \ . \tag{4.11}$$

Where the thickness of the steel, T_s, is such that most of the magnetic field is contained in order to maximise pull force, has been empirically determined, and can be approximated by

$$T_s = \frac{(T_m \times 0.2) + (D_m \times 0.2)}{2} \ . \tag{4.12}$$

Assuming a frame with four members of thickness T_f and height H_f is used, the weight of the frame is defined by

$$W_f(R_{pad}) = 4 \times \rho_a \times T_f \times H_f \times R_{pad} \ . \tag{4.13}$$

Finally, the weight of the footpad can be expressed as

$$W_{pad} = (n \times [W_m(D_m, T_m) + W_h + W_f(R_{pad})] + W_b) \ . \tag{4.14}$$

4.6 Performance Criteria

The performance criteria for the adhesion system are defined as follows.

The pull force is simply the number of magnets times the force of the magnets.

$$F_p = n \times F_m(D_m, T_m) \tag{4.15}$$

The slip force is the pull force multiplied by the coefficient of static friction.

$$F_s = n \times F_m(D_m, T_m) \times \mu_s \tag{4.16}$$

In calculating the bending moments, it is assumed the magnets are evenly distributed around the circumference of the adhesion system. Depending on the direction of the bending moment, the locations of the adhesion modules will effect the resulting moments.

$$M_x = \sum_{i=0}^{n-1} F_m(D_m, T_m) \times R_{pad} \times \cos(\frac{2 \times \pi}{n} \times i) \tag{4.17}$$

In order to accommodate both directions of bending, moments about the y axis are also calculated.

$$M_y = \sum_{i=0}^{n-1} F_m(D_m, T_m) \times R_{pad} \times \sin(\frac{2 \times \pi}{n} \times i) \tag{4.18}$$

The torsion moment takes into consideration the radius of the footpad and the slip force before the adhesion system rotates on the surface.

$$M_z = n \times F_m(D_m, T_m) \times R_{pad} \times \mu_s \tag{4.19}$$

4.7 Design Constraints

In order for the robot to perform a 180° plane transition as seen in Fig 4.9a, the footpad radius has an upper limit restricted by the length of members in the robot chain. Furthermore, the lower limit of the footpad radius is constrained by the minimum footpad size for a given magnet diameter as seen in Fig 4.9b.

Hence, Eqn 4.20 prevents an intersection of the magnets, ensures the construction of the footpad is feasible, and the 180° plane transition is possible.

$$0.15m \geq R_{pad} \geq \frac{D_m}{2 \times \sin(\pi/n)} \tag{4.20}$$

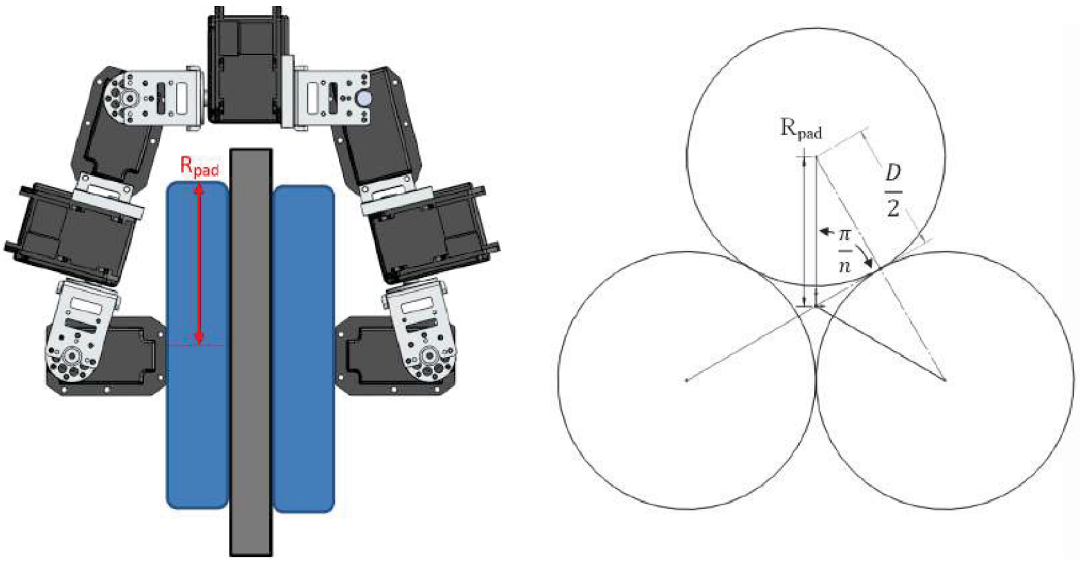

(a) (b)

FIGURE 4.9: Design constraints for foot pad. (a) Geometric constraints for footpad radius being limited by 180° plane transfer. (b) The minimum foot pad radius given the diameter of the magnets.

Limited by the torque specification of the selected actuators, the maximum footpad weight is W_{pmax}. Equation 4.21 limits the resulting footpad weight by W_{pmax}.

$$W_{max} \geq W_{pad} \tag{4.21}$$

Recalling the modes of failure, constraints are set on the performance criteria such that solutions with a failure case are ignored.

The pull force is constrained in Eqn 4.22 to ensure that the total system weight can be supported while inverted.

$$F_p \geq 2 \times W_{pad} + W_R \tag{4.22}$$

The slip force is constrained in Eqn 4.23 to ensure sufficient adhesion to overcome the weight of the robot when on a vertical surface.

$$F_s \geq (2 \times W_{pad} + W_R) \times \mu_s \tag{4.23}$$

A constraint on the bending moments in the x direction (Eqn 4.24) and y direction (Eqn 4.25) ensures that the footpad can support the climbing robot in a cantilevered position for either orientation.

$$M_x \geq M_R \tag{4.24}$$

$$M_y \geq M_R \tag{4.25}$$

The moment of the robot M_r can be determined by summing the moments around pivotal point of the adhesion system on a vertical wall. The total moment consists of the moments from each footpad and the inchworm robot's body, as defined in Eqn 4.26.

$$M_R = \frac{1}{2}H_{pad} \times W_{pad} + (\frac{1}{2}H_{pad} + \frac{1}{2}L_r) \times W_r + (H_{pad} + L_r + \frac{1}{2}H_{pad}) \times W_{pad} \tag{4.26}$$

Equation 4.27 ensures that the torsion capability of the footpad prevents the footpad from rotating due to the moment from the robot. Equation 4.28 describes this torsion moment due to the weight and length of the robot in a worse case scenario, when the robot is in a cantilevered pose.

$$M_z \geq M_T \tag{4.27}$$

Where,

$$M_T = \frac{1}{2}L_r \times W_r + (L_r + \frac{1}{2}H_{pad}) \times W_{pad} \tag{4.28}$$

It should be noted that Equations 4.26 and 4.28 have been determined based on the 7DOF inchworm configuration proposed in Chapter 3.

4.8 Construction of Optimally Designed Magnetic Adhesion System

Using the objective function presented, the fixed design variables for the robot configuration and the constraints identified, the magnetic adhesion system can be optimised.

4.8.1 Boundary Conditions and Application Parameters

In order to find the global minimum of the objective function, an exhaustive search has been performed. Boundary conditions are used to narrow the search for the optimal solution, and a step size for each parameter is specified. The number of magnets that could potentially be has been limited to $n = 3 : 10$ in order to ensure stability of the adhesion system. The foot pad radius $R_{pad} = 0 : 100$, the magnet diameter $D_m = 0 : 50mm$, the magnet thickness $T_m = 0 : 50mm$. The fixed design parameters are $H_p = 0.03m$, $L_r = 0.567m$, and $W_r = 1.2kg$, $W_{max} = 0.6kg$, $T_f = 0.003m$, $H_f = 0.01m$, $W_h = 0.120kg$, $W_b = 0.125kg$, $\rho_{Alum} = 2700kgm^{-3}$, $\rho_{NdFeB} = 7501kgm^{-3}$, $\mu_s = 0.6$.

4.8.2 Optimal Design Results

Performing a 'fmincon' search algorithm to optimise the four design parameters of the adhesion system, such that six performance criteria are maximised, multiple local minima were observed. Therefore, due to the limited range set by the boundary conditions and using a relatively large step size, it was feasible to use an exhaustive search to guarantee the global minimum solution of the objective function. With a step size of 1 mm for

the radius, magnet diameter and magnet thickness, the global minimum value of the objective function resulted in an adhesion system with a radius of 100mm, consisting of three adhesion modules, each with a magnet of 3mm thickness and 42mm diameter.

In order to visualise the optimisation results, Fig 4.10 shows the effect on the performance criteria with changes in magnet diameter and magnet thickness. The results are shown for the 100mm footpad radius consisting of 3 magnetic attachment modules. It can be observed that the optimal result for the magnet diameter and magnet thickness varies depending on the performance criteria being maximised. It should be noted that these results are optimised for an air gap of 5mm, due to the magnetic force model used, $F_m(D_m, T_m)$.

Figure 4.11 shows the effect on the performance criteria with changes in magnet diameter and footpad radius. The results are shown for the global optimum solution, with a 100mm footpad radius consisting of 3 magnetic attachment modules. Once again, it can be observed that the optimal result for the magnet diameter and footpad radius varies depending on the performance criteria being maximised.

This global optimum solution yielded the following results: F_p=279.2N, F_s=167.5N, M_x=18.6N, M_y=16.1Nm, M_z=16.8Nm, W_{pad}=540g. While this solution meets the optimal design requirements, it was not possible to source the exact magnet size, and the cost to produce so few magnets was too great. The closest available N52 grade magnet was found with a magnet diameter of 31.75mm and thickness 6.35mm. Running the optimiser again with the selected magnet dimensions fixed, a new footpad radius of 97mm was calculated with the following results: F_p=240.0N, F_s=144.0N, M_x=15.5Nm, M_y=13.4Nm, M_z=14.0Nm, W_{pad}=560g.

The change in magnet dimensions changes both the adhesion performance and weight negatively. The bending moment capability in the x direction is reduced by 3.1Nm, with an additional weight of 20g. However for the given magnet availability, this is the most optimal design to maximise the performance criteria.

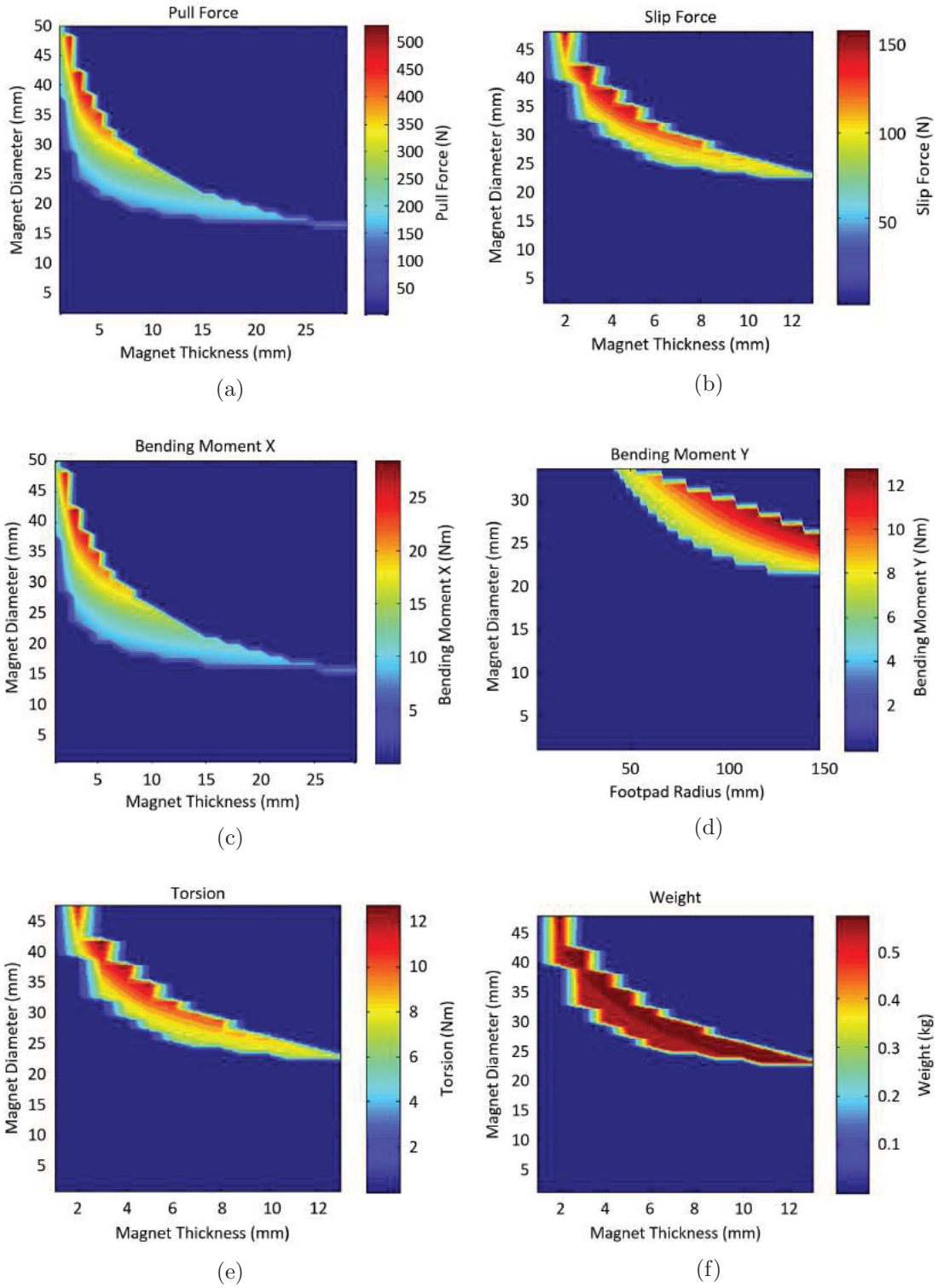

FIGURE 4.10: Optimisation results for each of the performance criteria, with changes in magnet diameter and magnet thickness, for a 100mm radius footpad consisting of 3 magnetic attachment modules. (a) Peeling force. (b) Slip force. (c) Bending Moment in x direction. (d) Bending Moment in y direction. (e) Torsion (f) Weight

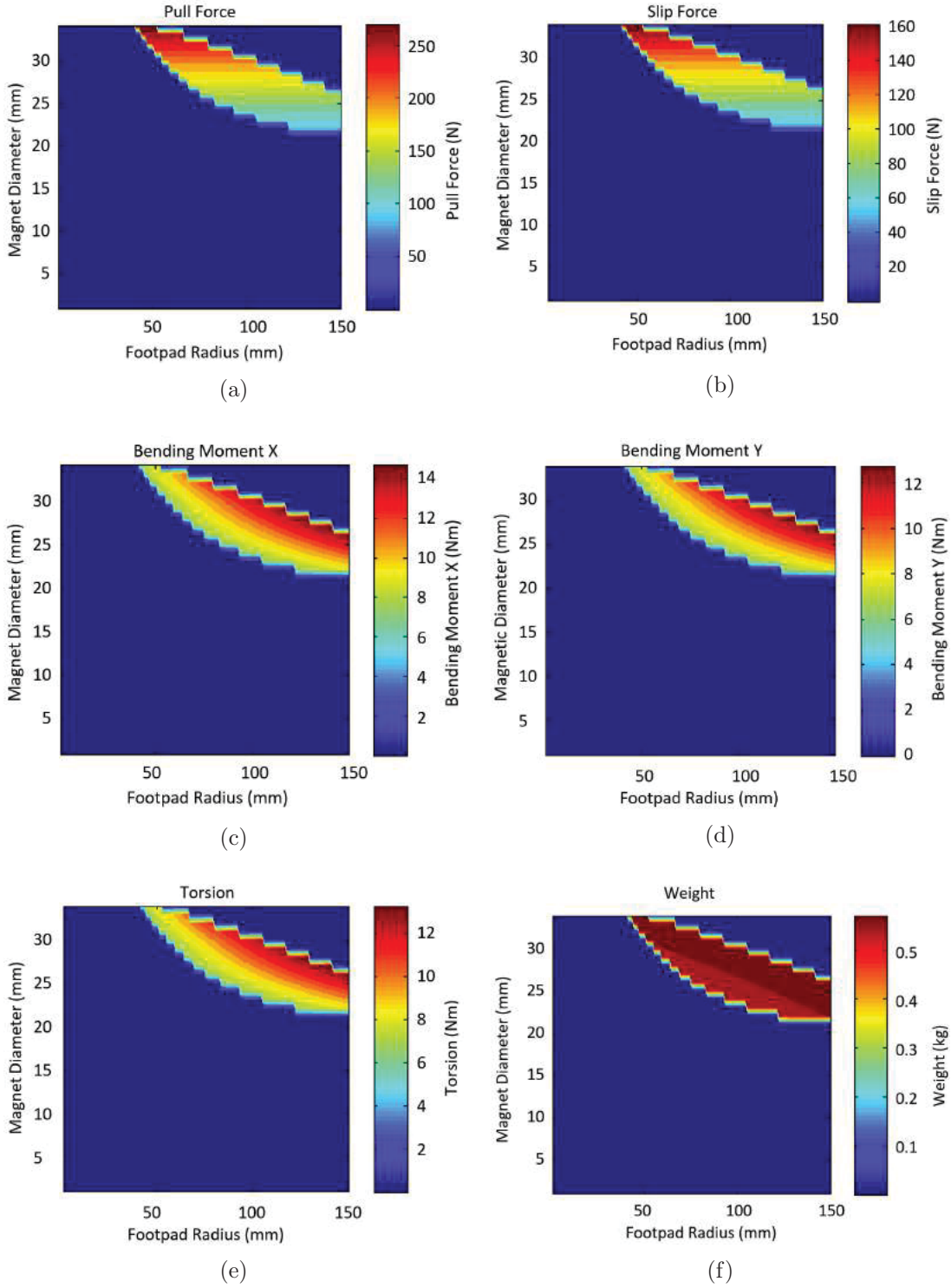

FIGURE 4.11: Optimisation results for each of the performance criteria, with changes in magnet diameter and footpad radius, for a 100mm radius footpad consisting of 3 magnetic attachment modules. (a) Peeling force. (b) Slip force. (c) Bending Moment in x direction. (d) Bending Moment in y direction. (e) Torsion (f) Weight

4.8.3 Magnetic Peeling Module

Based on the optimisation results for the selected magnet, the required torque for the peeling mechanism and motor to peel the magnet from the surface is determined. The peeling method uses a minimum expected air gap of 2mm due to the protective housing. Hence, the maximum expected holding force at 2mm is 15.6kg per magnet. It can be assumed that the force acts through the magnet's centre which is located 15.9mm from its rotation point. The torque required to peel the magnet from the surface is $2.43Nm$. An $11g$ micro-metal DC motor with a gear ratio of 1000:1, rated to 0.883Nm, was selected to drive the pinion gear with a further gear ratio of 10:1 to the quarter gear segment. The torque available to peel the selected magnet from the surface is $8.83Nm$. The constructed footpad can be seen in Fig 4.12.

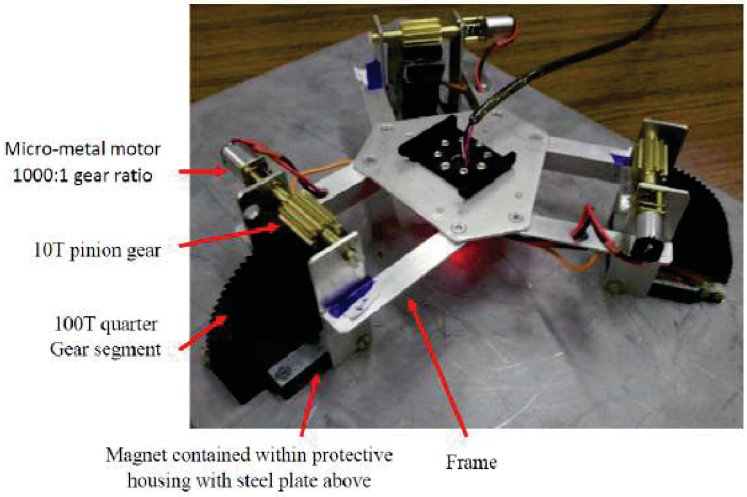

FIGURE 4.12: Constructed footpad from optimal design model, consisting of three magnetic attachment modules, 97mm footpad radius, magnet diameter of 31.75mm and magnet thickness 6.35mm.

4.9 Testing and Evaluation

The complete integration of three adhesion modules measures 612g in total. The increase is weight is due to the added control circuits, wiring and fixtures.

The footpad is seen in Fig 4.13a supporting more than 2.5x factor of safety in bending moment with a 0mm air gap. Figure 4.13b verifies the geometric constraints of the footpad

in the 180° plane transition, and Fig 4.13c shows the footpad supporting the inchworm climbing robot in cantilever.

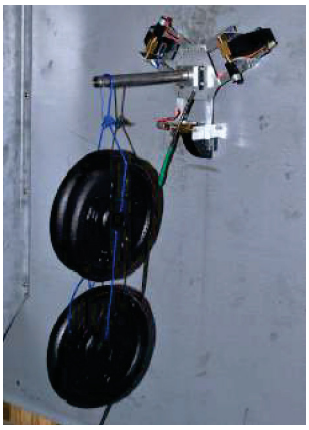

(a)

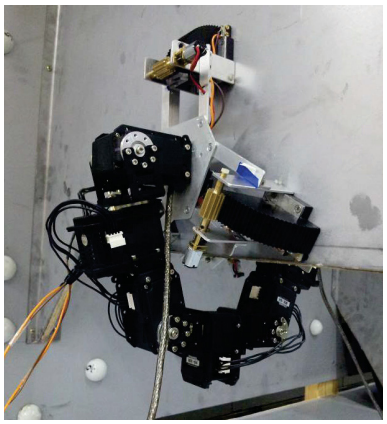

(b)

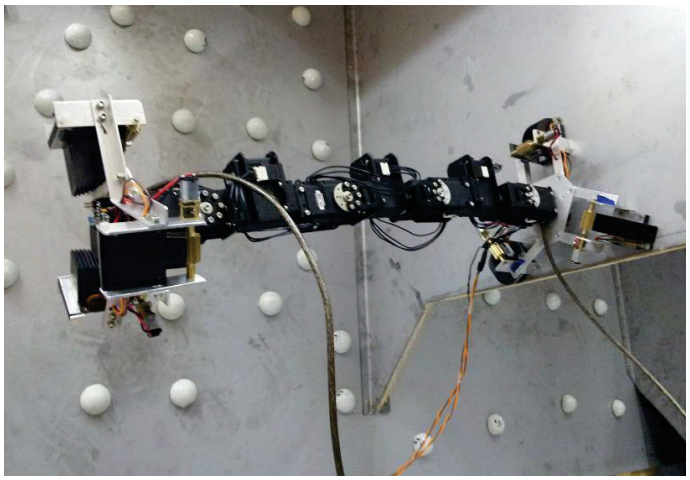

(c)

FIGURE 4.13: Construction and testing of prototype climbing robot and adhesion system. (a) Footpad supporting 18.4 Nm load. (b) Verification of geometric constraints in 180° plate transition. (c) Footpad supporting complete inchworm climbing robot in cantilever.

The test facility for the constructed foot pad uses 1.5mm steel sheet metal. MFEA showed that the minimum plate thickness to prevent saturation is 2.93mm for the given magnet dimensions. The theoretical pull force and bending moment have been adjusted for the 1.5mm sheet thickness using the linear relationship of sheet thickness to magnetic saturation. The theoretical results have been compared with the experimental results in Fig 4.14. The experimental results show close correlation with the force models used. Furthermore,

it demonstrates the capability of supporting the robot for air gaps up to 5mm as desired in the design model.

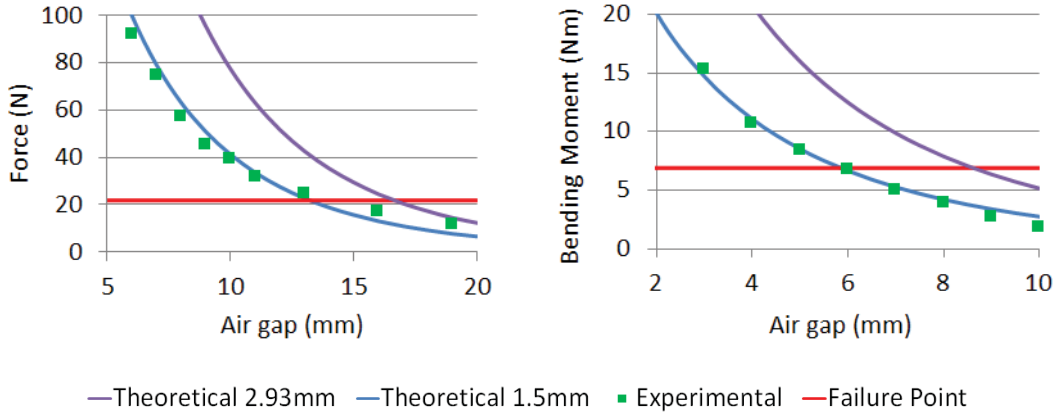

FIGURE 4.14: Comparison of theoretical results for 2.93mm sheet steel and 1.5mm sheet steel, experimental results, and failure point for pull force and bending moment in x direction. Pull force gauge was limited to 100N, therefore no data was collected beyond this force. FEA also predicts excessive deformation on frame. The air gap between the surface to the magnet due to the construction of the toe is 2mm.

4.10 Discussion and Conclusions

A novel permanent magnetic adhesion system has been presented with the ability to robustly support the intended payloads of the robot. In designing the adhesion system, different magnetic configurations have been evaluated to determine the best solution for the intended application scenario, in particular to accommodate the expected air gaps.

A novel peeling mechanism has been developed which peels a permanent magnet from a ferromagnetic surface. This device yields high adhesive strength to weight ratio, and ensures power-fail safe operation. An patent application has been published in Australia and Internationally for the magnetic peeling mechanism developed.

An optimisation model has been developed to determine the adhesion system design variables which maximise performance characteristics and minimise weight. The optimisation model can be adapted for use with other forms of adhesion and different inchworm robot configurations.

The primary limitation of optimisation model for the adhesion system is that discrete steps are used for the design variables. This poses two issues, the first issues is that the time taken to perform an exhaustive search, increases with the search resolution. Secondly, the most optimal solution may be missed if it happens to be between a step size. Using a step size of 1mm has proved sufficient due to tolerances in design and availability of magnets. A future approach will implement a genetic search algorithm for the global minimum.

Chapter 5

Experiments and Results

This chapter presents the experiments conducted in order to validate the design of the biologically inspired robot and the magnetic adhesion system. The outcomes of the tests, and the limitations of the robot are discussed.

A scaled and improved version of the inchworm robot is then presented, highlighting the improvements from lessons learnt through the testing and validation of the initial prototype. The improved version, referred to as CROC (Climbing RObotic Caterpillar), is tested extensively in laboratory conditions, before being tested and deployed for use by the Sydney Harbour Bridge inspectors. The robot is evaluated on its climbing ability, and the challenges faced in enabling climbing robots in real world applications is discussed.

5.1 Initial Testing and Evaluation for the Inchworm Robot

Having confirmed the kinematics of the inchworm robot configuration in Chapter 3 and performance of the magnetic adhesion system in Chapter 4, testing was first conducted in ideal laboratory conditions.

The robot was programed such that it would climb through a manhole partition plate on a representative bridge structure with ideal surface conditions as seen in Fig 5.1.

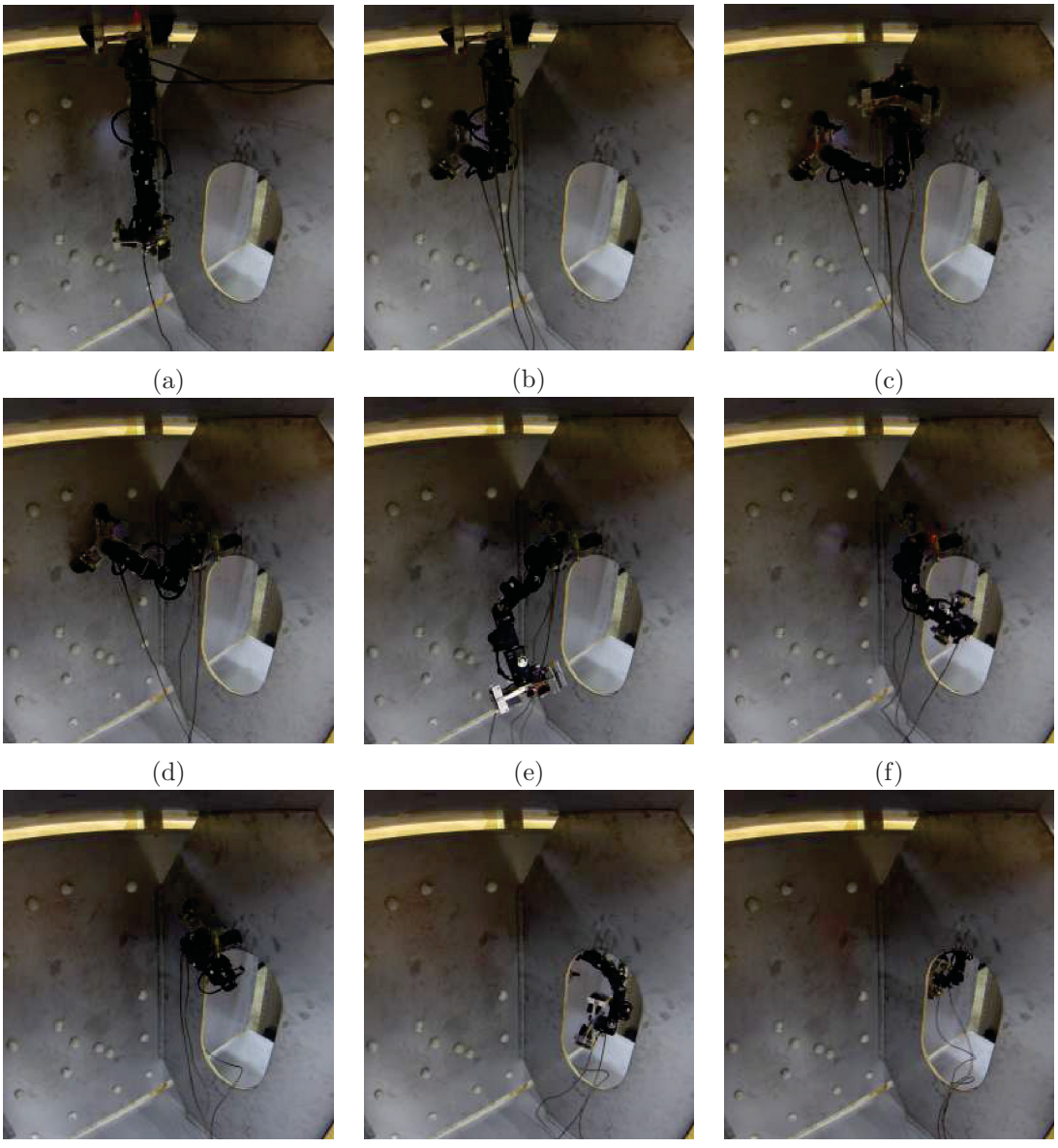

(a) (b) (c)

(d) (e) (f)

(g) (h) (i)

FIGURE 5.1: Mobility demonstration of the prototype inchworm inspired climbing robot. (a) Hanging from ceiling. (b) Transition to side wall. (c) Release from ceiling. (d) Transition to edge of manhole. (e) Release from sidewall. (f) Transition through manhole. (g) 180° transition and attachment to other side of manhole. (h) Transition of back foot through manhole. (i) Transition and attachment to side wall. Videos can be found here [106] and here [107]

At this stage the robot had no vision system therefore all trajectories were determined off-line; however the ability for the robot to transition through the manhole scenario and perform the 180° plane transition has been clearly demonstrated. This is the first demonstration known for an inchworm-inspired robot, including those preprogrammed, to perform the 180° transition. Moreover, this is the first known climbing robot with the ability to perform the 180° transition in any orientation with respect to gravity. This can be attributed to the adhesion system and robot configuration. Videos can be found here [106] and here [107]

5.1.1 Limitations

Initial testing demonstrated that the adhesion system could support the robot in a worst case scenario, i.e. that cantilevered pose, and the robot configuration enabled manoeuvring through challenging application scenarios. However, a number of limitations were noted in the design. As predicted in the discussions on scalability, deflections were observed throughout the body of the robot. These deflections can be attributed to compliance in the links, backlash in the joints, and deformation in the footpad base. These deflections were accommodated for in the motion planning algorithms whilst the robot did not carry any extra payload.

Having demonstrated the transitional abilities, the robot was fitted with the required inspection equipment and electronics to permit inspection, as seen in Fig 5.2. The added equipment included a 3D depth camera, power regulators, communication bus and controller, combined umbilical chord / tether, and embedded controllers for controlling the joints and feet. The weight of the equipment was distributed between either end of the robot in an effort not to hinder the workspace of any joints. Mounting the camera to one end also maximises the workspace whilst exploring the environment.

With the added weight at either end of the robot increased load torque is applied to the joints. Despite the added payload, the adhesion system could still support the robot, albeit with a reduced factor of safety. Several issues were identified due to the additional payload. The increased weight caused greater deflections; this was particularly problematic in fusing together the 3D points clouds which relied on accurate pose information. With

errors in the predicted pose information due to the deflections, the mapping results showed non-alignment in overlapping 3D data.

Finally, the added weight, diameter and stiffness of the tether became a hindrance in the mobility, particularly for flipping motions and for acrobatic motions, such as those performed during a manhole transition. In designing an improved inchworm robot, rigidity throughout the robot was a criterion to address.

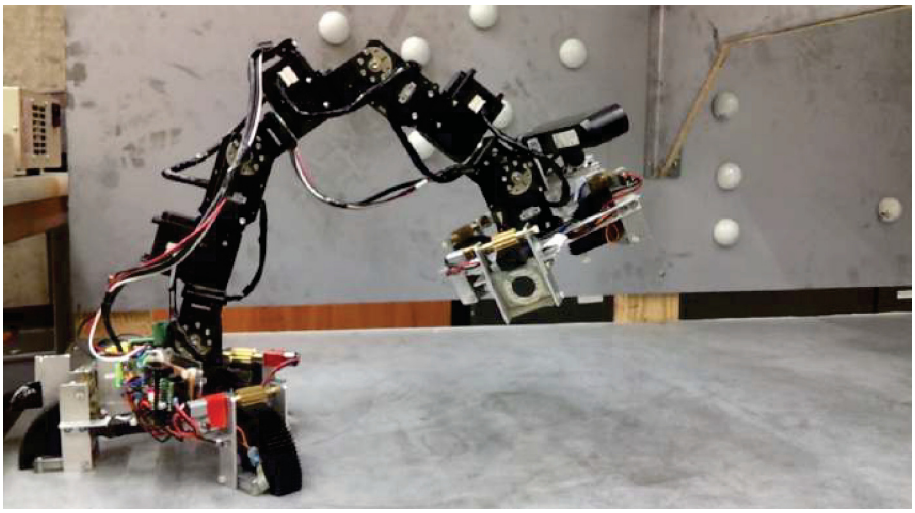

FIGURE 5.2: Prototype inchworm robot with required inspection equipment. Added payload causes deflections in robot and increased control complexity to compensate.

5.2 CROC: An Improved Inchworm Robot

5.2.1 Robot Overview

Although the proposed kinematic configuration in Chapter 3 has been proven to be dexterous, the actuator needs to be stronger in order to support the necessary inspection equipment and electronics. Therefore, scaling of the actuators was required.

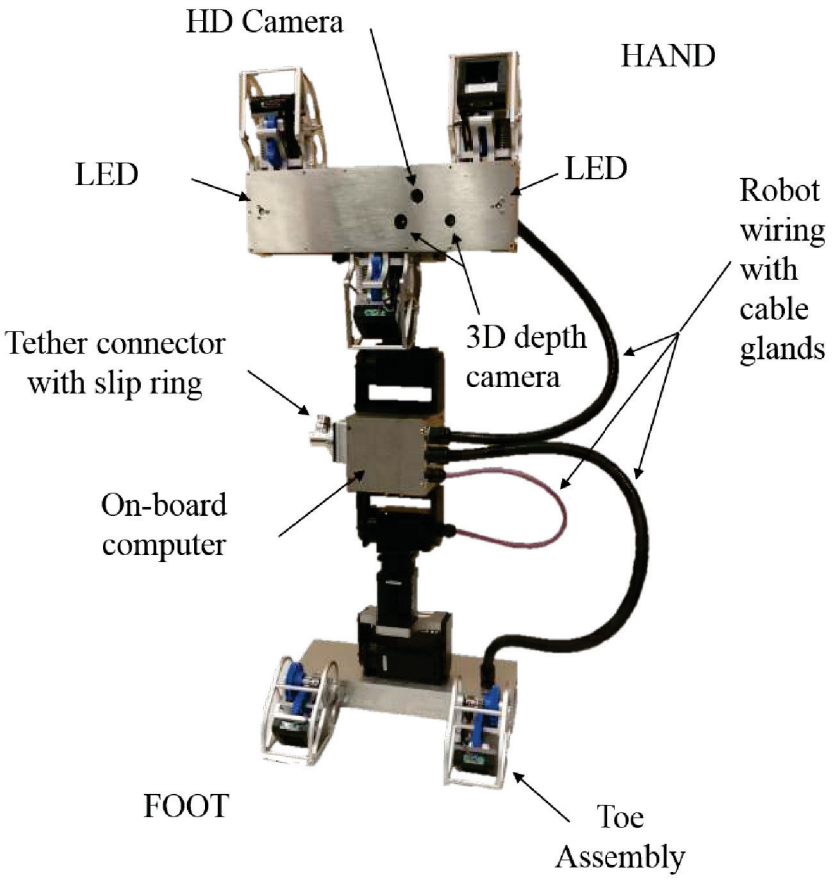

FIGURE 5.3: CROC: The Climbing RObot Caterpillar. Annotations indicate the major components of the robot.

The next motors up in size were the Dynamixel Pro motors. The static loads and adhesion requirements in using these actuators were re-evaluated, and they were determined to be feasible given the payload requirements and the required increase in performance for the adhesion system. Refer to Appendix B for table of loads applied to each motor in a cantilevered pose. Refer to Appendix C for table to torques in determining the required motor to peel the magnet.

The design of the revised robot, CROC, takes into account all the challenges faced and lessons learnt during the proof of concept. CROC, annotated in Fig 5.3 incorporates all the required equipment and achieves greater factors of safety in terms of adhesion capacity and joint torques.

The robot uses individual embedded controllers for each foot, an on-board ODROID-XU3 computer to monitor robot state, instruct actuators, and relay instructions and sensory information to the primary control unit. A HD Logitech C930e RGB camera is used to collect images for condition assessment.

The feet on either end of the robot are identical, although the LEDs, depth camera and RGB camera are only contained within on footpad, called the "HAND", as seen in Fig 5.4. All electronics including the cameras, and embedded controllers have been sealed within the foot pad housings to prevent containments from the environment entering. All wiring on the robot has been contained within cable glands to protect from pinching, wear and tear.

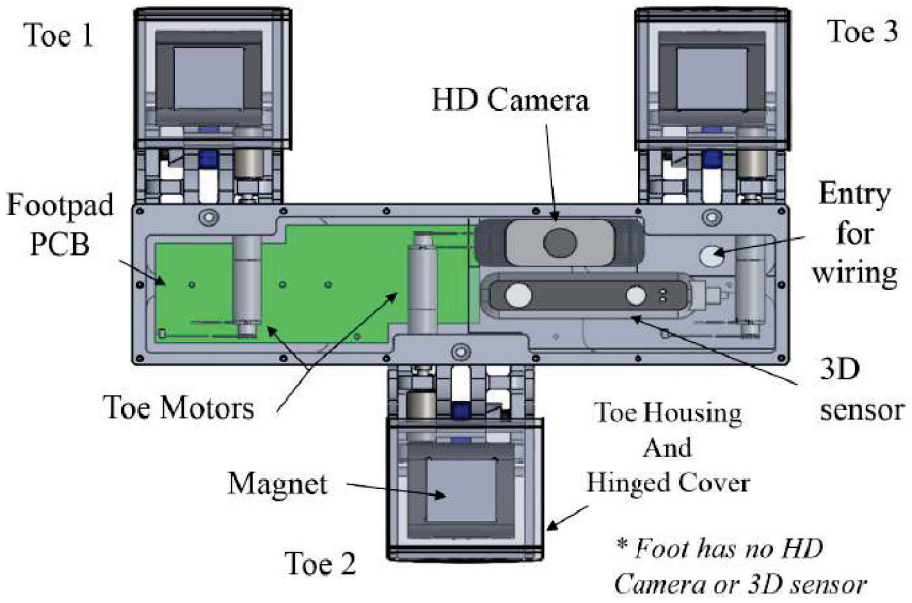

FIGURE 5.4: Revised foot pad for CROC, includes all required sensors to enable autonomous operation and inspection.

Improving rigidity was a primary focus on the new robot design. All load bearing systems were analysed with Finite Element Analysis (FEA) to increase rigidity and reduce weight. The primary load bearing systems include the footpad housing, the toe frame, and the links between motors. These parts were also machined from Al7075 to reduce weight and increase rigidity. Figure 5.5 shows the FEA analysis on the primary load bearing links used on joints 1 and 7. The brackets throughout the robot body have been limited to 0.2mm of deflection in a worst case scenario analysis.

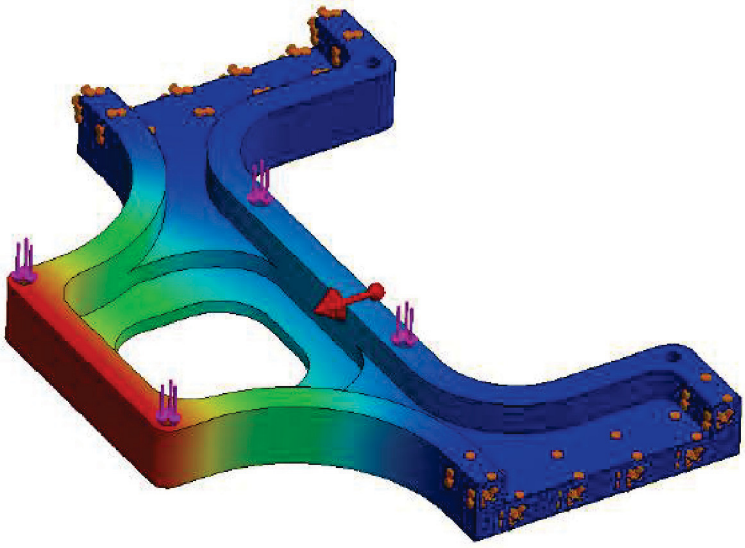

FIGURE 5.5: Finite Element Analysis of links. Figure shows the primary bracket used on joints 1 and 7. The bracket provides additional reach ability for the 180° plane transition, and is subject to the greatest load torque. FEA was used to reduce weight and minimise deflections under load.

The revised brackets introduce an offset between the z axis of the first joint to the second joint, and the sixth joint to seventh joint, as seen in Fig 5.6.

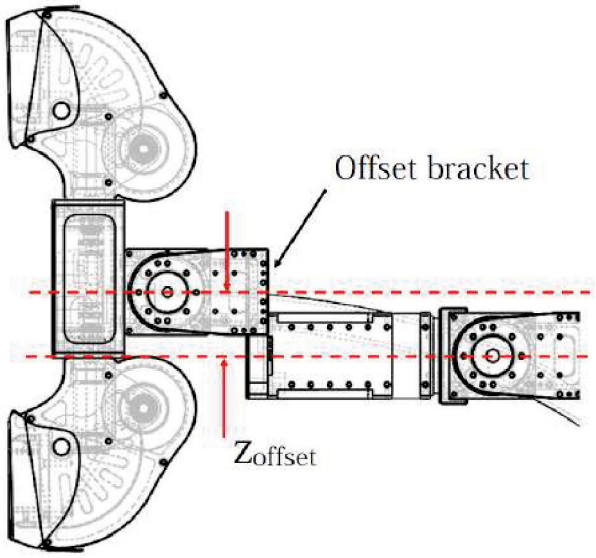

FIGURE 5.6: Offset bracket used on revised CROC configuration to enable better mobility during 180° plane transitions.

This offset provides three advantages. The first is the ability to rotate ±90° in both directions, which was previously limited by the centre toe in the 3-toe adhesion configuration. The second advantage is the ability to fold the body in between two toes and position the body closer to the surface. This increases the maximum thickness for the 180° plane transition. The most important trait, is the reduced total height of the robot when folded into a flat state. This allows the robot to fit through the manhole, shown in Fig 5.12b.

In addressing the issues faced with cable management, the primary tether to the robot was relocated to the centre of the robot. The tether is a high quality, high flex, robot wiring by IGUS which contains power and Ethernet communication from the external Operator Control Unit (OCU) to the on-board ODROID-XU3 computer. The tether connects to a load bearing slip ring, seen in Fig 5.7 to permit continuous rotation. This allows the robot to perform acrobatic and flipping manoeuvres without causing twists in the cable, or increasing the load for a particular foot.

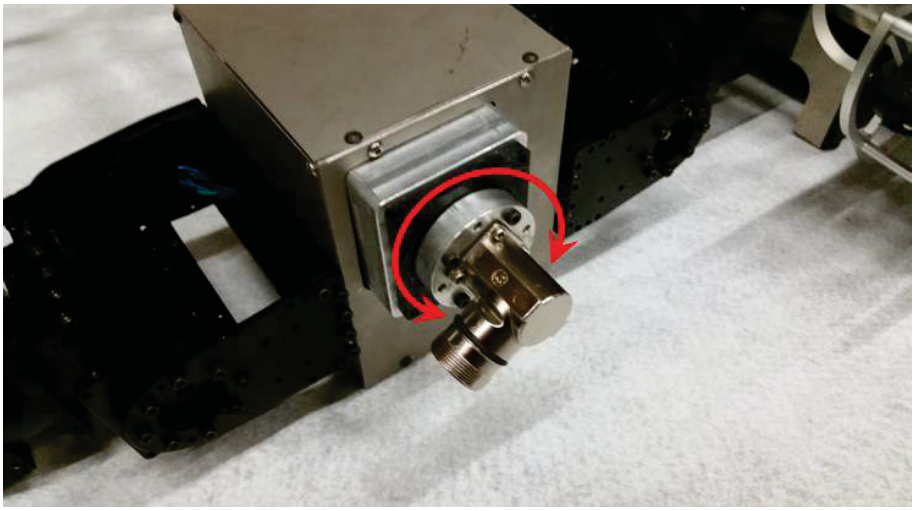

FIGURE 5.7: Close-up of slip ring used on CROC to allow continuous rotation of tether, and prevent twisting during flip step motions.

5.2.2 Adhesion System

5.2.2.1 Revised Peeling Mechanism

The magnetic peeling mechanism seen in Fig 5.8 was redesigned to increase rigidity, reliability, operating life, speed, and to provide a non-back-drivable capability. These improvements were achieved with better alignment, bearings, couplings, tighter tolerances, and higher quality parts.

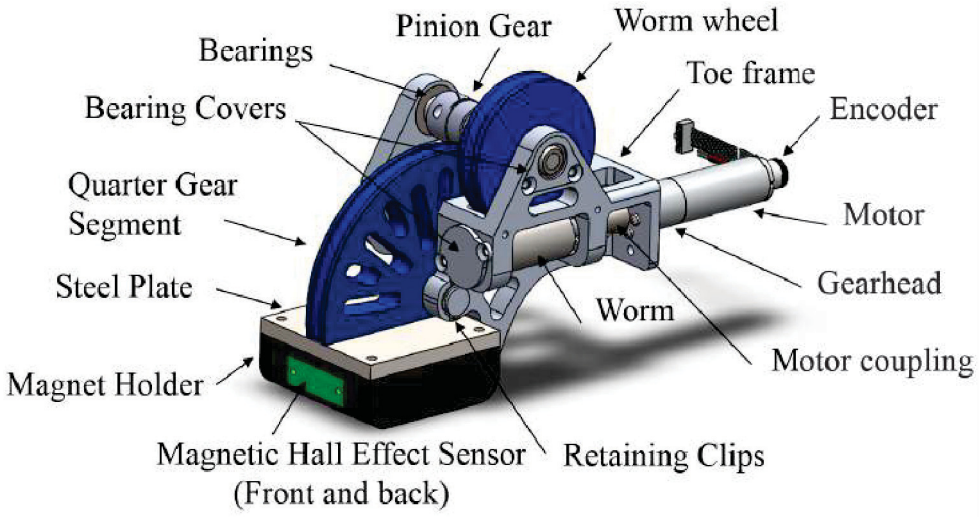

FIGURE 5.8: Magnetic adhesion module highlighting the primary components.

5.2.2.2 Revised Optimal Design

In optimising the design of the adhesion system, several of the constraint functions and fixed variables must be updated to accommodate changes in the design.

Firstly, to account for the added electronics, cameras and housing design parameters such as the toe frame dimensions, frame thickness and the shape, it is assumed that a hollow rectangular frame section is used, with its length being the radius of the adhesion system. The width and height of the hollow rectangular section are such that the electronics and cameras can be contained within, as illustrated in Fig 5.9. This design also increases the rigidity of the adhesion system.

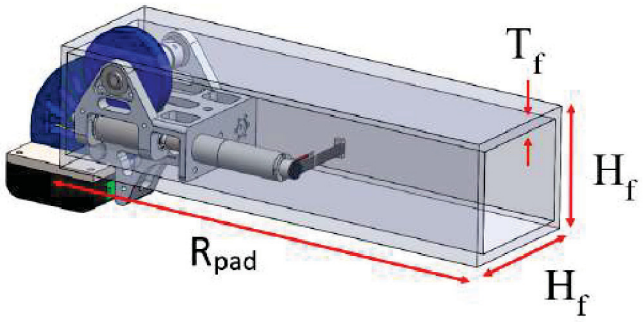

FIGURE 5.9: Revised frame design for optimisation model. A hollow rectangular section is assumed with length of R_{pad}, cross section length and height of H_f and thickness T_f. These parameters can be set to allow components such as electronics, cameras and sensors to be contained within the adhesion system.

The revised formulae for the frame weight is,

$$Vol_1 = H_f \times H_f \times R_{pad} \tag{5.1}$$

$$Vol_2 = (H_f - 2 \times T_f) \times (H_f - 2 \times T_f) \times R_{pad} \tag{5.2}$$

$$W_f = \rho_{Alum} \times (Vol_1 - Vol_2) \tag{5.3}$$

The revised peeling mechanism includes extra robustness in strength, rigidity and performance in comparison to the original peeling mechanism. An approximate scaling law between the mass of the revised peeling module and the torque has been determined through an empirical analysis. The torque required to peel the magnet M_m has been approximated by

$$M_m = F(D_m, T_m) \times \frac{D_m}{2} \tag{5.4}$$

$$W_{pm} = \sqrt[2]{\frac{M_m}{35}}. \tag{5.5}$$

Secondly, the properties used to normalise each of the performance criteria must be reconsidered with respect to the weight and performance characteristics of newly chosen actuators.

Performing a static torque analysis of the robot in a cantilevered pose, the maximum footpad weight, such that the joints do not operate above continuous operating current,

is determined to be 4kg. For full details of analysis, refer to Appendix B. A footpad weight above this, increases the expected torque of the first joint above its nominal torque. Therefore $W_{max} = 4kg$.

The weight of the robot minus the adhesion system is then approximated to be the sum of the weight for the seven joints, wiring, electronics and fasteners, being $W_r = 6kg$. The length of the robot minus the adhesion systems is $L_r = 0.64m$. The radius of the footpad is constrained to a maximum of $R_{pad} = 0.15m$, due to the width of the manholes. The height of the pad is must be at least $H_p = 0.05m$ so that the camera and 3D sensor can be contained with the unit. The weight of the components which will be contained within the footpad is $W_b = 0.5kg$. The characteristics of the frame which support the adhesion modules are $T_f = 0.003m$, $H_f = 0.05m$ and $\rho_{Alum} = 2700kgm^{-3}$. The density of the steel back plate is $\rho_{Steel} = 8000kgm^{-3}$ and the density of the magnets is $\rho_{NdFeB} = 7501kgm^{-3}$. A coefficient of static friction for rubber on a dry painted surface is used, $\mu_s = 0.6$.

The working code for the optimisation, exhaustive global search function, and plotting functions can be found in Appendix D.

The results from the objective function have been normalised between 0 to 1 and plotted in Fig 5.10 optimising for a 3mm air gap and in Fig 5.11 optimising for a 5mm air gap. Comparing the results in optimising for a 3mm air gap to a 5mm air gap, it is evident that when small air gaps there are two peaks present. One is for a large diameter and reduced thickness, and the other for a reduced diameter and larger thickness. Although a large diameter magnet with reduced thickness provides high holding forces with reduced weight, the torque required to peel the magnet is also increased. Consequently the mass of the peeling module also increases. In this instance the larger diameter is more optimal for the 3mm air gap scenario.

When considering the optimisation results a 5mm air gap, it is evident that the results favour a thicker magnet with smaller diameter, and the second peak is no longer present; in fact many solutions are no longer valid.

Identifying the global minimum from of objective function, the optimal design parameters for a 5mm air gap are determined to be, $R_{pad} = 150mm$, $D_m = 33.5mm$ and $T_m =$

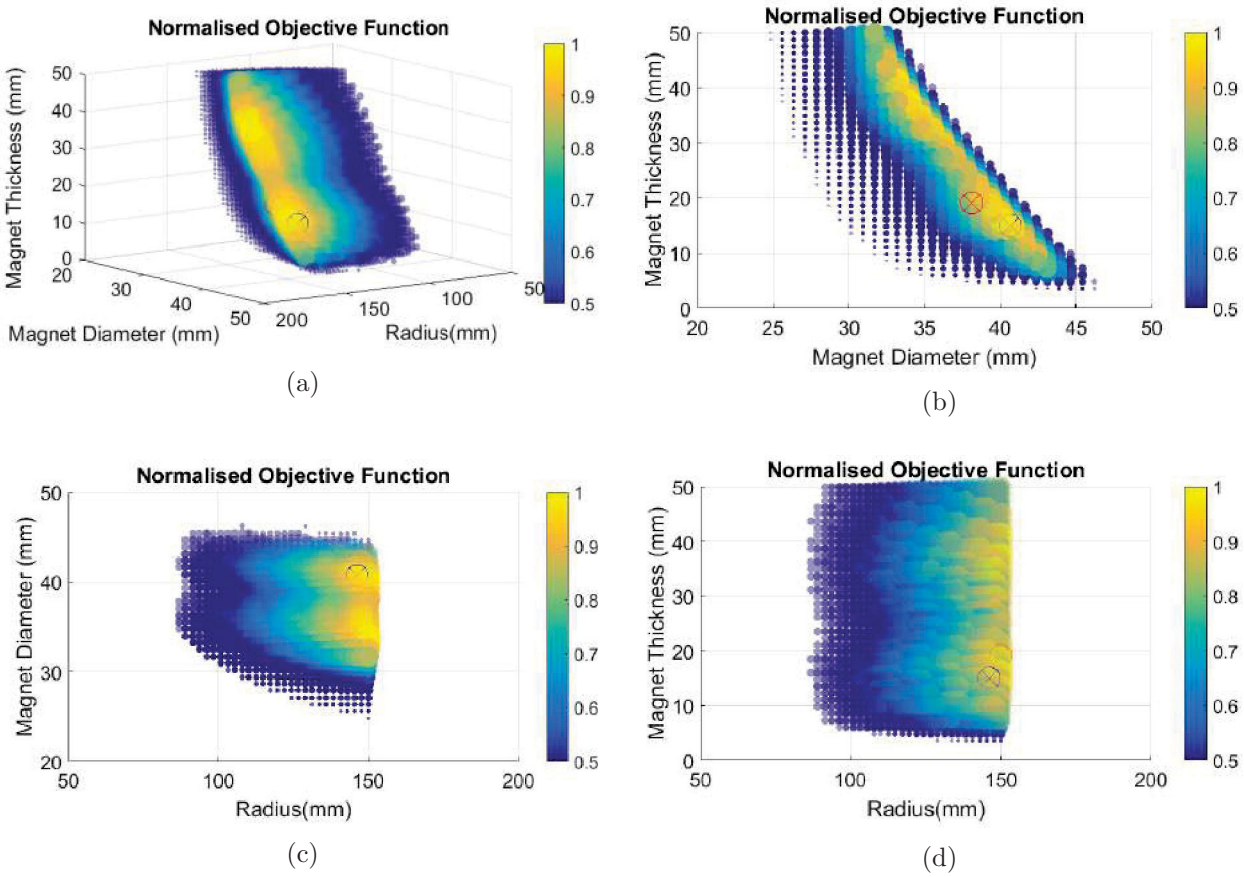

FIGURE 5.10: Results of the optimisation model for a 3mm air gap, plotting the objective function values. The number of magnets, n is not shown, however the objective function values are influenced by n. Objective function values have been normalised between 0 to 1 for plotting purposes, markers scale with increasing value, and colour of markers become yellow as they approach the global minimum of the objective function. The optimal solution is circled in blue and the constructed solution is circled in red. (a) Normalised objective function values comparing magnet diameter, magnet thickness and the radius of the adhesion system. (b) Normalised objective function values comparing the magnet diameter to the magnet thickness. (c) Normalised objective function values comparing magnet diameter to the radius of the adhesion system. (d) Normalised objective function values comparing magnet thickness to the radius of the adhesion system.

$39.9mm$. Once again, no off-the-shelf magnet for the given size was identified. The closest magnet in terms of weight, grade, strength was a rectangular $N52$ $38.1 \times 38.1 \times 19.1$ neodymium magnet. Entering these parameters into the equations used for the optimiser, the performance of the footpad was determined to be feasible for both 3mm and 5mm air gaps. Figures 5.10d and 5.11d plot the location of the selected magnet size against the optimised solutions. Table 5.1 summarises the difference in performance between the

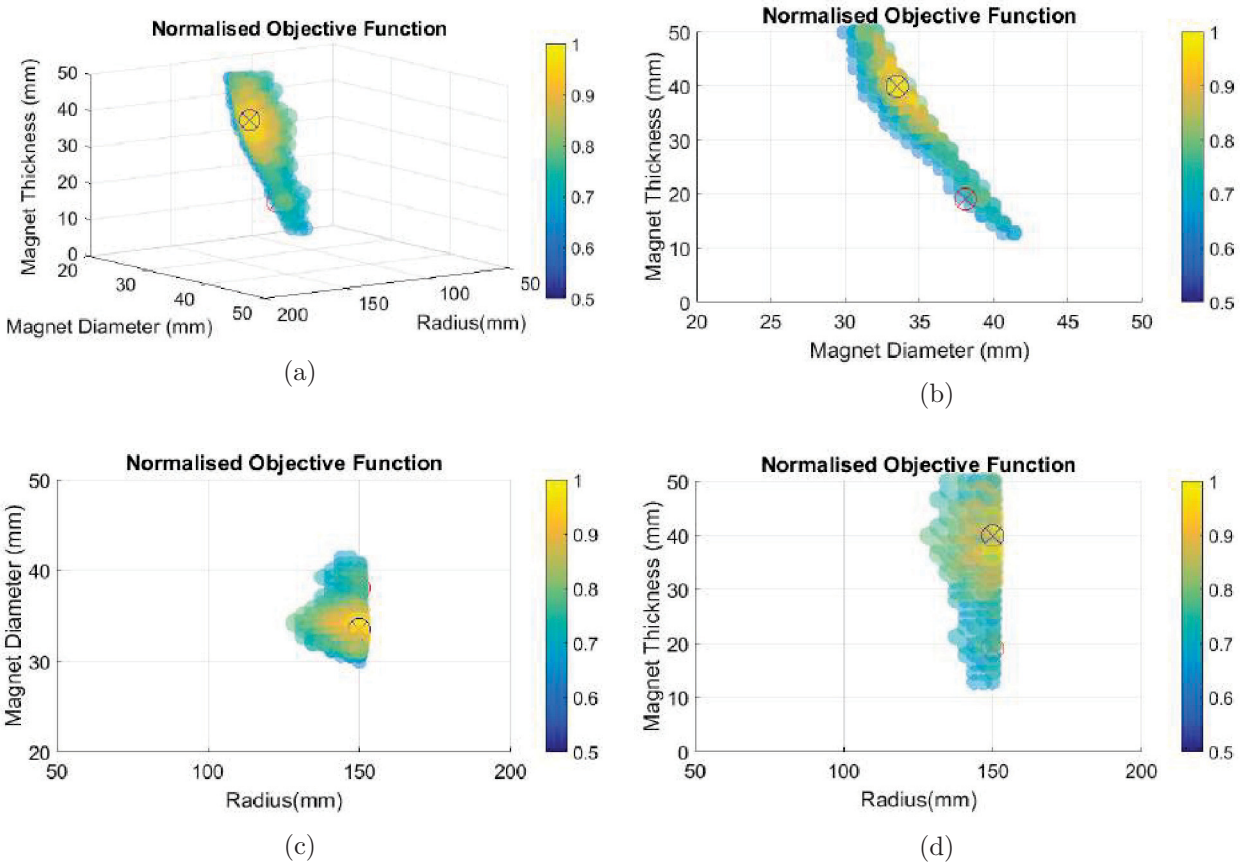

FIGURE 5.11: Results of the optimisation model for a 5mm air gap, plotting the objective function values. The number of magnets, n is not shown, however the objective function values are influenced by n. Objective function values have been normalised between 0 to 1 for plotting purposes, markers scale with increasing value, and colour of markers become yellow as they approach the global minimum of the objective function. The optimal solution is circled in blue and the constructed solution is circled in red. (a) Normalised objective function values comparing magnet diameter, magnet thickness and the radius of the adhesion system. (b) Normalised objective function values comparing the magnet diameter to the magnet thickness. (c) Normalised objective function values comparing magnet diameter to the radius of the adhesion system. (d) Normalised objective function values comparing magnet thickness to the radius of the adhesion system.

optimal solutions and the constructed solution.

TABLE 5.1: Comparison of optimal design results and constructed design results for a 3mm air gap and a 5mm air gap.

			Optimal Adhesion System 3mm Air Gap	Optimal Adhesion System 5mm Air Gap	Theoretical Adhesion System
3mm air gap	Design Variables	Number of Magnets	3	3	3
		Footpad Radius (mm)	146.2	150	150
		Magnet Diameter (mm)	40.7	33.5	38.1×38.1
		Magnet Thickness (mm)	15.0	39.9	19.05
		Weight (kg)	4.0	4.0	3.8
	Performance Criteria	Pull Force (N)	917.5	893.4	843.8
		Slip Force (N)	550.5	536.0	506.3
		Bending Moment X (Nm)	89.4	89.3	84.4
		Bending Moment Y (Nm)	77.4	77.4	73.1
		Torsion (Nm)	80.5	80.4	75.9
	Normalised Performance Criteria (FOS)	N_{F_p}	6.7	6.5	6.3
		N_{F_s}	6.7	6.5	6.3
		N_{M_x}	1.8	1.8	1.7
		N_{M_y}	1.5	1.6	1.5
		N_T	2.7	2.7	2.6
		N_{W_p}	0.12	0.13	0.13
		F_x	-40.3	-37.6	-34.1
5mm air gap	Performance Criteria	Pull Force (N)	370.9	638.5	575.4
		Slip Force (N)	618.1	383.1	345.2
		Bending Moment X (Nm)	60.2	63.8	57.5
		Bending Moment Y (Nm)	52.2	55.3	49.8
		Torsion (Nm)	54.2	57.5	51.8
	Normalised Performance Criteria (FOS)	N_{F_p}	4.5	4.7	4.3
		N_{F_s}	4.5	4.7	4.3
		N_{M_x}	1.2	1.3	1.1
		N_{M_y}	1.0	1.1	1.0
		N_T	1.8	1.94	1.76
		N_{W_p}	0.13	0.13	0.13
		F_x	-5.6	-7.7	-5.0

5.2.2.3 Constructed Adhesion System Overview

The configuration was revised such that the peeling orientations could effectively negotiate channel scenarios. By allowing all magnets to rotate in the same axis, the toes could be adjusted so that they sit flat on two different planes, or even on curved planes. In doing so, Toe 1 and Toe 3 rotate to less than 90°, whilst Toe 2 rotates over 90°, as pictured in Fig 5.12a .

The adhesion system configuration and the size of toes were verified against several known application scenarios on the Sydney Harbour Bridge. These include the ability to step between rivets, on channels (Fig 5.12a) and pass through, and stand on manhole partitions (Fig 5.12b). The width of the adhesion system has increased beyond the width of the manhole in order to accommodate the increase in weight and bending moment. Figure 5.12b compares the size of the footpad to the manhole size, and demonstrates how the robot body must be contained within the height of the footpad.

Each toe assembly is housed by a titanium hinged cover which encases the toe module and prevents the build up of ferromagnetic particles on the magnets whilst in the detached state, as seen in Fig 5.13 . The hinged cover allows the toe to attach to surfaces with $\pm 15°$ from a flat surface. Titanium sheet of 0.5mm thickness is used so that the air gap between the magnet and surface can be reduced, whilst maintaining strength of the covers.

A 1.5mm layer of natural rubber is adhered to the titanium cover to increase friction between the toe covers and the surface, and also to protect the surface. A Teflon sheet is used to allow slip between the magnet and the hinged titanium cover during attachment and detachment. A worm gear has been added to prevent back driving of the toes when they are not powered.

5.2.2.4 Sensing

Several methods of sensing were implemented for the robots' adhesion system. The first implementation used a mechanical on/off limit switch to detect contact with the surface plane. However the limit switches were not robust against surface irregularities and if not positioned accurately they were either subject to the full adhesive load or not switched

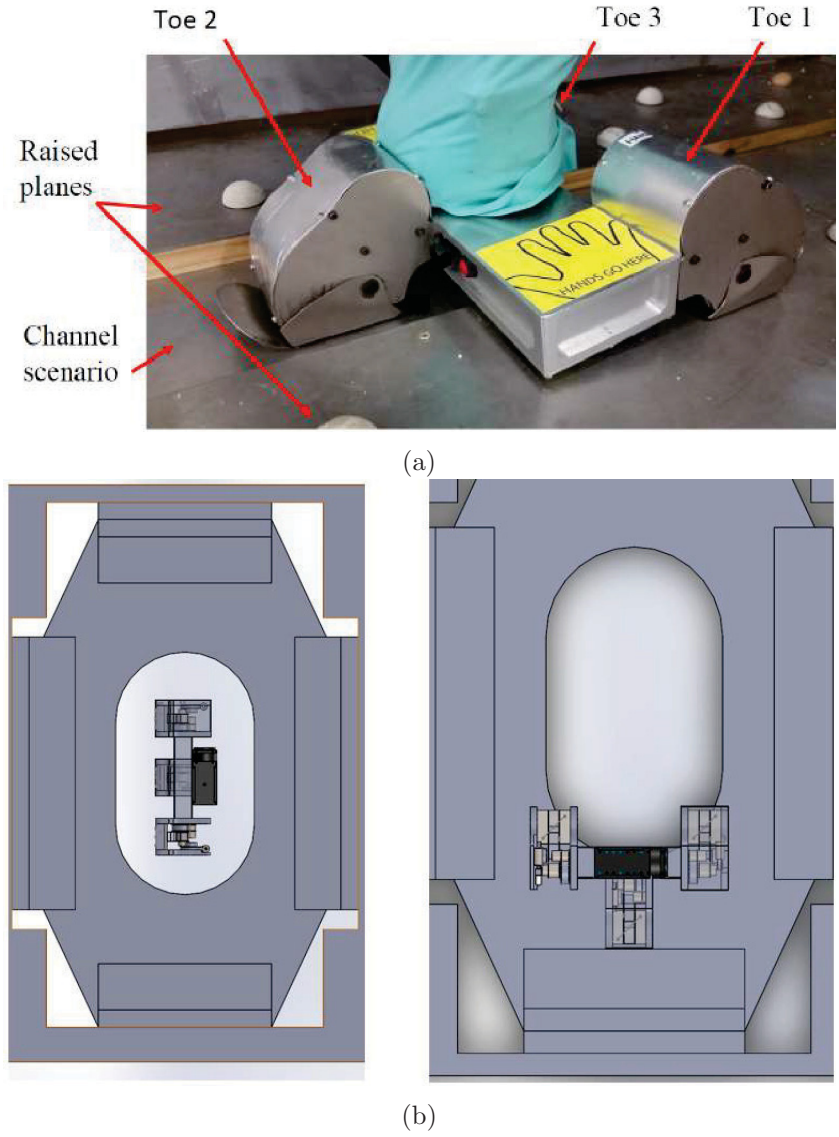

FIGURE 5.12: Modelling of newly optimised adhesion system against different application scenarios. (a) Channel scenario. (b) Passing through manhole. (c) Identifying potential attachment locations to manhole partition plate.

at the right time and magnet orientation. A custom surface contact sensor was designed using a spring loaded brass rod which would protrude from different locations surrounding the magnet as illustrated in Fig 5.14a. As the toe attaches to the surface, the springs are compressed and the rods retract into the toe. Analogue photo-interrupters are used to measure the change in light intensity as the brass posts interrupt the optical transmitter. The analogue output from the optical receiver is converted to a surface compliance rating to determine whether the toe has reached a fully attached state. The sensor operates like

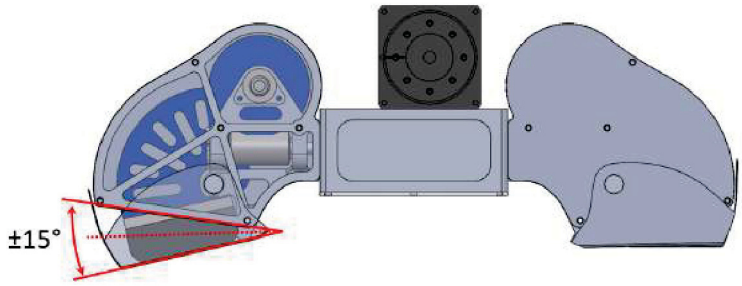

FIGURE 5.13: Hinged toe cover made from 0.5mm Titanium sheet, prevents build up of ferromagnetic material in the detached state, and permits attachment to varying inclinations required for walking along channels. 1.5mm rubber sole is adhered to underside of toe cover.

an analogue limit switch without being subject to the adhesive load. Testing the device posed several issues, firstly, there is no feedback regarding the actual adhesion strength. Secondly, since the device is not able to measure surface compliance directly under the toe, the sensor is not triggered on contact with surface irregularities and rivets.

To resolve these issues, an improved design using Force Sensing Resistors (FSRs) was investigated. A FSR was fixed directly to the underside of the magnet and coated in a layer of polyurethane, as illustrated in Fig 5.14b. The pressure applied to the FSR, changes the resistance of the device which can be used to a holding force. However, this configuration did not yield sufficient accuracy and repeatability, as the FSRs are largely pressure dependent, that is to say the force depends on the area of contact which largely fluctuates with surface irregularities.

Figure 5.14c illustrates an alternate FSR configuration, mounting the FSR between the magnet and a magnet enclosure. In this configuration the area of contact on the FSR is consistent due to the equal load distribution applied by the magnet. As the toe is brought into proximity to a ferromagnetic surface, the increasing force applied to the pad could be measured to within 10% accuracy with good repeatability. Unfortunately the force is approximately proportional to 2-3 power of the air gap, therefore the additional 1.5mm air significantly reduces the effectiveness of the adhesion system.

The final implementation of adhesion sensing involves measuring the magnetic flux density in the proximity of the magnet. Analogue bipolar Hall Effect sensors were mounted front and back of each magnet as illustrated in Fig 5.14d. As the magnet rotates toward the

surface, the sensor output responds linearly to increases in the magnetic flux density. Hall Effect sensors provide accurate and repeatable output for the magnetic flux density, allowing estimates of the adhesion force, and also the thickness of the air gap due to paint, dirt and rust when calibrated against an ideal surface. By comparing the sensor output for Hall Effect sensors on either side of a magnet, the adhesion system can also determine whether the orientation of toe is optimally aligned with the target surface to maximise the magnetic flux density surrounding the magnet. This can be achieved by adjusting the final position of the magnets until both outputs are maximised.

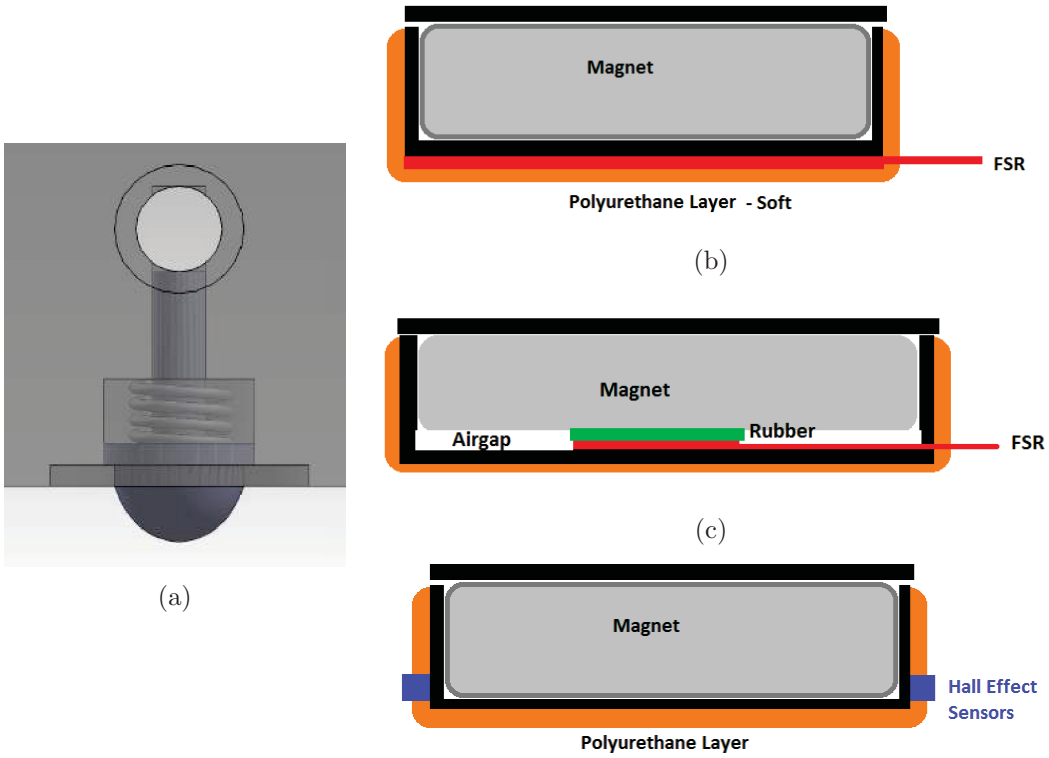

FIGURE 5.14: Methods of adhesion sensing tested. (a) Electromechanical opto-interrupter-sensing measures the travel of spring loaded rod on contact with surface. (b) Force Sensing Resistor (FSR) installed beneath magnetic toe measures the effective pressure due to applied magnetic force on contact with surface. (c) Alternate FSR configuration to measure applied pressure, does not required contact with surface, however increases the air gap. (d) Hall Effect sensors mounted on either side of the magnet measure the magnetic flux density which increases in proximity of ferromagnetic surface. The output is approximated to a holding force.

Each toe is also equipped with position encoders and current sensors. The position sensors provide feedback to the final resting angle that magnet stops at, which can also be used to indicate a surface irregularity. Current sensing and power regulation was also a noteworthy method of attachment sensing. By monitoring the current it is possible to determine whether a magnet is attached or not.

5.2.3 Climbing Ability

In determining the climbing capabilities of the improved robot design, several climbing traits have been considered and trialled in a test structure representative of a hollow box girder section from the Sydney Harbour Bridge.

5.2.3.1 Locomotion Gaits

The robot has two primary forward stepping gaits; these are referred to as the shuffle step and the flip step. The shuffle step, is inspired by the inchworm, and may be necessary when approaching obstacles so that it can adjust its approach distance and perform a particular manoeuvre. The shuffle step can travel up to 640mm for a single step going from its minimum step length of 170mm. The flip step allows the robot to travel 1280mm in a single step.

5.2.3.2 Planar Climbing Ability

The robot's capability to climbing planar surfaces in any orientation with respect to gravity is tested. Figures 5.15a to 5.15f demonstrate the robot climbing on the floor in an upright orientation. The robot is able to perform the shuffle and flip step on ferromagnetic surfaces with the full step size. It is able to use a flip step with a step size up to 340mm on non-ferromagnetic surfaces. The step size is limited on non-ferromagnetic surfaces due to instability from lack of adhesion. Figures 5.15g to 5.15l demonstrate the robot climbing horizontally on the wall, Fig 5.15m to 5.15r demonstrate climbing inverted on a ceiling, Fig 5.16i to 5.16g demonstrate vertical climbing.

5.2.3.3 Plane Transitions

The robot's ability to perform all plane transitions between 0° to 180° both concave and convex, in any orientation with respect to gravity has been tested. Within the robot's entire workspace there are no stability issues relating to adhesion or joint torques, even under dynamic loads. Figures 5.16 shows the robot transitioning from the floor plane to the vertical plane, proceeding up the vertical plane then transitioning the ceiling. This example demonstrates the robot climbing in a worse case foot pad orientation, whereby orienting the single toe upwards significantly reduces the total adhesive bending moment, by almost half.

Figure 5.17 demonstrates further complex transitional capabilities of the robot. Figures 5.17a to 5.17h show the robot performing the 180° thin plane transition, while Fig 5.17i to 5.17l shows the robot performing a discontinuity transition between two planes.

The robot has clearly been demonstrated with the ability to perform complex climbing motions and transitions in orientation with respect to gravity.

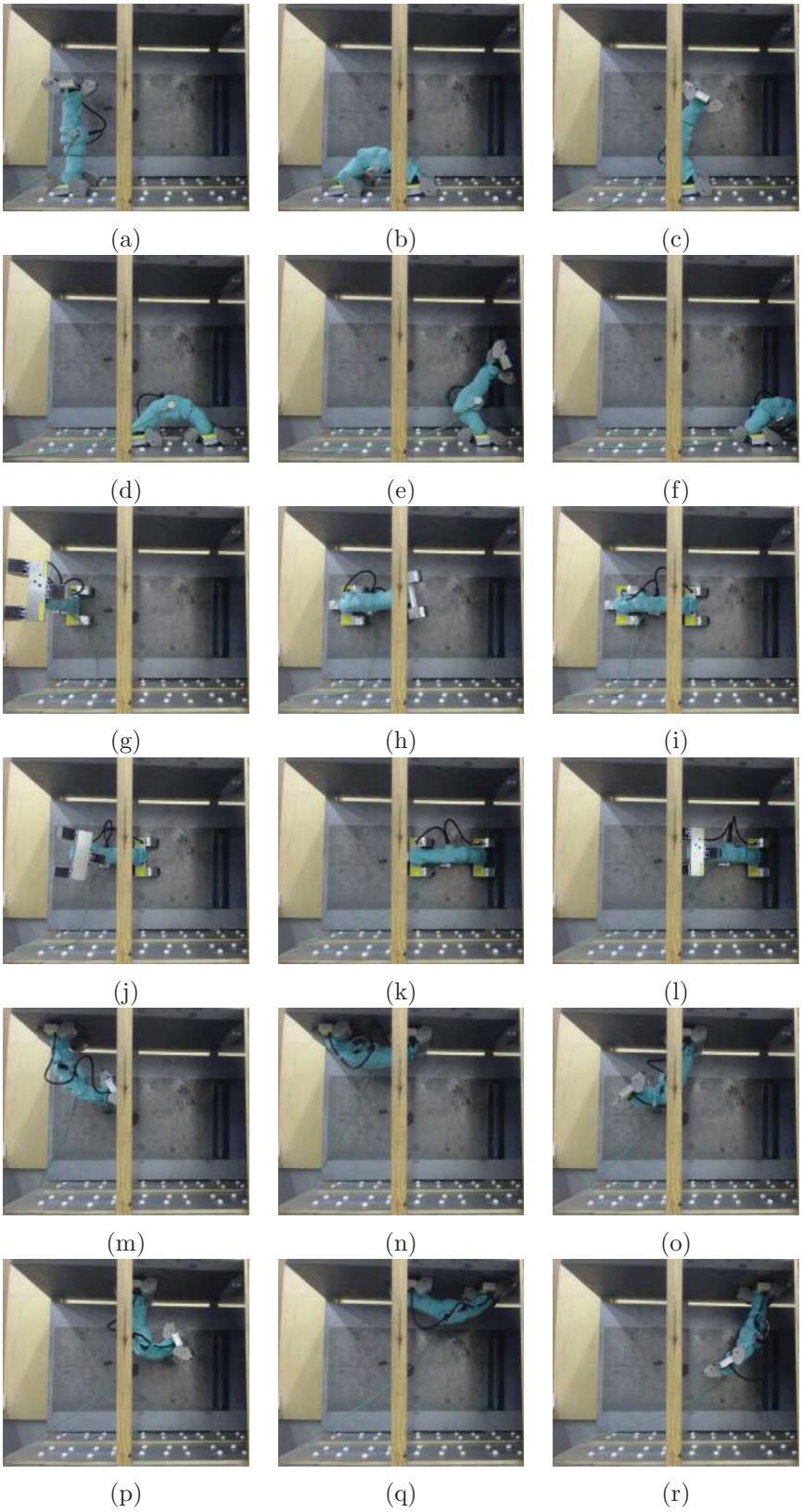

FIGURE 5.15: Demonstration of the inchworm-inspired climbing robot performing floor, wall, roof climbing. (a)-(f) Upright floor climbing in the test environment. (g)-(l) Horizontal wall climbing. (m)-(r) Inverted ceiling climbing.

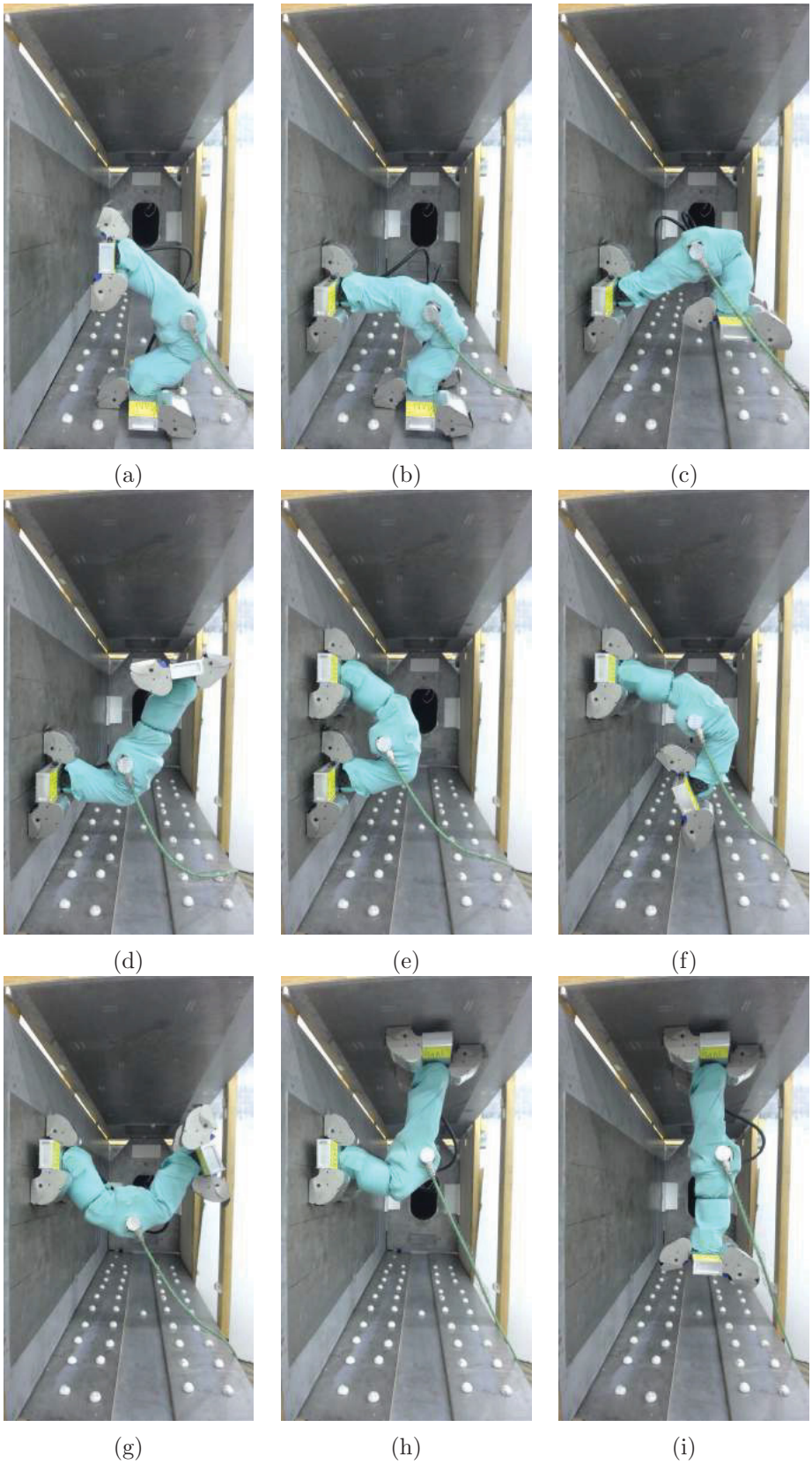

FIGURE 5.16: Demonstration of the inchworm-inspired climbing robot performing concave plane transitions. Climbing in orientation of weakest adhesion moment, one toe up. (a)-(c) Concave plane transition from floor to wall. (d)-(f) Vertical wall climbing. (g)-(i) Concave plane transition from floor to wall.

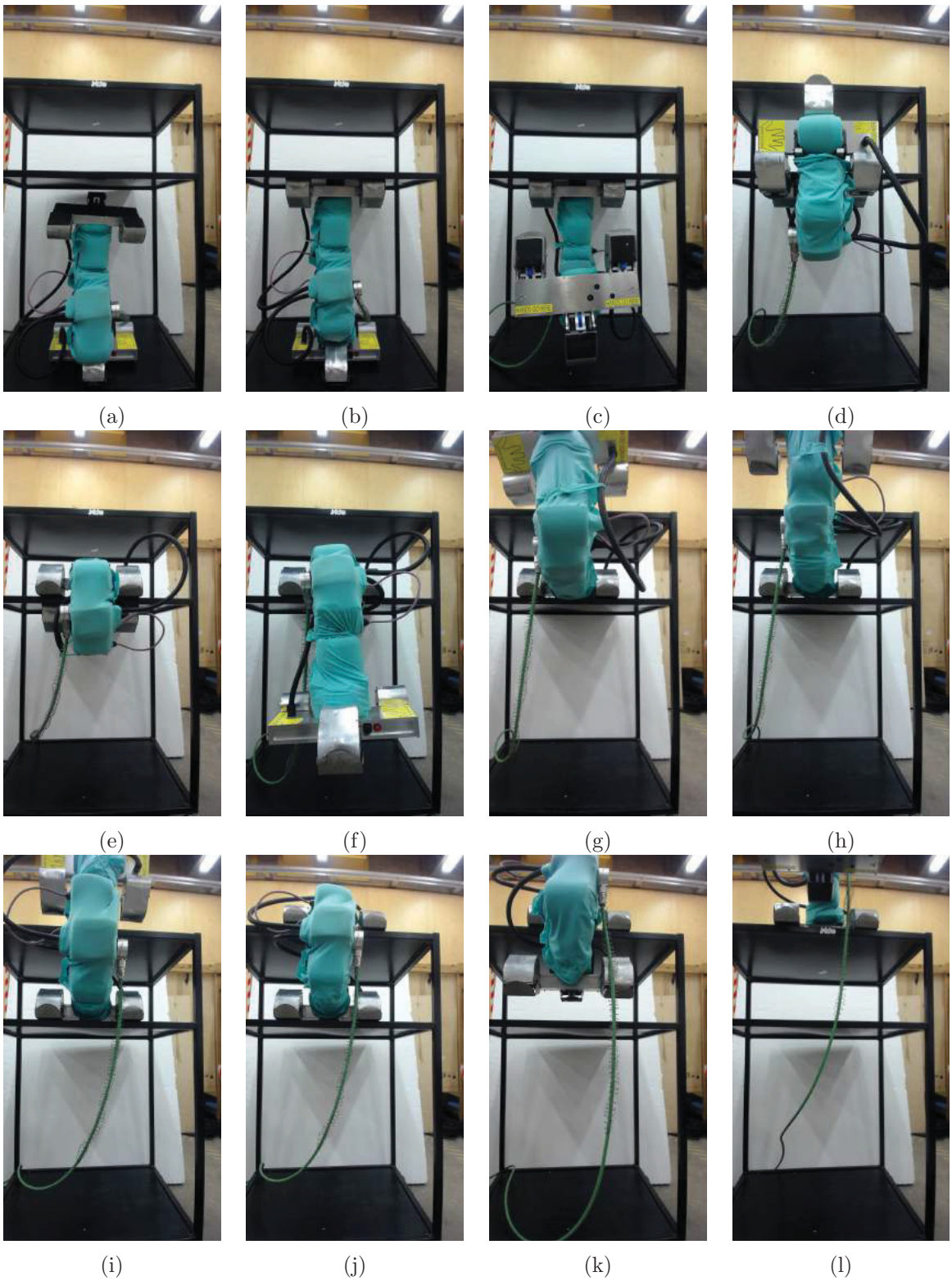

FIGURE 5.17: Demonstration of the inchworm-inspired climbing robot performing 180° plane transition and discontinuity transition.

5.2.4 Real World Deployment: Results, Challenges and Lessons Learnt

Despite the significant research into climbing robots for applications in industry, there is little information available on the practical deployment of such robots. Through the course of over 50 site trials in the archways of the Sydney Harbour Bridge many challenges have been faced. The results from these trials are presented and the lessons learnt are briefly discussed to aid in the design of climbing robots for practical use.

5.2.4.1 Deployment

A significant consideration is how the robot will be deployed. There are many constraints in the deployment including the system weight, system size, length of tether, power requirements and the access to site. The archways of the Sydney Harbour Bridge present a level 6 containment zone, requiring access to confined spaces whilst being at heights. Furthermore in order to access the intended site, 134m above water, the equipment must be light enough and ergonomic to carry. The two backpack carry frames seen in Fig 5.18 were developed to carry the robot, control unit and tether. Each back pack weighs 18kg.

(a) (b)

FIGURE 5.18: Backpacks used to deploy robot at site. (a) Two backpacks are shown, top, containing control unit and tether, bottom, containing robot. (b) Each backpack is 18kg and uses ergonomic straps for the inspectors to carry.

Before performing an inspection, review of WHS requirements are mandatory. Although climbing robots are primarily intended to reduce WHS issues, they have the potential to impose new issues such as ergonomics and falling objects from heights. Whilst working at heights, all systems must be tethered to the structure as seen in Fig 5.19a . In this respect, the tether system has been designed such that it is strong enough to support the

weight of the robot. In order to place the robot into the confined space, a tripod and hoist are used to reduce manual handling as shown in Fig 5.19b.

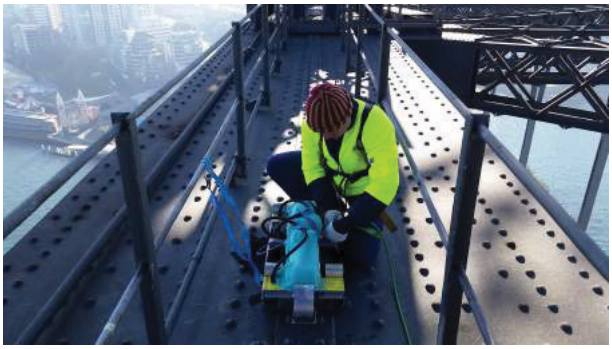

(a)

(b)

FIGURE 5.19: RMS Bridge Inspector deploying CROC at site. (a) Robot system is secured to structure, tether is being attached. (b) Robot is lowered into the confined space of the arch.

5.2.4.2 Operation

A user interface has been developed to guide the bridge inspectors through the set-up procedure. Following the on-screen prompts from the user interface, the robot is lowered into the confined space, the head of the robot attaches to the wall, and the foot detaches from the hoist system, as seen in Fig 5.20a to 5.20c. It then proceeds to perform fully autonomous operation under the supervision of the bridge inspectors as seen in Fig 5.20d to 5.20o. During the fully autonomous operation the robot performs exploration, mapping, localisation, motion planning, and collision avoidance operations for each step. The task definition for the robot has been programmed such that the robot climbs along the chord,

collecting inspection images until instructed to stop. A video of the full operation can be found at [108] .

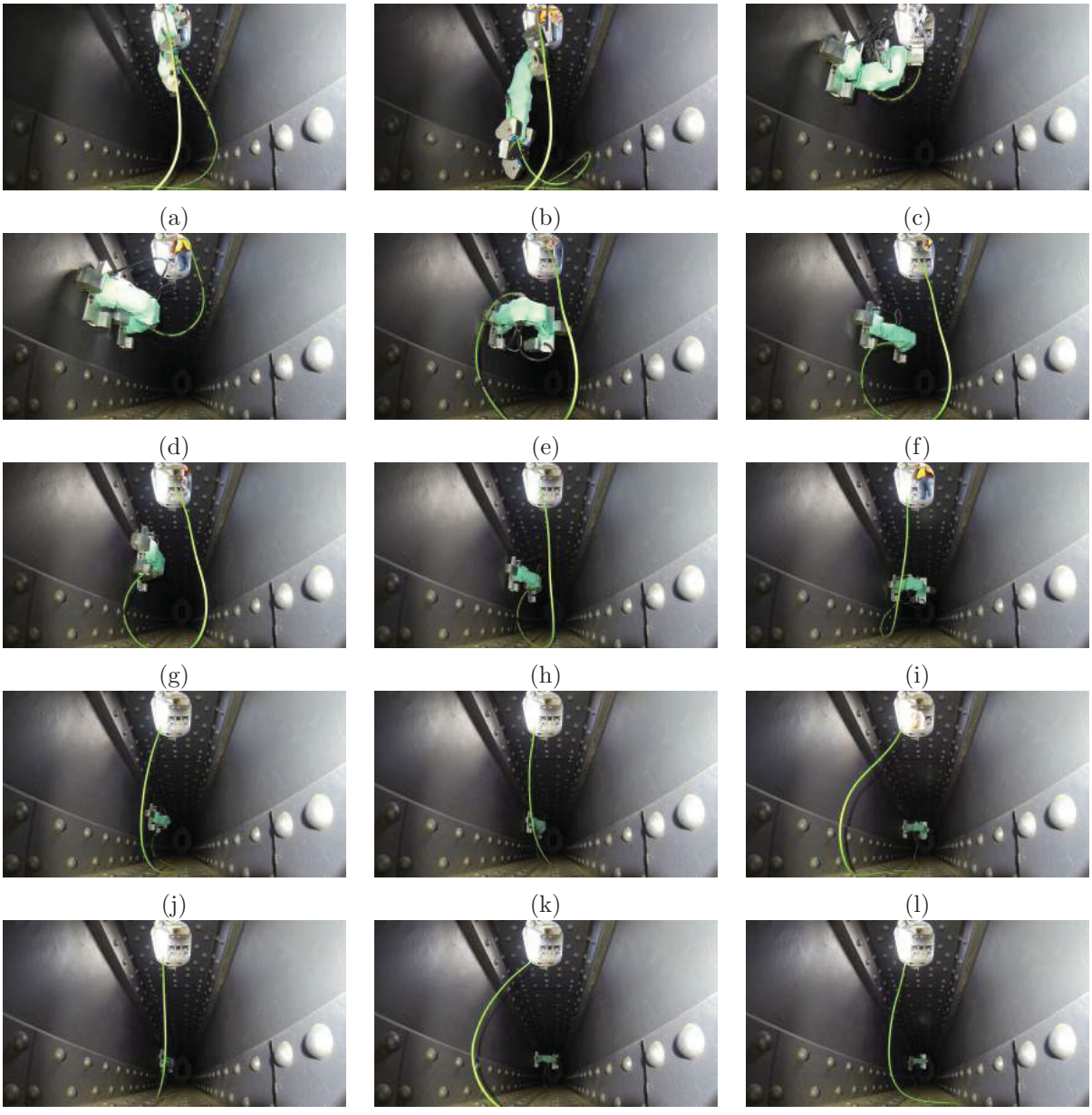

FIGURE 5.20: CROC inspecting internal box girder section on the Sydney Harbour Bridge. More information on the intelligence and a video of the operation can be found at [108] .

5.2.4.3 Robot Intelligence

CROC is able to operate fully autonomously once deployed. There has been significant research on efficient algorithms on mapping, visual processing, situation awareness, localisation, planning and collision avoidance in order to develop the intelligence required for CROC to operate autonomously in such complex scenarios.

These algorithms are not within the scope of this thesis, for more information refer to the following research papers.

- P. Quin, G. Paul, A. Alempijevic, D.K. Liu, G. Dissanayake (2013), Efficient Neighbourhood-Based Information Gain Approach for Exploration of Complex 3D Environments, Proceedings of the 2013 IEEE International Conference on Robotics and Automation (ICRA), Karlsruhe, Germany, May 6-10, 2013, pp1335-1340.
- Phillip Quin, Gavin Paul, Dikai Liu, Alen Alempijevic (2013), Nearest Neighbour Exploration with Backtracking for Robotic Exploration of Complex 3D Environments, Proceedings of Australasian Conference on Robotics and Automation, 2-4 Dec 2013, University of New South Wales, Sydney Australia, 8 pages
- G. Paul, S. Mao, L. Liu, and R. Xiong, Mapping Repetitive Structural Tunnel Environments for a Biologically Inspired Climbing Robot, in Proceedings of the 18th International Conference on CLAWAR, 2015, pp. 110.
- G. Paul, P. Quin, C. Yang, and D. Liu, Key Feature-based Approach for Efficient Exploration of Structured Environments, in Robotics and Biomimetics (ROBIO), 2015 IEEE International Conference on, 2015.
- G. Paul, P. Quin, A. Wing, K. To, and D. Liu, A Sliding Window Approach to Exploration for 3D Map Building Using a Biologically Inspired Bridge Inspection Robot, in Proceedings of the IEEE International Conference on CYBER Technology in Automation, Control, and Intelligent Systems, 2015, pp. 10971102.

Figure 5.21 demonstrates the process in which CROC has mapped the environment, identified and located a manhole, assessed numerous possible candidates for safe attachment

points, determined the quickest path to the manhole and calculated a safe moving trajectory between each of the attachment points.

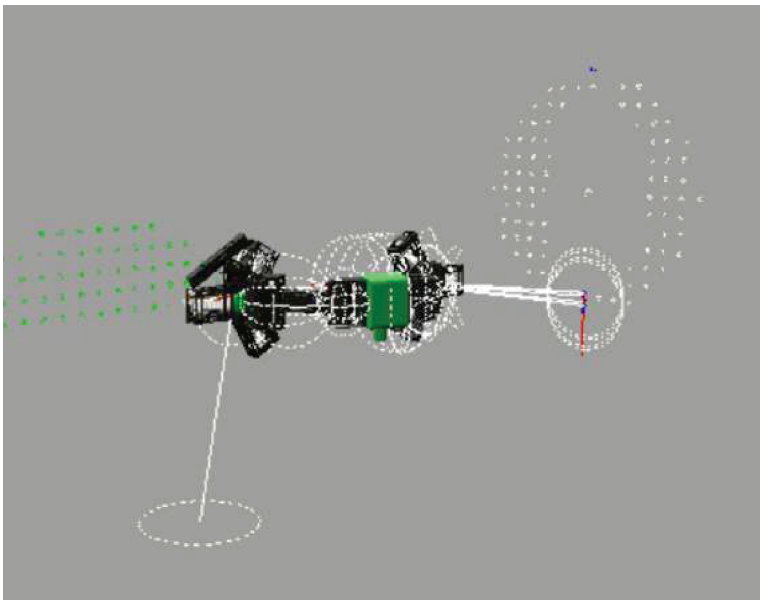

FIGURE 5.21: CROC performing planning in lead up to reach manhole and perform manhole transition.

5.2.5 Discussion on Limitations

Following the extensive testing of the robot, several limitations have been identified. These do not effect the deployment for the given task definition; however it may effect deployment in other application scenarios.

- **Narrow sections:** Due to the size of the foot pad, the robot is limited to walking on planes which are at least as wide as the footpad, being 300mm. Truss section which are narrower than this can not support the robot and would require an alternative footpad design, preferably a mechanical gripper.
- **Deflection in body:** Although the robot has increased rigidity compared to the prototype robot, deflection in the body is still noted and compensated for. In a worst-case scenario, being a cantilevered pose, the robot observes $\pm 1.5°$, and 23mm deflection. In typical operating conditions the robot experiences $0.6°$ and 10mm

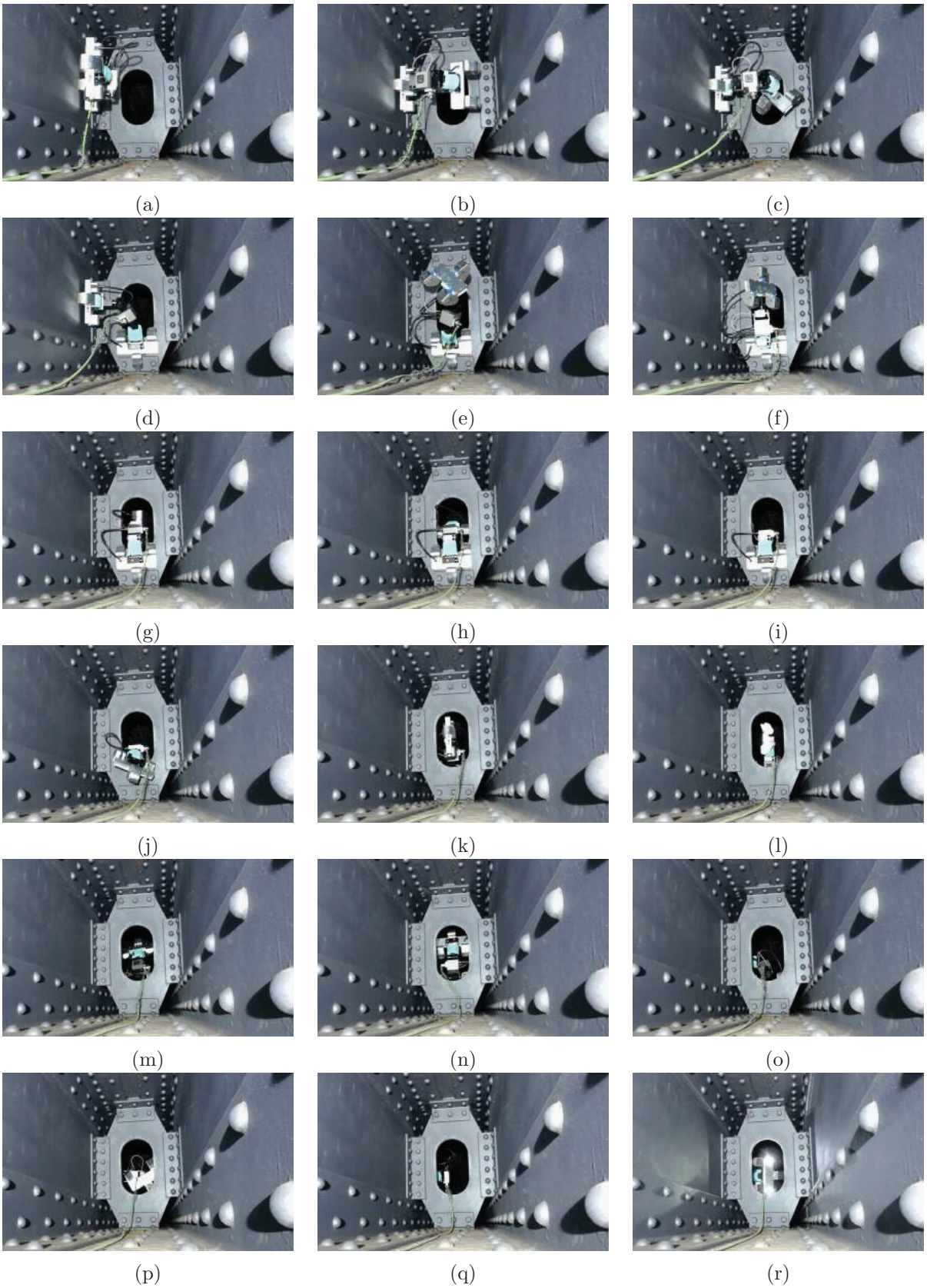

FIGURE 5.22: CROC performing 180° plane transition though a manhole on site at the Sydney Harbour Bridge. Video of the manhole transfer can be found at [108] .

deflection. The deflection is largely based on the orientation of the actuators and brackets during motion, and the load due to the pose.

- **No brakes:** The actuators have no built in brakes, therefore in high torque poses the robot is susceptible to eventually over heating. The brakes would aid to maintain a pose without using power and prevent overheating.

- **Transition discontinuities:** The robot is only capable of transitioning discontinuities within its workspace, up to its maximum step size of 600mm.

- 180° **plane transitions:** The robot is only able to perform 180° plane transitions up to 100mm in thickness. This is limited by the link lengths.

- **Steel substrate and air gap:** The magnetic adhesion system is limited by an air gap of up to a maximum of 7mm, which may be due to a build-up in dirt, rust and/or paint. There is also a requirement for the steel surface to be greater than 5mm in thickness to maintain the designed factor of safety. Assuming no air gap is present, the steel thickness may be 1.5mm before reaching the fail point of the adhesion system. The type of steel will also affect the magnetic force and performance of the adhesion system, all performance calculations have been based on structural steel. It should be noted that some steels may be non-magnetic by nature.

- **Radius of curvature:** The design of the magnetic adhesion modules limits the usable attachment angles of the magnets. The angle has been designed to accommodate the channel scenario where toes need to extend up to ±10° from horizontal. This also accommodates steel pipes with a radius greater than 450mm.

- **Tether management:** The tether poses several challenges for the operation of the robot. In its current state the robot has no knowledge or sensory feedback for the location of the tether. Future research will focus on modelling and sensing the tether location to provide information, such as strain, to avoid tension and twisting in the cable. In its current operation, the robot has some strategies to avoid trajectories or attachment locations that are likely to lead to an entanglement. The tether has a weight of 150grams per metre, at significant lengths or heights this will cause large drag forces which will affect the adhesion performance.

- **Payload:** The payload capability of the robot is largely attributed to the target material, the surface conditions and the desired factor of safety. Due to the symmetry in the design of the robot, an extra 350gram of equipment can be installed in the foot of the robot whilst maintaining equivalent adhesion performance. Table 5.1 can be used to determine the factor of safety at 3mm and 5mm air gaps for the given design. Strategies in the operation of the robot can be used to avoid poses where large adhesive moments are required.

Chapter 6

Conclusions

The aim of this research has been to develop a climbing robot with high capability in overcoming complex obstacles such as the manhole scenarios found in the archways of the Sydney Harbour Bridge. In developing the climbing robot the research focused on designing a robot configuration and adhesion system which could tackle the challenges faced by the current state of the art climbing robots on complex steel structures.

As a result of this research, CROC, a biologically inspired climbing robot has been designed and developed to accommodate the task definition and intended application scenarios. CROC robot has been demonstrated with greater mobility in comparison to the known state of the art climbing robots, with the ability to perform 180° plane transitions and climb through manholes in real world inspection sites.

CROC has high potential for inspection of steel infrastructure in diverse industries around the world; these include the transport industry with steel infrastructure such as bridges; the maritime industry with shipyards and ship hulls; the energy industry with transmission towers, silos, coal chutes and surge bins. With increasing stringency in WHS regulations, robots like CROC will be in high demand. Where most climbing robots have lacked the ability to cope with the challenges faced in real world deployment, CROC has demonstrated a robust climbing ability and advanced autonomous operation.

6.1 Summary of Contributions

6.1.1 A Unique Biologically Inspired 7 DOF Robot Configuration with High Mobility

Biological inspiration from the inchworm caterpillar, namely the Geomtriade family of Lepidoptera, was used in developing CROC. This was based on investigating, and understanding how they are able to achieve their high mobility and manoeuvrability, and their ability to firmly grasp structures.

It has been discovered that the inchworm caterpillar follows isometric scaling, while inchworm type robots with rigid structures and serial actuator configurations are not scalable. This is a limitation due to the conflicting scaling laws between subsystems, in particular a control requirement to maintain rigidity for precise controllability, and technological limitations preventing actuators to scale with the required scaling laws.

The mobility of CROC is primarily due to the unique robot kinematics which permits high manoeuvrability. The robot configuration has been clearly demonstrated, achieving superior climbing ability on planar surfaces, and in performing complex plane transitions, both convex and concave up to $\pm 180°$, at any orientation with respect to gravity. The climbing ability allows the robot to access previously inaccessible inspection locations and carry out a broad range of tasks which require manipulation. This superior mobility extends the state of the art for known climbing robots.

Due to the configuration of the robot it is able to perform advanced manipulation tasks which benefits operations such as exploration, mapping, inspection and maintenance tasks.

6.1.2 A Novel Magnetic Adhesion Module

A magnetic adhesion module was designed and developed, which yields low weight, high capacity, high robustness to surfaces conditions, and is power-fail safe ensuring safe operation. The patented system uses a gear train with a quarter gear segment to provide attached and detached states on ferromagnetic structures.

6.1.3 An Optimisation Model to Design an Adhesion System

A generic optimisation model which can be fitted to different application requirements has been formulated. Given a particular adhesion module, the optimisation model maximises performance characteristics, and minimises the system weight and size. Experimental results and field trials validate the design model and performance for given constraints. The magnetic adhesion system is reliable and power-fail safe, therefore deployable for real world conditions on inchworm type climbing robots.

6.1.4 A Practically Deployable Climbing Robot for the Inspection of Steel Structures

The integration of the biologically inspired robot configuration and the novel adhesion system form a climbing robot for inspection of complex environments. The robot extends the state of the art in climbing robotics with its ability for traversing complex steel structures.

CROC has been integrated with all the necessary sensors, communication and computing hardware such that it is able to perform fully autonomous operation in complex and unknown environments. This is rarely demonstrated in climbing robots.

The climbing ability of CROC was initially demonstrated in a replica steel bridge structure, validating its ability to climb on planar surfaces, perform the full range of convex and concave plane transitions, and perform 180° plane transitions, all of which can be performed in any orientation with respect to gravity. Following verification in laboratory conditions, the robot has been extensively tested and deployed for use by RMS bridge inspectors in the intended environment, with over 50 site trials in the archways of the Sydney Harbour Bridge.

6.2 Discussion of Limitations

Despite the benefits of CROC, some limitations are noted in this research. These limitations should be considered for further research in improving CROC.

6.2.1 Robot Configuration

The design of the robot presented is not scalable. This means that for each change in the robot configuration, a full design review is required. In order to mimic the scalability of the inchworm robot, compliant actuators must be investigated. The robot configuration also limits the transitional ability across discontinuities of up to its body length, 180° plane transitions are limited in thickness by 100mm.

6.2.2 Adhesion System

The optimal design model requires a separate force model for every air gap and magnetic configuration that is to be consider. Obtaining these models is not a particularly easy task and the results should be verified experimentally. The magnetic configuration is chosen such that ferromagnetic surfaces with thickness of greater than 5mm are preferred; thinner steel surfaces may benefit from a different magnetic configuration with more adhesion modules. The current implementation of the adhesion modules is limited to use on round surfaces, such as steel pipes, given the radius of curvature is greater than 450mm. This is limited by the radius of the footpad and the quarter segment gear. For adhering to pipes of small radius the 90° gear segment could be increased further, to say 120° with minimal effect on the design and performance.

6.3 Future Work

There are several opportunities for future work. These can be split in three pathways; improvements to the current robot for inspection of ferromagnetic structures; expanding the capability of the robot for inspection of non-ferromagnetic structures; and expanding the task definition of the robot to include maintenance tasks.

6.3.1 Improvements to Current Robot for Inspection of Ferromagnetic Structures

Although the robot is able to carry out its task definition, there are several improvements which are proposed for the current system. This mainly concerns the intelligence, inspection outputs, speed, efficiency and climbing ability, and advancements with technology.

CROC is a suitable platform for developing and testing advanced algorithms and even artificial intelligence. The robot is already capable of environmental and situational awareness through sophisticated algorithms across exploration, mapping, localisation, planning and collision avoidance. These algorithms allow CROC to operate autonomously in completely unknown environments. In order to increase the speed of operation and inspection procedures, prior knowledge of the environment has been provided to reduce computations. With more efficient algorithms and improved computing hardware, the robot would be more capable in new environments. With research into machine learning, the robot could learn from its past operations to improve future operations. For example, the first planning operation in a new environment may take a long time to determine an optimal trajectory or path. However, using the knowledge of this path as a prediction for the next trajectory or path may improve computation speed. Likewise, using experiences in overcoming one obstacle may aid in overcoming another similar obstacle in the future. The robot can improve on future operations by learning from past operations, for example, by analysing differences in joint torques, trajectory speeds or complexity, completeness of maps or adhesion strengths.

CROC is able to collect 3D maps, HD RGB images and video which are used by inspectors for condition assessment. However, the robot could potentially carry out more detailed inspection and analysis of sites. In order to do this, the robot could be equipped with additional sensing hardware including Hyper-spectral imaging and numerous forms of Non-Destructive Testing (NDT) such as Hall Effect, eddy current and ultra sound. Incorporating these sensors would allow the robot to carry out detail analysis and automated condition assessment which previously has not been possible by humans due to the limitations in physically accessing the site to be inspected.

Further research with CROC can focus on studying dynamics, increase speed, trajectory efficiency and climbing ability.

CROC was largely determined with a analytical and empirical approaches, therefore there is much room for optimisation in the with changes in the configuration, link lengths and joint offsets across a larger set of application scenarios. Tools such as the Robotics Toolbox by Peter Corke can be used to study and evaluate performance measures such the robots workspace, manipulability and manoeuvrability.

6.3.2 Expand Capability of Robot for Inspection of Non-Ferromagnetic Structures

The second potential pathway for the future of CROC is by expanding its inspection capabilities for other structures. Whilst the magnetic footpad serves as a reliable means of adhesion for many steel structures, some limitations have been noted; in particular the constraint due to the size of the footpad, the maximum curvature of the surface limits its ability on pipes, minimum requirement in the thickness of the steel structure, and most importantly the structure's surface material must be ferromagnetic. Most steel structures can be accommodated through minor configuration changes to the magnetic adhesion system, however non-ferromagnetic structures such as wood, concrete, glass, and stainless steel would require a significant redesign of the adhesion system. An adhesion system for these applications should consider mechanical grasping to maintain high adhesion strength and the ability to ensure power-fail safe designs. Those which cannot use mechanical grasping would require careful consideration of the trade-off between advantages and disadvantages for various adhesion methods, perhaps even reconsider the means of locomotion.

Further research can be realised in dynamic locomotion. Whilst the activation and deactivation time of the magnetic adhesion system are not suitable for dynamic locomotion, alternate adhesion systems, such as mechanical grippers, may provide avenues for increasing the speed of the robot through swinging motions.

6.3.3 Expand Task Definition of the Robot to Include Maintenance Tasks

With CROC being used to inspect sites where there are high risks posed to humans, it is intuitive to think that a human would face even greater risks in performing maintenance tasks at the same sites. Therefore a robot that could carry out the required maintenance tasks on the spot is a necessary pathway for the climbing robot. There are many challenges introduced in designing a climbing robot which incorporates a means of cleaning paint, dirt and rust from structures which require maintenance. The cleaning of the surface may be achieved by grit blasting or laser blasting with a unit mounted on the head of the robot. Following the cleaning of the surface, the robot should then proceed to spray paint the surface.

Incorporating the elements of cleaning and blasting is both a challenge in redesigning the robot and enabling autonomous operation. The weight of the units at the head of the robot would require actuators that are more powerful than the current state of the art.

Appendix A

Static Analysis for Prototype Inchworm Robot

Table A.1: Properties for each component of prototype inchworm robot body

Components	Length	Units	Description
U Bracket	0.0360	m	Centre hole to hold point
	0.018	kg	Weight of the bracket
Straight Bracket	0.0009	m	Width
	0.0026	kg	Weight of the bracket
Plate Bracket	0.0065	m	Width
	0.012	kg	Weight of the bracket
Gear Horn	0.0020	m	Width
	0.0026	kg	Weight of the gear horn
Motor 1 MX-106	0.0651	m	Length along rotation face
	0.046	m	Width along rotation axis
	0.0402	m	Breath of rotation face
	0.012	m	Rotation point to short edge
	0.0531	m	Rotation point to long edge
	0.153	kg	Weight of the motor
Motor 2 MX-64	0.0611	m	Length along rotation face
	0.041	m	Width along rotation axis
	0.0402	m	Breath of rotation face
	0.012	m	Rotation point to short edge
	0.0491	m	Rotation point to long edge
	0.126	kg	Weight of the motor
Pad	0.04	m	Height of the pad
	0.623	kg	Weight of the pad
Gravity	9.81	m/s	Gravity

TABLE A.2: Moments for each component of prototype inchworm robot

	Pad	Joint 1	Gear	Bracket	Gear	Joint 2	Bracket	Bracket	Joint 3	Gear	Bracket	Bracket	Joint 4
Length to COG	0.0200	0.0726	0.0931	0.1111	0.1301	0.1541	0.1804	0.1841	0.2171	0.2376	0.2556	0.2769	0.3031
Weight	1.2000	0.1530	0.0026	0.0180	0.0026	0.1530	0.0120	0.0026	0.1530	0.0026	0.0180	0.0120	0.1530
Total Moment Experienced	10.67	10.43	10.33	10.32	10.30	10.30	10.07	10.05	10.04	9.72	9.71	9.67	9.63

Continued from previously column

	Gear	Bracket	Gear	Joint 5	Bracket	Bracket	Joint 6	Gear	Bracket	Gear	Joint 7	Pad
Length to COG	0.3271	0.3461	0.3641	0.3967	0.4177	0.4214	0.4477	0.4717	0.4907	0.5087	0.5412	0.5818
Weight	0.0026	0.0180	0.0026	0.1530	0.0026	0.0120	0.1530	0.0026	0.0180	0.0026	0.1530	1.2000
Total Moment Experienced	9.18	9.17	9.11	9.10	8.50	8.49	8.44	7.77	7.76	7.67	7.66	6.85

Appendix B

Static Analysis for Revised Inchworm Robot

Table B.1: Properties for each component of revised inchworm robot body

Components	Length	Units	Description
U Bracket	0.04	m	Centre hole to hold point
	0.04	kg	Weight of the bracket
Flat Bracket	0.005	m	Width
	0.004	kg	Weight of the bracket
Horn	0.005	m	Width
	0.004	kg	Weight of the bracket
Gear Horn	0.0020	m	Width
	0.0026	kg	Weight of the gear horn
Motor Type 1 H54-200W Joints 1,7	0.126	m	Length
	0.054	m	Width
	0.054	m	Height
	0.855	kg	Weight of the motor
Motor Type 2 H54-100W Joints 2,3,4,5,6	0.108	m	Length
	0.054	m	Width
	0.054	m	Height
	0.73	kg	Weight of the motor
Pad	0.1	m	Height of the pad
	4	kg	Weight of the pad
Gravity	9.81	m/s	Gravity

TABLE B.2: Moments for each component of revised inchworm robot

	Joint 1			Joint 2		Joint 3		Joint 4		
	Footpad	H54 in Rx	U-Bracket	Horn	H54 in Rz	U-Bracket	H54 in Rx	F-Bracket	H54 in Rz	Horn
Running Total (m)	0.100	0.127	0.167	0.172	0.280	0.320	0.347	0.352	0.460	0.465
Length to Centre of Gravity (m)	0.050	0.114	0.147	0.170	0.226	0.300	0.334	0.350	0.406	0.463
Weights (kg)	4.000	0.855	0.040	0.040	0.730	0.040	0.730	0.040	0.730	0.040
Total Moment Experienced (Nm)	**47.3**	**40.2**			**27.3**		**24.0**		**14.4**	
Current Draw (Amps)		9.75			6.9		5.7		3.6	

Continued from previous column

	Joint 5			Joint 6		Joint 7			
	F-Bracket	H-54 in Rx	U-Bracket	H54 in Rz	Horn	U-Bracket	H54 in Rx	Footpad	Totals
Running Total (m)	0.470	0.497	0.537	0.645	0.650	0.690	0.717	0.817	0.697 m
Length to Centre of Gravity (m)	0.468	0.484	0.517	0.591	0.648	0.670	0.704	0.767	
Weights (kg)	0.040	0.730	0.040	0.730	0.040	0.040	0.855	4.000	13.72 kg
Total Moment Experienced (Nm)		**12.1**		**4.2**			**2.6**		
Current Draw (Amps)		3		1.8			1.5		32.25 Amps

Appendix C

Table of Torques in Designing Magnetic Toe Module - Revised Inchworm Robot

TABLE C.1: Table of torques for magnetic toe module - Revised inchworm robot

Airgap	Magnet Force	Torque to Peel Magnet	Gear 1 - Segment		Gear 2 - Pinion 1		Gear 3 - Worm Gear		Worm		Motor	Motor Torque 40% eff
			Force out	Torque	Force in	Torque	Force Out	Torque	Force in	Torque	Torque	
mm	N	Nm	N	Nm	N	Nm	N	Nm	N	Nm	Nm	
0.00	843.67	16.92	338.31	16.92	338.31	2.37	94.73	2.37	94.73	0.047	0.047	0.118
1.00	570.01	11.43	228.57	11.43	228.57	1.60	64.00	1.60	64.00	0.032	0.032	0.080
2.00	446.31	8.95	178.97	8.95	178.97	1.25	50.11	1.25	50.11	0.025	0.025	0.063
3.00	362.12	7.26	145.21	7.26	145.21	1.02	40.66	1.02	40.66	0.020	0.020	0.051
4.00	299.87	6.01	120.25	6.01	120.25	0.84	33.67	0.84	33.67	0.017	0.017	0.042
5.00	251.77	5.05	100.96	5.05	100.96	0.71	28.27	0.71	28.27	0.014	0.014	0.035
6.00	213.54	4.28	85.63	4.28	85.63	0.60	23.98	0.60	23.98	0.012	0.012	0.030
7.00	182.62	3.66	73.23	3.66	73.23	0.51	20.50	0.51	20.50	0.010	0.010	0.026
8.00	157.21	3.15	63.04	3.15	63.04	0.44	17.65	0.44	17.65	0.009	0.009	0.022
9.00	136.07	2.73	54.57	2.73	54.57	0.38	15.28	0.38	15.28	0.008	0.008	0.019
10.00	118.32	2.37	47.45	2.37	47.45	0.33	13.28	0.33	13.28	0.007	0.007	0.017

Appendix D

Matlab Code for Adhesion System Optimiser

```
function [ObjFx3DPlot, ObjFx,  solution, outputs] = AdhesionSystemOptimiser()
% AdhesionSystemOptimiser  Optimises an adhesion system.
%   [fx, fxAll,  solution, outputs] = AdhesionSystemOptimiser()
%
%   Optimises an adhesion system: Refer to Thesis titled: Design of a
%   Biologically Inspired Climbing Robot and an Adhesion Mechanism for
%   Reliable and Versatile Climbing in Complex Steel Structures Chapters 4
%   and 5
%   Author: Peter Ward
%   Centre for Autonomous Systems, University of Technology
%   Sydney
%   email: Peter.Ward@uts.edu.au
%   Website: www.https://www.uts.edu.au/research-and-teaching/...
%   our-research/centre-autonomous-systems/about-cas/our-people/...
%   postgraduate/peter
%   May 2013; Last revision: 12-Jan-2016

%% ------------- BEGIN CODE --------------
% Flag to determine which objective function to use Objective function 1 is
% the default -1Fp*Fs*Bx*By*T*Wp and does not require any tuning of
% paramenters Objective function 2 is -1*(Fp+Fs+Bx+By+T+Wp) and requires
```

```
% careful tuning of the weightings
objectiveFx = 1;

% Flag to check the performance inequalities, this should be left as 1.
% i.e. does the performance meet the minimum requirements required
checkInequalities = 1;

% Flag to check the system constraints, this should be left as 1. i.e. is
% the design suitable for the application scenario
checkConstraints = 1;

% After determining the optimal solution, the results are graphed.
plotObjectiveFunction = 1;

% Flag to show the contrcuted footpad size on the plot in comparison to
% optimal design
showContructed = 1;
cRadius = 150.0;
cDiametre = 38.1;
cThickness = 19.1;

% Design Variables and System Constants These varaibles depend on the robot
% configuration, and should be set or estimated accordingly, they should be
% reduced where possible

% baseMass: is the mass of all components that will be contained with in
% the footpad and are not included in the mass of the robot. This includes
% components such as cameras, wiring, sensors, pcbs, circuits, controllers
% e.t.c.
baseMass = 0.5; % kg

% minPadHeight: is the minimum possible height of the footpad due to the
% components which must be contained in the footpad. This may be the height
% of the cameras, and may include clearances between the surface and the
% footpad. i.e. camera height of 45mm + surface clearance of 25mm for
% rivets. The pad height may end up greater than this, due to the sizing of
% the optimised magnet. This dimension is used in determining the overal
% bending moment of the robot in a cantilevered pose.
minPadHeight = 40; % mm
```

```
% This is the mass of the robot which includes the actuators, wiring,
% brackets, fasteners, sensors etc. It includes anything that is not
% associated with the adheison systems.
robotMass = 6; % kg

% The length of the robot between the first joint to the last joint, not
% including the predicted length of the adhesion system. This includes link
% lengths between the joints.
robotLength = 640; % mm

% staticFriction: Coefficient of Static Friction between the pad and a
% surface, i.e. the friction between a rubber pad and a dry painted steel
% surface.
staticFriction = 0.6;

% maxPadRadius: This is constraint on the maximum pad radius due to the
% intended application scenario. i.e. if the pad must fit through a hole a
% particular size, or step on a member of a particular size
maxPadRadius = 150; % (mm)

% gravity: Assuming the robot is used on Earth
gravity = 9.81; % (m/s)

% maxNoMagnets: The max number of magnet we want to consider. The number of
% magnets used is largely determined by sclaing laws and scaling rates of
% the peeling mechanisms, in particular the scaling of weight with changes
% to magnet size. In active systems such as vacum the weight increases at a
% slower rate than the weight of passive systems such as permanent magnetic
% adheison.
maxNoMagnets = 10;

% maxPadMass: This is limited by the stall torque of the actuators and is
% determined by a worst case scenario / cantilevered robot. A static
% analysis is required to determine the maximum pad mass at stall torque.
maxPadMass = 4; % kg

% idealPadMass: This is limited by the continuous operating torque of the
% actuators for a worst case scenario / cantilevered robot. A static
```

```
% analysis is required to determine the ideal pad mass.
idealPadMass = baseMass; %4.5; % kg

% airGap: This is the air gap we want to optimise the pad for, best to
% optimise for the most commonly used airgap, however all airgaps should be
% considered in the design of the adheison system for safe use. It is
% reccommended to optimise for the max air gap expected. It should also be
% noted that with significant increases in intended operating air gap,
% solutions will dissapear and there may be no valid solutions to the
% optimisation. airGap is only directly relevant to magnetic type of
% adhesion, and requires a force model such as Fm(Dm,Tm).
airGap = 3; %mm

% The number of samples used in interpolating the magnet diameter,
% thickness and radius. Note these make up the size of a 4D matrix.
% Choose these carefully, start small, so that computation is faster.
% Use larger sample size for more refined optimal solution
samplesRadius = 30; %65
samplesDiameter = 25; %60
samplesThickness = 15; %10

% Each air gap has a different look up table for the magnetic force model,
% each force model has different x and y axis. Ideally they should have
% the same dimensions, and could be arranged into a 3D array.
if airGap == 0
    load magDiametre7Counts.mat;
    magDiametreArray = magDiametre7Counts;
    load magThickness14Counts.mat;
    magThicknessArray = magThickness14Counts;
elseif airGap == 2
    load magDiametre10Counts.mat;
    magDiametreArray = magDiametre10Counts;
    load magThickness14Counts.mat;
    magThicknessArray = magThickness14Counts;
elseif airGap == 3
    load magDiametre10Counts.mat;
    magDiametreArray = magDiametre10Counts;
    load magThickness14Counts.mat;
    magThicknessArray = magThickness14Counts;
```

```
elseif airGap == 5
    load magDiametre7Counts.mat;
    magDiametreArray = magDiametre7Counts;
    load magThickness14Counts.mat;
    magThicknessArray = magThickness14Counts;
else
    error('Air gap must be 0,2,3 or 5mm')
end

% Get the min and max of each array, then sample between the two with the
% specified number of samples
maxDiameter = max(magDiametreArray);
minDiameter = min(magDiametreArray);
diametreArray = minDiameter:((maxDiameter-minDiameter)/ ...
                                        (samplesDiameter-1)):maxDiameter;

maxThickness = max(magThicknessArray);
minThickness = min(magThicknessArray);
thicknessArray = minThickness:((maxThickness-minThickness)/ ...
                                        (samplesThickness-1)):maxThickness;

% Get the values for radius, mag diam, mag height
radius = 0:(maxPadRadius/(samplesRadius-1)):maxPadRadius;

% Get the length
lenDiametre = numel(diametreArray);
lenThickness = numel(thicknessArray);
lenRadius = numel(radius);

% The optimal solutions will be stored in here
solution = [];
% The performance criteria will be stored in here
outputs = [];

% ObjFx stores all of the objective function values for every discrete
% value of number of magnets, radius, diameter, and thickness
ObjFx = zeros(maxNoMagnets,lenRadius,lenDiametre,lenThickness);

% ObjFx3D Plot is used to store all of the objective function values for
```

```
% plotting purposes. As the no of modules used is typically most
% constrained, this is not represented in the 3D plots.
ObjFx3DPlot = zeros(lenRadius,lenDiametre,lenThickness);

% To find global minimum, track the performance criteria and fx
[minfx,minfx2,optimalThickness,optimalDiametre,optimalPadRadius]=deal(9e99);
[maxfx,gSlipForce,gPullForce,gBendingMomentX,gBendingMomentY,gTorsion, ...
    gMass,gindex1,gindex2,gindex3,maxNormalisedSlipForce, ...
    maxNormalisedPullForce,maxNormalisedBendingMomentX, ...
    maxNormalisedBendingMomentY,maxNormalisedTorsion, ...
    maxNormalisedMass,optimalNoMagnets,solutions] = deal(0);

for noMagnets = 3:maxNoMagnets
    for index1 = 1:lenRadius % progress through each radii
        padRadius = radius(index1);
        for index2 = 1:lenDiametre % progress through each diameter
            diametre = diametreArray(index2);
            for index3 = 1:lenThickness % progress through each thickness
                thickness = thicknessArray(index3);

                % To get the objective function value, we must
                % 1. Determine the performance criteria
                % 2. Check the performance constraintes
                % 3. Check the geometric constraints
                % 4. Normalise the criteria
                % 5. Obtain the objective function value

                % This is the force model for a disc magnet with a steel
                % back plate. It can be replaced by another depending on
                % the type of adhesion being used. This force model uses a
                % look up table and interpolates for the force for a give
                % diameter, thickness and airgap.
                magForce = force(diametre,thickness,airGap);
                if isnan(magForce)
                    ObjFx(noMagnets,index1,index2,index3) = NaN;
                    continue;
                end;

                % The mass of the magnet clearly depends on its diameter
```

```
        % and thickness.
        magMass = magnetMass(diametre, thickness);

        % The height of the peeling mechanism used (therefore pad),
        % is approximately 1.5 times the magnet diameter.
        % However we also check to see whether it is less than the
        % minimum pad height, which may be limited by cameras,
        % electronics etc.
        padHeight = (1.5*diametre);
        if padHeight < minPadHeight
            padHeight = minPadHeight;
        end

        % Pull Force
        pullForce = noMagnets*magForce;

        % Slip Force
        slipForce = pullForce*staticFriction;

        % Bending Moment X
        N = 0:noMagnets-1;
        bendingMomentX = magForce*padRadius/ ...
                              1000*sum(abs(cos(2*pi/noMagnets*N)));

        % Bending Moment Y
        bendingMomentY = magForce*padRadius/ ...
                              1000*sum(abs(sin(2*pi/noMagnets*N)));

        % Torsion
    Torsion  = noMagnets*(padRadius/1000)*magForce*staticFriction;

        % Mass of pad
        padMass = noMagnets* ...
(magMass+housingMass(diametre,thickness)+frameMass(padRadius)) ...
                                                    + baseMass;

        % Max Pull Force
        minRequiredPullForce = gravity*(2*padMass+robotMass);
```

```
    % Max Slip Force
    minRequiredSlipForce = minRequiredPullForce*staticFriction;

    % Max Bending Moment, in a worst case scenario
    minRequiredBendingMomentX = 0.5*(padHeight/1000)* ...
                                          padMass*gravity + ...
      0.5*((padHeight+robotLength)/1000)*robotMass*gravity + ...
((padHeight+robotLength+0.5*padHeight)/1000) * padMass*gravity;

    % Max Bending Moment, in a worst case scenario for the
    % footpad orientation of wall
    minRequiredBendingMomentY = 0.5*(padHeight/1000)* ...
                                         padMass*gravity + ...
     0.5*((padHeight+robotLength)/1000)*robotMass*gravity + ...
  ((padHeight+robotLength+0.5*padHeight)/1000)*padMass*gravity;

    % Max Torsion - in a worst case scenario, this is the load
    % of the robot causing the footpad to rotate on the surface
 minRequiredTorsion  = minRequiredBendingMomentX*staticFriction;

    % Performance Constraints
    % Check the inequalities to see if system is feasible
    % If not feasible, get rid of solution, and go to next one
    if(checkInequalities == 1)

        % Is the pull force enough to support the robot?
        if pullForce < minRequiredPullForce
            ObjFx(noMagnets,index1,index2,index3) = NaN;
            continue;

        % Is the slip force enough to support the robot?
        elseif slipForce < minRequiredSlipForce;
             ObjFx(noMagnets,index1,index2,index3) = NaN;
            continue;

        % Is the x bending moment enough to support the robot?
        elseif bendingMomentX < minRequiredBendingMomentX
             ObjFx(noMagnets,index1,index2,index3) = NaN;
             continue;
```

```
            % Is the y bending moment enough to support the robot?
            elseif bendingMomentY < minRequiredBendingMomentY
                ObjFx(noMagnets,index1,index2,index3) = NaN;
                continue;

            % Is the torsion moment enough to support the robot?
            elseif Torsion < minRequiredTorsion
                ObjFx(noMagnets,index1,index2,index3) = NaN;
                continue;
            end;
        end;

        % Design Constraints, i.e. Geometric and Mass
        if (checkConstraints == 1);
            % Is the adhesion module too big considering the
            % radius of the adhesion system
            if (diametre/2)/sin(pi/noMagnets) > padRadius
                ObjFx(noMagnets,index1,index2,index3) = NaN;
                continue;
            % Is the radius of the adhesion system bigger than the
            % maximum allowable?
            elseif padRadius > maxPadRadius
                ObjFx(noMagnets,index1,index2,index3) = NaN;
                continue;

            % Is the mass of the adhesion system less than the
            % maximum, such that the motor torques operate at or
            % below nominal torque
            elseif padMass > maxPadMass
                ObjFx(noMagnets,index1,index2,index3) = NaN;
                continue;
            end
        end

    % If all the inequalities and constraints pass we have a solution!
    solutions = solutions+1; % Lets keep track of them.

    % We must then normalise the performance outcomes against the
```

```
 % required performance criteria.
 % By doing so, each of the normalised performance criteria
 % will represent the factor of safety (FOS) for that criteria


% Determine whether we are trying to maximise or minimise
% the performance criteria
normalisedSlipForce = ...
    normalise(slipForce,minRequiredSlipForce,'maximise');

normalisedPullForce = ...
    normalise(pullForce,minRequiredPullForce,'maximise');

normalisedBendingMomentX = ...
    normalise(bendingMomentX,minRequiredBendingMomentX,'maximise');

normalisedBendingMomentY = ...
    normalise(bendingMomentY,minRequiredBendingMomentY,'maximise');

normalisedTorsion = normalise(Torsion,minRequiredTorsion,'maximise');

normalisedMass = normalise(padMass,idealPadMass,'minimise');

        % We can now determine the objective function value
        % This is the default objective function
        if (objectiveFx == 1)
            ObjFx(noMagnets,index1,index2,index3) = -1 * ...
                (normalisedSlipForce*normalisedPullForce* ...
                normalisedBendingMomentX*normalisedBendingMomentY* ...
                normalisedTorsion*normalisedMass);

            % We also update the plot value, however because we
            % aren't tracking the no. magnets we must make sure we
            % are replacing a more optimal solution
            if (ObjFx(noMagnets,index1,index2,index3) < ...
                                ObjFx3DPlot(index1,index2,index3))
                 ObjFx3DPlot(index1,index2,index3) = ...
                            ObjFx(noMagnets, index1,index2,index3);
            end
```

```
                % This is an experimental objective function, with
                % summation of the normalised criteria. This allows weights
                % of the criteria however requires careful manual tuning.
                elseif (objectiveFx == 2)
                    % Weightings could be applied to the performance
                    % criteria if desired, altneratively extra FOS could be
                    % added
                    %            sf      pf   bx   by   t    w
                    %weightings = [0.01   0.01   3    3    3    100];
                    weightings = [0.1   0.1  1    1    1    1];

                    ObjFx(noMagnets, index1,index2,index3) = -1* ...
      (normalisedSlipForce*weightings(1)+normalisedPullForce*weightings(2)+...
normalisedBendingMomentX*weightings(3)+normalisedBendingMomentY*weightings(4)+...
            normalisedTorsion*weightings(5)+normalisedMass*weightings(6));

                    if (ObjFx(noMagnets, index1,index2,index3) < ...
                                        ObjFx3DPlot(index1,index2,index3))
                         ObjFx3DPlot(index1,index2,index3) = ...
                                    ObjFx(noMagnets,index1,index2,index3);
                    end
                end


                % The objective function should be negative if the
                % performance criteria are normalised properly. Therefore
                % the most negative or global minimum of the objective fx
                % is what we are after. If a more negative value is found
                % we store the performance criteria.

                if ObjFx(noMagnets, index1,index2,index3) < minfx2
                    optimalNoMagnets = noMagnets;
                    minfx =  ObjFx3DPlot(index1,index2,index3);
                    minfx2 =  ObjFx(noMagnets,index1,index2,index3);
                    optimalThickness    = thickness;
                    optimalDiametre     = diametre;
                    optimalPadRadius       = padRadius;
                    gSlipForce      = slipForce;
                    gPullForce      = pullForce;
```

```
                    gBendingMomentX  = bendingMomentX;
                    gBendingMomentY  = bendingMomentY;
                    gTorsion        = Torsion;
                    gMass         = padMass;

                    gindex1 = index1;
                    gindex2 = index2;
                    gindex3 = index3;

                    maxNormalisedSlipForce = normalisedSlipForce;
                    maxNormalisedPullForce = normalisedPullForce;
                    maxNormalisedBendingMomentX = normalisedBendingMomentX;
                    maxNormalisedBendingMomentY = normalisedBendingMomentY;
                    maxNormalisedTorsion = normalisedTorsion;
                    maxNormalisedMass = normalisedMass;

                end
            end

        end
    end
end


sprintf('Solutions: %f \r', solutions)

sprintf([' maxNormalisedSlipForce = %f \n maxNormalisedPullForce = %f' ...
    '\n maxNormalisedBendingMomentX = %f \n maxNormalisedBendingMomentY = %f' ...
    '\n maxNormalisedTorsion = %f \n maxNormalisedMass = %f'], ...
   maxNormalisedSlipForce,maxNormalisedPullForce,maxNormalisedBendingMomentX,...
   maxNormalisedBendingMomentY,maxNormalisedTorsion,maxNormalisedMass)

sprintf(' gindex1 = %f \n gindex2 = %f \n gindex3 = %f', gindex1,gindex2,gindex3)

sprintf([' minfx = %0.3f  \n minfx2 = %0.3f  \n Optimal No. Magnets = %f'...
    '\n Optimal Thickness = %0.1f mm  \n Optimal Diameter = %0.1f mm' ...
    '\n Optimal Radius = %0.1f mm'],...
    minfx, minfx2, optimalNoMagnets,...
    optimalThickness,optimalDiametre,optimalPadRadius)
```

```
sprintf([' SlipForce = %0.1f  \n PullForce = %0.1f N  \n'...
    'BendingMomentX = %0.1f Nm    \n BendingMomentY = %0.1f Nm'...
    '\n Torsion = %0.1f Nm    \n Mass = %0.1f kg'],...
    gSlipForce,gPullForce,gBendingMomentX,gBendingMomentY,gTorsion,gMass)

solution = [solution, [minfx, optimalNoMagnets, optimalThickness, ...
                                    optimalDiametre, optimalPadRadius]' ];
outputs = [outputs, [gSlipForce, gPullForce, ...
                        gBendingMomentX,gBendingMomentX, gTorsion, gMass]'];

if (plotObjectiveFunction == 1)
    plotColour = -1*ObjFx3DPlot;
    plotColour(isnan(plotColour)) = 0.000001;
    plotColour(find(plotColour <= 0)) = 0.000001;
    maxPlotColour = max(plotColour(:));
    plotColour = plotColour./maxPlotColour;
    plotColour = plotColour(:);

    % plot size needs to be greater than 0, and real, then scaled
    plotSize = -1*ObjFx3DPlot;
    plotSize(isnan(plotSize)) = 0.000001;
    plotSize(find(plotSize <= 0)) = 0.000001;
    maxPlotSize = max(plotSize(:));
    plotSize = plotSize./maxPlotSize;

    % scale the plot size disproportionately
    plotSize = 500*plotSize.^2;
    plotSize = plotSize(:);

    [X , Y, Z] = ndgrid(radius, diametreArray, thicknessArray);
    figure('Color',[1 1 1]);

    % Plot 1: Thickness vs Diameter vs Radius
    subplot(2,2,1);
    hold on;
    fig1 = scatter3( X(:), Y(:), Z(:), plotSize, plotColour, 'filled');
    view(-60,60);
    axis([0 maxPadRadius 0 max(diametreArray) 0 max(thicknessArray)]);
```

```
alpha(fig1,.5);
grid on;

plot3(optimalPadRadius, optimalDiametre, optimalThickness,...
                                                    'bx','MarkerSize',20)
plot3(optimalPadRadius, optimalDiametre, optimalThickness,...
                                                    'bo','MarkerSize',20)

if showContructed
    plot3(cRadius, cDiametre, cThickness,'rx','MarkerSize',20)
    plot3(cRadius, cDiametre, cThickness,'ro','MarkerSize',20)
end

title('Normalised Objective Function','FontSize', 18);
xlabel('Radius(mm)','FontSize', 18);
ylabel('Magnet Diameter (mm)','FontSize', 18);
zlabel('Magnet Thickness (mm)', 'FontSize', 18);
set(gca,'fontsize',18)
colorbar;
[cmin,cmax] = caxis;
caxis([0.5,cmax]);

% Plot 4: Thickness vs Diameter
subplot(2,2,2);
grid on;
hold on;
%axis vis3d
fig2 = scatter3( X(:), Y(:), Z(:), plotSize, plotColour, 'filled');
axis([0 maxPadRadius 0 max(diametreArray) 0 max(thicknessArray)]);
alpha(fig2,.5);

plot3(optimalPadRadius, optimalDiametre, optimalThickness,...
                                                    'bx','MarkerSize',20)
plot3(optimalPadRadius, optimalDiametre, optimalThickness,...
                                                    'bo','MarkerSize',20)

if showContructed
    plot3(cRadius, cDiametre, cThickness,'rx','MarkerSize',20)
    plot3(cRadius, cDiametre, cThickness,'ro','MarkerSize',20)
```

```
end

title('Normalised Objective Function','FontSize', 18);
xlabel('Radius(mm)','FontSize', 18);
ylabel('Magnet Diameter (mm)','FontSize', 18);
zlabel('Magnet Thickness (mm)', 'FontSize', 18);
set(gca,'fontsize',18)
colorbar;
[cmin,cmax] = caxis;
caxis([0.5,cmax]);
view([1 0 0]);

% Plot 3: Thickness vs Radius
subplot(2,2,3);
hold on;
grid on;
%axis vis3d
fig3 = scatter3( X(:), Y(:), Z(:), plotSize, plotColour, 'filled');
axis([0 maxPadRadius 0 max(diametreArray) 0 max(thicknessArray)]);
alpha(fig3,.5);

plot3(optimalPadRadius, optimalDiametre, optimalThickness,...
                                                    'bx','MarkerSize',20)
plot3(optimalPadRadius, optimalDiametre, optimalThickness,...
                                                    'bo','MarkerSize',20)

if showContructed
plot3(cRadius, cDiametre, cThickness,'rx','MarkerSize',20)
plot3(cRadius, cDiametre, cThickness,'ro','MarkerSize',20)
end

title('Normalised Objective Function','FontSize', 18);
xlabel('Radius(mm)','FontSize', 18);
ylabel('Magnet Diameter (mm)','FontSize', 18);
zlabel('Magnet Thickness (mm)', 'FontSize', 18);
set(gca,'fontsize',18)
colorbar;
[cmin,cmax] = caxis;
caxis([0.5,cmax]);
```

```
view([0 -1 0]);

% Plot 4: Diameter vs Radius
subplot(2,2,4);
hold on;
grid on;
fig4 = scatter3( X(:), Y(:), Z(:), plotSize, plotColour, 'filled');
axis([0 maxPadRadius 0 max(diametreArray) 0 max(thicknessArray)]);
alpha(fig4,.5);

plot3(optimalPadRadius, optimalDiametre, optimalThickness,...
                                                    'bx','MarkerSize',20)
plot3(optimalPadRadius, optimalDiametre, optimalThickness,...
                                                    'bo','MarkerSize',20)

if showContructed
plot3(cRadius, cDiametre, cThickness,'rx','MarkerSize',20)
plot3(cRadius, cDiametre, cThickness,'ro','MarkerSize',20)
end

title('Normalised Objective Function','FontSize', 18);
xlabel('Radius(mm)','FontSize', 18);
ylabel('Magnet Diameter (mm)','FontSize', 18);
zlabel('Magnet Thickness (mm)', 'FontSize', 18);
set(gca,'fontsize',18)
colorbar;
[cmin,cmax] = caxis;
caxis([0.5,cmax]);
view([0 0 1])

% A few additional custom plot settings to suitable for displaying the
% current optimisation results
subplot(2,2,1);
axis([50 200 20 50 0 50]);
view(144.2,16.1);
%view([0.1 0.2 0.1])
subplot(2,2,2);
axis([50 200 20 50 0 50]);
subplot(2,2,3);
```

```
    axis([50 200 0 50 0 50]);
    set(gca,'Ydir','reverse');
    subplot(2,2,4);
    axis([50 200 20 50 0 50]);
end

end

%% normalise(variable, maximum, type)
% Normalises a variable with a maximum value between 0 to 1
% variable: The variable to be normalised
% maximum: The maximum value which corelates to the new 1 value
% type: 'maximise' or 'minimise'
% If 'minimise' is used the varaible is normalised between 1 to 0
function normalisedValue = normalise(variable, maximum, type)
    if strcmp(type, 'maximise')
        normalisedValue = variable/maximum;
    elseif strcmp(type, 'minimise')
        normalisedValue = maximum/variable;
    else
        warning('Invalid normalisation parameter')
    end
end

%% force(diametre,thickness,airGap)
% This is the force model for a disc magnet with a steel
% back plate. It can be replaced by another depending on
% the type of adhesion being used. This force model uses a
% look up table and interpolates for the force for a give
% diameter, thickness and airgap.
% diametre: mm
% thickness: mm
% airGap: mm
% force: Newtons
function fm = force(diametre,thickness,airGap)
    gravity = 9.81;
    load magDiametre7Counts.mat;
    load magDiametre10Counts.mat;
    load magThickness14Counts.mat;
```

```
    if airGap == 0
        load force0mm.mat;
        % convert from pounds to kg to newtons
        force0mm = 0.453592 * gravity * force0mm;
        fm = interp2(magDiametre7Counts, magThickness14Counts,...
                                            force0mm, diametre, thickness);
    elseif airGap == 2
        load force2mm.mat;
        % convert from pounds to kg to newtons
        force2mm = 0.453592 * gravity * force2mm ;
        fm = interp2(magDiametre10Counts, magThickness14Counts,...
                                            force2mm, diametre, thickness);
    elseif airGap == 3
        load force3mm.mat;
        % convert from pounds to kg to newtons
        force3mm = 0.45392 * gravity * force3mm ;
        fm = interp2(magDiametre10Counts, magThickness14Counts,...
                                            force3mm, diametre, thickness);
    elseif airGap == 5
        load force5mm.mat;
        % convert from pounds to kg to newtons
        force5mm = 0.453592 * gravity * force5mm ;
        fm = interp2(magDiametre7Counts, magThickness14Counts,...
                                            force5mm, diametre, thickness);
    else
        error('Air gap must be 0 or 5mm')
    end
end

%% frameMass(padRadius)
% Determines the mass of the frame for a gien radius of the adhesion system
% This function assumes a hollow hollow rectangluar beam is used to support
% the module, of thickness frameThickness, and width and height of
% frameHeight, length pad Radius
% padRadius: mm
% frameMass: kg
function frameMass = frameMass(padRadius) % diametre and thickness are in mm
    frameDensity = 2700;  % Density kg/m3
    frameThickness = 3; %mm
```

```
    frameHeight = 50; %mm
    totalVol = (frameHeight/1000)*(frameHeight/1000)*(padRadius/1000);
    innerVol = ((frameHeight-2*frameThickness)/1000)*...
                    ((frameHeight-2*frameThickness)/1000)*(padRadius/1000);
    frameMass =  frameDensity * ( totalVol - innerVol ); % mass is in kg
end

%% housingMass(diametre,thickness)
% Determines the mass of magnetic assembly peeling module inc. gear train,
% motor, housing, axle, large gear, pinion gear.
% This has been determined emprically by analsysing different scaled
% versions of the peeling module in Solidworks and through static
% analysis
% diameter: mm
% thickness: mm
% housingMass: kg
function housingMass = housingMass(diametre,thickness)
% Calculates the torque required to peel the magnet and converts it to a
% mass based on performance criteria identified for the peeling mechanism
magForce = force(diametre,thickness,0);
% torque required to peel magnet
torque = (magForce*diametre/2/1000);
housingMass = nthroot( (torque/35) ,2);
end

%% magnetMass
% Takes a magnet diameter and thickness to determine the weight of the
% magnet and the weight of the assocaited steel back plate in order to
% maintain most of the magnetic field. This has been determined emprically
% with a statistically significant data set.
% diameter: mm
% thickness: mm
% magnetMass: kg
function magnetMass = magnetMass(diametre, thickness)
steelThickness = ((thickness*0.2)+(diametre*0.2))/2;
steelDensity = 8000;  % Density kg/m3
steelMass = (pi*((1.5*diametre/1000)/2)^2*(steelThickness/1000))*steelDensity;
magnetDensity = 7501.25418;  % Density kg/m3
magnetMass = (pi*((diametre/1000)/2)^2*(thickness/1000))*magnetDensity;
```

```
magnetMass = magnetMass + steelMass;
end
%%
%------------- END OF CODE --------------

%   @TODO
%   enter fixed variables as function inputs
%   seperate plotting function
%   enter scaling laws for subsytems as an input, i.e. weight to torque
%   fix force model look up table i.e. 3D lookup table with
%   standardised x(diameter),y(thickness),z axis(air gap).
%
%   Please send suggestions for improvement of the above optimisation
%   to Peter Ward at this email address: Peter.Ward@uts.edu.au
%   Your contribution towards improving this optimisation will be greatly
%   appreciated and acknowledged.
```

Bibliography

[1] Hans Peter Moravec. Robot. URL http://www.britannica.com/technology/robot-technology.

[2] Shimon Y. Nof. *Handbook of Industrial Robotics (2nd ed.)*. John Wiley & Sons. ISBN 0-471-17783-0.

[3] C H Hare. Protective Coatings for Bridge Steel. Technical report, Transportation Research Board, Washington, DC. URL http://www.trb.org/Publications/Pages/262.aspx.

[4] Leonard J. Bond. Bridge Inspection. URL http://www.ndt-ed.org/AboutNDT/SelectedApplications/Bridge_Inspection/Bridge_Inspection.htm.

[5] Nicole Martino, D Ph, and Amber Caulkins. The Road to Better Bridges : Strategies for Maintaining Infrastructure. Technical report, The Collaborative, Providence, RI 02903. URL http://collaborativeri.org/wp-content/uploads/2015/05/The-Road-to-Better-Bridges-Strategies-for-Maintaining-Infrastructure.pdf.

[6] Brian Leshko. Access Methods for Bridge Inspections. URL http://www.structuremag.org/wp-content/uploads/2014/08/C-StructuralForensics-Leshko-Oct081.pdf.

[7] Ciaran MacCarron. *Confined Space Fatalities*. Phd thesis, Edith Cowan University.

[8] Confined Space Fatalities... a closer look at the numbers. URL http://www.rocorescue.com/roco-rescue-blog/confined-space-fatalities-a-closer-look-at-the-numbers.

[9] Jeremy Koonce, Todd Demski, Mike Rowe, and Nate Morriss. *Bridge Inspection Access to Minimize Operational Impacts*. PhD thesis, AREMA.

[10] John Robinson and Mount Townsend Solutions Pty Ltd. Life Cycle Costs of Industrial Protective Coatings. URL `http://manual.ingal.com.au/INGAL_Manual_Version4_Web.pdf`.

[11] Quintin Lake. Brooklyn. URL `http://archive.quintinlake.com/`.

[12] New South Wales Road and Transport Authority. Sydney Harbour Bridge Conservation Management Plan 2007. *Godden Mackay Logan Ltd*, page 114.

[13] Road Transport Authority. RTA Bridge Inspection Procudure Manual - Protective Coatings. Technical report, Road and Transport Authority, Sydney.

[14] DroneBuff. What's the best quadcopter? - Drone Buff. URL `http://dronebuff.com/whats-best-quadcopter/#toc-flight-time`.

[15] Jian Zhu, Dong Sun, and Shiu Kit Tso. Development of a tracked climbing robot. *Journal of Intelligent and Robotic Systems: Theory and Applications*, 35(4):427–444. ISSN 09210296. doi: 10.1023/A:1022383216233.

[16] J Krahn, Y Liu, a Sadeghi, and C Menon. A tailless timing belt climbing platform utilizing dry adhesives with mushroom caps. *Smart Materials and Structures*, 20(11):115021. ISSN 0964-1726. doi: 10.1088/0964-1726/20/11/115021. URL `http://stacks.iop.org/0964-1726/20/i=11/a=115021?key=crossref.c31540ae0099374b2f98176bc2373db0`.

[17] Shunichi Yoshida. Development of Small-Size Window Cleaning Robot By Wall Climbing Mechanism. *ISARC*, pages 215–220.

[18] Guangzhao Cui, Keke Liang, Jinchao Guo, and Huiping Li. Design of a Climbing Robot Based on Electrically Controllable Adhesion Technology. In *International Conference on Solid State and Materials*, volume 22, pages 90–95, Los Angeles, USA. IERI. ISBN 9781612750231.

[19] Harsha Prahlad, Ron Pelrine, Scott Stanford, John Marlow, and Roy Kornbluh. Electroadhesive robots - Wall climbing robots enabled by a novel, robust, and

electrically controllable adhesion technology. *Proceedings - IEEE International Conference on Robotics and Automation*, pages 3028–3033. ISSN 10504729. doi: 10.1109/ROBOT.2008.4543670.

[20] Frederic Rochat, Patrick Schoeneich, Olivier Truong-Dat Nguyen, and Francesco Mondada. TRIPILLAR: Miniature magnetic caterpillar climbing robot with plane transition ability. In O Tosun, H L Akin, M O Tokhi, and G S Virk, editors, *Proceedings of 12th International conference on climbing and walking robots and the support technologies for mobile machines (CLAWAR)*, pages 343–350, Istanbul. World Scientific. URL `http://www.clawar2009.org/`.

[21] FILIPPO BONACCORSO, CARLO BRUNO, DOMENICO LONGO, and GIOVANNI MUSCATO. STRUCTURE AND MODEL IDENTIFICATION OF A VORTEX-BASED SUCTION CUP. In *Advances in Mobile Robotics*, pages 303–310. WORLD SCIENTIFIC. ISBN 978-981-283-576-5. doi: 10.1142/9789812835772_0037. URL `http://www.worldscientific.com/doi/10.1142/9789812835772_0037`.

[22] Zhijian Jiang, Jun Li, Xueshan Gao, Ningjun Fan, and Boyu Wei. Study on pneumatic wall climbing robot adhesion principle and suction control. In *Robotics and Biomimetics. IEEE International Conference on*, ROBIO, pages 1812–1817, Bangkok, Thailand. doi: 10.1109/ROBIO.2009.4913277.

[23] Dawei Zhang, Zhenbo Li, and Jiapin Chen. Design and Optimization of an Omnidirectional Permanent-Magnetic Wheeled Wall-Climbing Microrobot with MEMS-Based Electromagnetic Micromotors. *Advanced Robotics*, 26(1-2):197–218. ISSN 0169-1864. doi: 10.1163/016918611X607716. URL `http://www.tandfonline.com/doi/abs/10.1163/016918611X607716`.

[24] M Eich and T Vogele. Design and control of a lightweight magnetic climbing robot for vessel inspection. In *Control Automation, 2011 19th Mediterranean Conference on*, MED, pages 1200–1205, Corfu, Greece. doi: 10.1109/MED.2011.5983075.

[25] Weimin Shen, J Gu, and Yanjun Shen. Proposed wall climbing robot with permanent magnetic tracks for inspecting oil tanks. In *Mechatronics and Automation, 2005*

IEEE International Conference, volume 4, pages 2072 – 2077 Vol. 4. doi: 10.1109/ICMA.2005.1626882.

[26] Mahmoud Tavakoli, Carlos Viegas, Lino Marques, J. Norberto Pires, and Aníbal T. De Almeida. OmniClimbers: Omni-directional magnetic wheeled climbing robots for inspection of ferromagnetic structures. *Robotics and Autonomous Systems*, 61 (9):997–1007. ISSN 09218890. doi: 10.1016/j.robot.2013.05.005.

[27] Hwang Kim, Dongmok Kim, Hojoon Yang, Kyouhee Lee, Kunchan Seo, Doyoung Chang, and Jongwon Kim. Development of a wall-climbing robot using a tracked wheel mechanism. *Journal of Mechanical Science and Technology*, 22(8):1490–1498. ISSN 1738-494X. doi: 10.1007/s12206-008-0413-x. URL `http://link.springer.com/10.1007/s12206-008-0413-x`.

[28] Giuk Lee, Kunchan Seo, Seokwoo Lee, Junhwan Park, Hwang Kim, Jongwon Kim, and TaeWon Seo. Compliant track-wheeled climbing robot with transitioning ability and high-payload capacity. *2011 IEEE International Conference on Robotics and Biomimetics*, pages 2020–2024. doi: 10.1109/ROBIO.2011.6181588. URL `http://ieeexplore.ieee.org/lpdocs/epic03/wrapper.htm?arnumber=6181588`.

[29] Wolfgang Fischer, Fabien Tâche, and Roland Siegwart. Magnetic wall climbing robot for thin surfaces with specific obstacles. *Springer Tracts in Advanced Robotics*, 42: 551–561. ISSN 16107438. doi: 10.1007/978-3-540-75404-6_53.

[30] Jianzhong Shang, Bryan Bridge, Tariq Sattar, Shyamal Mondal, and Alina Brenner. Development of a climbing robot for inspection of long weld lines. *Industrial Robot: An International Journal*, 35(3):217–223. ISSN 0143-991X. doi: 10.1108/01439910810868534.

[31] Frederic Rochat, Patrick Schoeneich, Barthelemy Luthi, Francesco Mondada, Hannes Bleuler, and Roland Moser. Cy-mag3D: A Simple And Miniature Climbing Robot With Advance Mobility In Ferromagnetic Environment. *Emerging Trends in Mobile Robotics - Proceedings of the 13th International Conference on Climbing and Walking Robots and the Support Technologies for Mobile Machines*, pages 383–390.

doi: 10.1142/9789814329927_0048. URL http://eproceedings.worldscinet.com/9789814329927/9789814329927_0048.html.

[32] Autonomous Systems, E T H Zürich, and Ch Zürich. Very Compact Climbing Robot rolling on Magnetic Hexagonal Cam-Discs, with High Mobility on Obstacles but Minimal Mechanical Complexity. In *Joint 41th International Symposium on Robotics 2010 and 6th German Conference on Robotics 2010*, pages 1239–1245, Zürich. Eidgenössische Technische Hochschule Zürich, Autonomous System Lab. ISBN 978-3-8007-3273-9. URL http://dx.doi.org/10.3929/ethz-a-010027617.

[33] Seokwoo Lee Junhwan Park Hwang Kim Jongwon Kim TaeWon Seo Giuk Lee Kunchan Seo. Compliant Track-Wheeled Climbing Robot with Transitioning Ability and High-Payload Capacity. In *IEEE International Conference on Robotics and Biomimetics (ROBIO)*. IEEE.

[34] Giuk Lee, Geeyun Wu, Jongwon Kim, and Taewon Seo. High-payload climbing and transitioning by compliant locomotion with magnetic adhesion. *Robotics and Autonomous Systems*, 60(10):1308–1316. ISSN 09218890. doi: 10.1016/j.robot.2012.06.003. URL http://dx.doi.org/10.1016/j.robot.2012.06.003.

[35] Giuk Lee, Geeyun Wu, Sun Ho Kim, Jongwon Kim, and TaeWon Seo. Combot: Compliant climbing robotic platform with transitioning capability and payload capacity. In *Robotics and Automation (ICRA), 2012 IEEE International Conference on*, pages 2737–2742. doi: 10.1109/ICRA.2012.6224799.

[36] Giuk Lee, Geeyun Wu, Jongwon Kim, and Taewon Seo. High-payload climbing and transitioning by compliant locomotion with magnetic adhesion. *Robotics and Autonomous Systems*, 60(10):1308–1316. ISSN 09218890. doi: 10.1016/j.robot.2012.06.003. URL http://dx.doi.org/10.1016/j.robot.2012.06.003.

[37] Metin Sitti. Under-actuated tank-like climbing robot with various transitioning capabilities. *2011 IEEE International Conference on Robotics and Automation*, pages 777–782. doi: 10.1109/ICRA.2011.5979533. URL http://ieeexplore.ieee.org/lpdocs/epic03/wrapper.htm?arnumber=5979533.

[38] Wolfgang Fischer, Christoph Hürzeler, and Roland Siegwart. Lightweight magnetic foot with variable force, for docking/landing with micro-helicopters on rust-covered walls in boiler furnaces. In *Proc. of the 13th International Conference on Climbing and Walking Robots 2010 (CLAWAR)*, pages 407–414, Nagoya, Japan. Eidgenössische Technische Hochschule Zürich, Autonomous System Lab.

[39] Mark Yim, Sam Homans, and Kimon Roufas. Climbing with Snake-Like Robots. *IFAC Workshop on Mobile Robot Technology 2001*.

[40] Keigo Watanabe, Guang Lei Liu, and Kiyotaka Izumi. Pattern Analyses for Semi-Looper Type Robots with Multiple Links. pages 2–7.

[41] Yutaka Mizota, Yusuke Goto, and Taro Nakamura. Development of a Wall Climbing Robot Using the Mobile Mechanism of Continuous Traveling Waves Propagation. In *IEEE International Conference on Robotics and Biomimetics (ROBIO)*, pages 1508–1513, Shenzhen, China. IEEE. ISBN 9781479927449.

[42] Huai-Ti Lin, Gary G Leisk, and Barry Trimmer. GoQBot: a caterpillar-inspired soft-bodied rolling robot. *Bioinspiration & biomimetics*, 6(2):026007. ISSN 1748-3182. doi: 10.1088/1748-3182/6/2/026007.

[43] H. X. Zhang, J. Gonzalez-Gomez, S. Y. Chen, and J. W. Zhang. Embedded intelligent capability of a modular robotic system. *2008 IEEE International Conference on Robotics and Biomimetics, ROBIO 2008*, pages 2061–2066. doi: 10.1109/ROBIO.2009.4913319.

[44] Douglas Adams. *So long, and thanks for all the fish*. Harmony Books, London, Pan. ISBN 0517554399. URL `https://goo.gl/prto7K`.

[45] Aaron Greenfield, AA Rizzi, and Howie Choset. Dynamic Ambiguities in Frictional Rigid-body Systems with Application to Climbing via Bracing. In *Proceedings of the 2005 IEEE International Conference on Robotics and Automation*, pages 1947–1952, Barcelona, Spain. IEEE. ISBN 0-7803-8914-X. doi: 10.1109/ROBOT.2005.1570398. URL `http://ieeexplore.ieee.org/xpls/abs_all.jsp?arnumber=1570398http://ieeexplore.ieee.org/lpdocs/epic03/wrapper.htm?arnumber=1570398`.

[46] Cornell Wright, Austin Buchan, Ben Brown, Jason Geist, Michael Schwerin, David Rollinson, Matthew Tesch, and Howie Choset. Design and Architecture of the Unified Modular Snake Robot. In *Proceedings - IEEE International Conference on Robotics and Automation*, pages 4347–4354. ISBN 9781467314039. doi: 10.1109/ICRA.2012.6225255.

[47] Ozgur Unver, Michael Murphy, and Metin Sitti. Geckobot and Waalbot: Small-Scale Wall Climbing Robots. URL `http://arc.aiaa.org/doi/abs/10.2514/6.2005-6940`.

[48] Hongjun Chen, Weihua Sheng, Ning Xi, and Jindong Tan. Motion Control of a Micro Biped Robot for Nondestructive Structure Inspection. In *Proceedings of the 2005 IEEE International Conference on Robotics and Automation*, pages 478–483, Barcelona, Spain. IEEE. ISBN 0-7803-8914-X. doi: 10.1109/ROBOT.2005.1570164. URL `http://ieeexplore.ieee.org/lpdocs/epic03/wrapper.htm?arnumber=1570164`.

[49] Sangbae Kim, Matthew Spenko, Salomon Trujillo, Barrett Heyneman, Virgilio Mattoli, and Mark R. Cutkosky. Whole body adhesion: hierarchical, directional and distributed control of adhesive forces for a climbing robot. In *Proceedings 2007 IEEE International Conference on Robotics and Automation*, pages 1268–1273, Roma, Italy. IEEE. ISBN 1-4244-0602-1. doi: 10.1109/ROBOT.2007.363159. URL `http://ieeexplore.ieee.org/lpdocs/epic03/wrapper.htm?arnumber=4209263`.

[50] A Asbeck, S Dastoor, A Parness, L Fullerton, N Esparza, D Soto, B Heyneman, and M Cutkosky. Climbing rough vertical surfaces with hierarchical directional adhesion. In *Robotics and Automation, 2009. ICRA '09. IEEE International Conference on*, pages 2675–2680.

[51] M. Armada, P. G. de Santos, M. a. Jimenez, and M. Prieto. Application of CLAWAR Machines. *The International Journal of Robotics Research*, 22(3-4):251–264. ISSN 0278-3649. doi: 10.1177/0278364903022003009. URL `http://ijr.sagepub.com/cgi/doi/10.1177/0278364903022003009`.

[52] M Armada, M Prieto, T Akinfiev, H Montes, S Nabulsi, R Ponticelli, J Sarria, J Estremera, S Ros, J Grieco, and G Fernandez. On the Design and Development of Climbing and Walking Robots for the Maritime Industries. *Journal of Maritime Research*, II(1):9–32.

[53] A Gimenez C. Balaguer and A Jardon. Climbing Robots Mobility for Inspection and Maintenance of 3D Complex Environments. In *Autonomous Robots*, volume 18, page 157169, The Netherlands. Springer Science + Business Media, Inc.

[54] J. C. Resino, A. Jardón, A. Gimenez, and C. Balaguer. Analysis of the direct and inverse kinematics of ROMA II Robot. *Proceedings of the 8th International Conference on Climbing and Walking Robots and the Support Technologies for Mobile Machines, CLAWAR 2005*, pages 869–874. doi: 10.1007/3-540-26415-9-104. URL `http://www.scopus.com/inward/record.url?eid=2-s2.0-61649083913&partnerID=tZOtx3y1`.

[55] A. Hirose, R. Nagakubo, and S. Toyama. Machine That Can Walk and Climb on Floors, Walls and Ceilings.pdf. In *Fifth International Conference on Advanced Robotics, 'Robots in Unstructured Environments'*, pages 753–758, Pisa, Italy. ICAR.

[56] Akihiko Nagakubo and Shigeo Hirose. Walking and Running of the Quadruped Wall-Climbing Robot. *Proceedings of the 1994 IEEE International Conference on Robotics and Automation*, 2:1005–1012. ISSN 10504729. doi: 10.1109/ROBOT.1994.351225. URL `http://ieeexplore.ieee.org/lpdocs/epic03/wrapper.htm?arnumber=351225`.

[57] Yasong Li, Ausama Ahmed, Dan Sameoto, and Carlo Menon. Abigaille II: toward the development of a spider-inspired climbing robot. *Robotica*, 30(01):79–89. ISSN 0263-5747. doi: 10.1017/S0263574711000373. URL `http://www.journals.cambridge.org/abstract_S0263574711000373`.

[58] B L Luk, A A Collie, and J Billingsley. Robug 11 : an Intelligent Wall Climbing Robot. *Proceedings of the 1991 IEEE International Conference on Robotics and Automation*, pages 2342–2347. doi: 10.1109/ROBOT.1991.131752.

[59] Michael Murphy, William Tso, Michael Tanzini, and Metin Sitti. Waalbot: An Agile Small-Scale Wall Climbing Robot Utilizing Pressure Sensitive Adhesives. *2006 IEEE/RSJ International Conference on Intelligent Robots and Systems*, pages 3411–3416. doi: 10.1109/IROS.2006.282578. URL `http://ieeexplore.ieee.org/lpdocs/epic03/wrapper.htm?arnumber=4058928`.

[60] Werner Brockmann and M Florian. Climbing Without a Vacuum Pump. *Climbing and Walking Robots (CLAWAR)*, pages 1–8.

[61] K D Kotay and D L Rus. Navigating 3D steel web structures with an inchworm robot. In *Intelligent Robots and Systems '96, IROS 96, Proceedings of the 1996 IEEE/RSJ International Conference on*, volume 1, pages 368 –375 vol.1. doi: 10.1109/IROS.1996.570701.

[62] Hyungseok Kim, Taehun Kang, Vo Gia Loc, and Hyouk Ryeol Choi. Gait Planning of Quadruped Walking and Climbing Robot for Locomotion in 3D Environment. *Proceedings of the 2005 IEEE International Conference on Robotics and Automation*, 2005(April):2733–2738. ISSN 10504729. doi: 10.1109/ROBOT.2005.1570527. URL `http://ieeexplore.ieee.org/lpdocs/epic03/wrapper.htm?arnumber=1570527`.

[63] Tachun Kang, Hyungseok Kim, Theyoung Son, and Hyoukryeol Choi. Design of quadruped walking and climbing robot. In RSJ, editor, *Proceedings 2003 IEEE/RSJ International Conference on Intelligent Robots and Systems (IROS)*, volume 1, pages 619–624, Las Vegas, Nevada. IEEE. ISBN 0-7803-7860-1. doi: 10.1109/IROS.2003.1250698. URL `http://ieeexplore.ieee.org/lpdocs/epic03/wrapper.htm?arnumber=1250698`.

[64] Zhiqiang Bi, Yisheng Guan, Shizhong Chen, Haifei Zhu, and Hong Zhang. A miniature biped wall-climbing robot for inspection of magnetic metal surfaces. In *2012 IEEE International Conference on Robotics and Biomimetics (ROBIO)*, pages 324–329. IEEE. ISBN 978-1-4673-2127-3. doi: 10.1109/ROBIO.2012.6490987. URL `http://ieeexplore.ieee.org/lpdocs/epic03/wrapper.htm?arnumber=6490987`.

[65] Mahmoud Tavakoli, Ali Marjovi, Lino Marques, and Aníbal T. De Almeida. 3DCLIMBER: A climbing robot for inspection of 3D human made structures. *2008 IEEE/RSJ International Conference on Intelligent Robots and Systems, IROS*, pages 4130–4135. doi: 10.1109/IROS.2008.4651024.

[66] A J Huete, J G Victores, S Martinez, A Gimenez, and C Balaguer. Personal Autonomy Rehabilitation in Home Environments by a Portable Assistive Robot. *Systems, Man, and Cybernetics, Part C: Applications and Reviews, IEEE Transactions on*, 42(4):561–570. ISSN 1094-6977. doi: 10.1109/TSMCC.2011.2159201.

[67] A. J. Huete, Juan G Victores, S. Martinez, A. Gimenez, and Carlos Balaguer. Personal Autonomy Rehabilitation in Home Environments by a Portable Assistive Robot. *IEEE Transactions on Systems, Man, and Cybernetics, Part C (Applications and Reviews)*, 42(4):561–570. ISSN 1094-6977. doi: 10.1109/TSMCC.2011.2159201. URL `http://ieeexplore.ieee.org/lpdocs/epic03/wrapper.htm?arnumber=5959995`.

[68] C. Balaguer, A. Gimenez, A.J. Huete, A.M. Sabatini, M. Topping, and G. Bolmsjo. The MATS robot: service climbing robot for personal assistance. *IEEE Robotics & Automation Magazine*, 13(1):51–58. ISSN 1070-9932. doi: 10.1109/MRA.2006.1598053. URL `http://ieeexplore.ieee.org/lpdocs/epic03/wrapper.htm?arnumber=1598053`.

[69] RT Pack, J.L. Christopher, and K. Kawamura. A Rubbertuator-based structure-climbing inspection robot. In *Proceedings of International Conference on Robotics and Automation*, volume 3, pages 1869–1874. IEEE. ISBN 0-7803-3612-7. doi: 10.1109/ROBOT.1997.619060. URL `http://ieeexplore.ieee.org/xpls/abs_all.jsp?arnumber=619060http://ieeexplore.ieee.org/lpdocs/epic03/wrapper.htm?arnumber=619060`.

[70] Manuel; Armada and Pablo Gonzalez de Santos. Climbing, walking and intervention robots. *Industrial Robot: An International Journal*, 24(2):158–163. ISSN 0143-991X. doi: 10.1108/01439919710165716. URL `http://www.emeraldinsight.com/doi/abs/10.1108/01439919710165716`.

[71] FREDERIC ROCHAT, RICARDO BEIRA, HANNES BLEULER, and FRANCESCO MONDADA. TREMO: An Inspection Climbing Inchworm Based On Magnetic Switchable Device. In *Field Robotics*, pages 421–428, Paris, France. World Scientific. ISBN 978-981-4374-27-9. doi: 10.1142/9789814374286_0049. URL http://www.worldscientific.com/doi/10.1142/9789814374286_0049.

[72] Greg Peters. *UTS RVC: The Design and Construction of a Protoype Climbing Robot.* Thesis, University of Technology, Sydney.

[73] Gavin Banh. *UTS RVC: Computer Aided Design of a Climbing Robot.* Thesis, University of Technology, Sydney.

[74] Haifei Zhu, Yisheng Guan, Chuanwu Cai, Li Jiang, Xianmin Zhang, and Hong Zhang. W-Climbot: A modular biped wall-climbing robot. *2010 IEEE International Conference on Mechatronics and Automation*, pages 1399–1404. doi: 10.1109/ICMA.2010.5589064. URL http://ieeexplore.ieee.org/lpdocs/epic03/wrapper.htm?arnumber=5589064.

[75] M Minor, H Dulimarta, G. Danghi, R. Mukherjee, R. Lal Tummala, and D. Aslam. Design, implementation, and evaluation of an under-actuated miniature biped climbing robot. In *Proceedings. 2000 IEEE/RSJ International Conference on Intelligent Robots and Systems (IROS 2000) (Cat. No.00CH37113)*, volume 3, pages 1999–2005. IEEE. ISBN 0-7803-6348-5. doi: 10.1109/IROS.2000.895264. URL http://ieeexplore.ieee.org/xpls/abs_all.jsp?arnumber=895264http://ieeexplore.ieee.org/lpdocs/epic03/wrapper.htm?arnumber=895264.

[76] María A Jiménez Manuel Prieto Manuel Armada Pablo González de Santos. Application of CLAWAR Machines. In *The International Journal of Robotics Research*, chapter 22, page 251 to 264. SAGE Publications, Industrial Automation InstituteC-SIC 28500 La Poveda, Madrid, Spain.

[77] Liyu Wang, Lina Graber, and Fumiya Iida. Climbing vertical terrains with a self-contained robot. *2012 IEEE/RSJ International Conference on Intelligent Robots and Systems*, pages 305–310. ISSN 2153-0858. doi: 10.1109/IROS.

2012.6385848. URL http://ieeexplore.ieee.org/lpdocs/epic03/wrapper.htm?arnumber=6385848.

[78] Fumiya Iida and Iida Fumiya. *Self-Contained High Payload Robot For Climbing On Multiple Vertical Environments*. PhD thesis, Swiss Federal Institute of Technology Zurich.

[79] Donald Ruffatto, Jainam Shah, and Matthew Spenko. Increasing the adhesion force of electrostatic adhesives using optimized electrode geometry and a novel manufacturing process. *Journal of Electrostatics*, 72(2):147–155. ISSN 03043886. doi: 10.1016/j.elstat.2014.01.001. URL http://dx.doi.org/10.1016/j.elstat.2014.01.001.

[80] JACOB N. ISRAELACHVILI. INTERMOLECULAR AND SURFACE The Forces Between Atoms and Molecules : Principles and Concepts. *Interactions*, pages 3152–3158. ISSN 1098-6596. doi: 10.1002/elps.201000212.

[81] K Autumn, Y a Liang, S T Hsieh, W Zesch, W P Chan, T W Kenny, R Fearing, and R J Full. Adhesive force of a single gecko foot-hair. *Nature*, 405(6787):681–685. ISSN 0028-0836. doi: 10.1038/35015073.

[82] Kellar Autumn. How Gecko Toes Stick. *American Scientist*, 94(2):124. ISSN 0003-0996. doi: 10.1511/2006.58.987. URL http://www.americanscientist.org/issues/feature/2006/2/how-gecko-toes-stick.

[83] A. Saunders, D. I. Goldman, R. J. Full, and M. Buehler. The RiSE Climbing Robot: Body and Leg Design. In Grant R. Gerhart, Charles M. Shoemaker, and Douglas W. Gage, editors, *Proc. of SPIE*, volume 6230, pages 1–13. Georgia Institute of Technology Society of Photo-optical Instrumentation Engineers (SPIE). doi: 10.1117/12.666150. URL http://hdl.handle.net/1853/44549.

[84] Burak Aksak, Michael P Murphy, and Metin Sitti. Gecko inspired micro-fibrillar adhesives for wall climbing robots on micro/nanoscale rough surfaces. In *2008 IEEE International Conference on Robotics and Automation*, ICRA 2008, pages 3058–3063, Pasadena, USA. IEEE. ISBN 978-1-4244-1646-2. doi: 10.1109/ROBOT.

2008.4543675. URL http://ieeexplore.ieee.org/lpdocs/epic03/wrapper.htm?arnumber=4543675.

[85] Satya P. Krosuri and Mark A. Minor. Design, modeling, control, and evaluation of a hybrid hip joint miniature climbing robot. *The International Journal of Robotics Research*, 24(12):1033.

[86] Domenico Longo and Giovanni Muscato. Adhesion Techniques for Climbing Robots: State of the Art and Experimental Considerations. *Proceedings of the 11th International Conference on Climbing and Walking Robots (CLAWAR)*, pages 6–28. doi: 10.1142/97898128357720003. URL http://eproceedings.worldscinet.com/9789812835772/9789812835772_0003.html.

[87] Aaron Parness, Mathew Frost, Nitish Thatte, Jonathan P King, Kevin Witkoe, Moises Nevarez, Michael Garrett, Hrand Aghazarian, and Brett Kennedy. Gravity-independent Rock-climbing Robot and a Sample Acquisition Tool with Microspine Grippers. *Journal of Field Robotics*, 30(6):897–915. ISSN 15564959. doi: 10.1002/rob.21476. URL http://doi.wiley.com/10.1002/rob.21476.

[88] E García M Prieto S Nabulsi M. A. Armada P. G. de Santos. Design of mobile robots. In *Proceedings of the 2005 CLAWAR: Introductory Mobile Robotics Workshop*, pages 2890–2895, London, UK.

[89] B E Shores and M A Minor. Design, kinematic analysis, and quasi-steady control of a morphic rolling disk biped climbing robot. In *Proceedings of the 2005 IEEE International Conference on Robotics and Automation*.

[90] X Dianguo Z Yanzheng S Hao G Xueshan W. Yan L. Shuliang. Development and application of wall-climbing robots. In *Proceedings of the 1999 IEEE International Conference on Robotics and Automation*, pages 1207–1212, Detroit, Michigan, USA.

[91] Goudsmit. Electromagnets - Goudsmit Magnetic Supplies. URL http://www.goudsmitmagnets.com/en/pot-electro-magnets/15-electromagnets.html.

[92] K Gilpin, A Knaian, and D Rus. Robot pebbles: One centimeter modules for programmable matter through self-disassembly. In *Robotics and Automation, 2010*

IEEE International Conference on, ICRA, pages 2485–2492, Anchorage, Alaska. doi: 10.1109/ROBOT.2010.5509817.

[93] Ara Nerses Knaian. *Electropermanent Magnetic Connectors and Actuators: Devices and Their Application in Programmable Matter*. PhD thesis, M.S. Massachusetts Institute of Technology. URL `http://hdl.handle.net/1721.1/60151`.

[94] Peter Ward and Dikai Liu. Design of a high capacity Electro Permanent Magnetic adhesion for climbing robots. *2012 IEEE International Conference on Robotics and Biomimetics (ROBIO)*, pages 217–222. doi: 10.1109/ROBIO.2012.6490969. URL `http://ieeexplore.ieee.org/lpdocs/epic03/wrapper.htm?arnumber=6490969`.

[95] Peter Ward and Dikai Liu. Design of a High Capacity Electro Permanent Magnetic Adhesion for Climbing Robots. In Huosheng Hu Hong Zhang, editor, *Proceedings of the 2012 IEEE International Conference on Robotics and Biomimetrics*, pages 217–222, Guangzhou, China. ROBIO, IEEE.

[96] Frederic Rochat, Patrick Schoeneich, Michael Bonani, Stephane Magnenat, Francesco Mondada, and Tokhi Mohammad O Mochiyama Hiromi Virk Gurvinder S Hannes Bleuler Fujimoto Hideo. Design of Magnetic Switchable Device (MSD) and applications in climbing robot. In *Climbing and Walking Robots and the Support Technologies for Mobile Machines.The 13th International Conference on*, CLAWAR 2010, pages 375–382, Nagoya, Japan. World Scientific.

[97] Linnea Ingeborg Natasja Nathalie van Griethuijsen. *Behavioural Repsonses to Mechano-sensory Information in a Soft-Bodied Terrestrial Animal*. PhD thesis, Tufts University. URL `http://search.proquest.com/docview/1026562199`.

[98] Sachin Chorge. Simple eyes - Biology Online. URL `http://www.biology-online.org/articles/sense-organs-insects/simple-eyes.html`.

[99] Debbie Hadley. 10 Fascinating Facts About Caterpillars. URL `http://insects.about.com/od/butterfliesmoths/a/10-Cool-Facts-About-Caterpillars.htm`.

[100] Joseph Berger. Spiny Looper Phigalia Titea (Cramer). *University of Georgia, Lakewood, Colorado, United States*, Bugwood.or:Image Number:

5438910. URL http://www.insectimages.org/browse/detail.cfm?imgnum=5438910#sthash.gYFqjEXn.dpuf.

[101] Introduction to Scaling Laws. URL https://www.av8n.com/physics/scaling.htm.

[102] David Allen. *How Mechanics Shaped the Modern World*. Springer Science & Business Media. ISBN 978-3-319-01701-3. URL http://www.springer.com/fr/book/9783319017006.

[103] K J Waldron and C Hubert. Scaling of robotic mechanisms. *Robotics and Automation, 2000. Proceedings. ICRA'00. IEEE International Conference on*, 1(April): 40–45.

[104] Lucinda Treadwell. an Introduction To the Identification of Caterpillars. URL http://www.insectsexplained.com/caterpillars.pdf.

[105] Gyorgy Csoka. Geometrid moth (Lycia hirtaria) Image No. 5371153-PPT. URL Bugwood.org.

[106] University of Technology Sydney and Centre for Autonomous Systems. CROC Prototype Testing in Lab with manhole Transition. URL https://www.youtube.com/watch?v=t2W4d4MmQq8.

[107] University of Technology Sydney and Centre for Autonomous Systems. CROC on site testing. URL https://www.youtube.com/watch?v=KVWGSonki_c.

[108] UTS CAS RMS. CROC: A Biologically Inspired Climbing Robot for Autonomous Inspection of Steel Infrastructure. URL https://www.youtube.com/watch?v=AP9KTw1WmLs.